Universidade de Aveiro Departamento de Química
2019

Catarina Corte-Real Côncio Sousa

Modelling of Friction and Convective Coefficients in a Dry Transformer

Catarina Corte-Real Côncio Sousa

Modelação dos Coeficientes de Fricção e Convecção num Transformador Seco

dissertação apresentada à Universidade de Aveiro para cumprimento dos requisitos necessários à obtenção do grau de Mestre em Engenharia Química, realizada sob a orientação científica de Luis Sánchez, Engenheiro Sénior I&D da Efacec Power Solutions, SGPS SA, e Carlos Manuel Silva, Professor Associado do Departamento de Química da Universidade de Aveiro.

Dedico este trabalho à minha mãe pelo incansável apoio emocional durante todo o meu percurso acadêmico.

o júri

Presidente	Prof. Doutora Maria Inês de Portugal Branco
	Professora Auxiliar do Departamento de Química da Universidade de Aveiro
Arguente	Prof. Doutor Francisco Avelino da Silva Freitas
	Professor Auxiliar do Departamento de Química da Universidade de Aveiro
Vogal	Prof. Doutor Carlos Manuel Santos da Silva
	Professor Associado do Departamento de Química da Universidade de Aveiro

agradecimentos

Gostaria de agradecer primeiramente à Universidade de Aveiro e à Efacec pela oportunidade da elaboração desta tese de Mestrado. Do mesmo modo, aos meus orientadores, Eng. Luis Sánchez e Professor Carlos Manuel Silva, pelo seu apoio e orientação. Um especial agradecimento ao Márcio Quintela pela sua disponibilidade e apoio.

palavras-chave Transferência de Calor por Convecção; CFD; Transformadores secos; Modelação Térmica

resumo Esta dissertação baseia-se no estudo, axi-simétrico 2D, de transferência de calor por convecção, em condutas de refrigeração de transformadores secos, por meio de simulações de CFD (ANSYS *Fluent*). O objetivo foi a definição de um modelo matemático descritivo dos coeficientes médios de transferência de calor por convecção e de fricção, em relação à convecção natural e forçada, num canal cilíndrico vertical anular, sob condições de fluxo de calor uniforme nas paredes. O fluido de refrigeração neste tipo de transformador é o ar, por convecção natural e um sistema AC é assumido na base do transformador para convecção forçada. Todas as condições do sistema e propriedades do fluido foram construídas e definidas no programa *Fluent*. Foram realizados vários testes prévios, principalmente para selecionar adequadamente a malha de estudo e o modelo fluido-dinâmico. O estudo paramétrico foi construído tendo em conta 45 geometrias, 8 fluxos de calor na parede, 4 velocidades para simulações de convecção forçada, enquanto para convecção natural foi criada e assumida uma correlação linear de velocidade de fluxo de calor. Isto corresponde a 1800 simulações. Após análise e tratamento dos dados, foi realizada uma regressão não linear no MATLAB, visando as funções descritivas dos coeficientes referidos. Obteve-se um ajuste adequado através de redes neurais artificiais (RNA), fornecendo previsões do coeficiente de convecção de erros relativos inferiores a 12% para aproximadamente 80% dos casos e inferior a 15% para aproximadamente 70% dos casos de coeficiente de atrito, relativamente aos resultados obtidos das simulações. Concluiu-se uma precisão superada das previsões de RNA, comparada com o modelo mais adequado de literatura considerado, para o coeficiente de transferência de calor por convecção.

keywords

Convection Heat Transfer; CFD analysis; Dry Transformers; Thermal Modelling

abstract

This thesis stands for a 2D axisymmetric study of convection heat transfer, within cooler ducts of dry type transformers, by means of CFD simulations (*ANSYS Fluent*). The purpose was the definition of descriptive functions for the mean heat transfer and friction coefficients, regarding free and forced convection, within a vertical cylindrical annular duct, under isoflux conditions (uniform wall heat flux). Dry-transformer type uses air as cooling system by natural convection and an AC system is assumed at the base of the transformer for forced convection. All system conditions and fluid properties were constructed and defined at *Fluent* program. Several pre-tests were performed, mainly in order to properly select the studied mesh and fluid-dynamic model. The parametric study was assembled accounting for 45 geometry's designs, 8 values for wall heat flux, 4 velocities for forced convection simulations, while for natural convection a linear correlation heat flux-velocity was assumed. This corresponds to 1800 simulations. After data analysis and treatment, a non-linear regression was performed in MATLAB, aiming for the descriptive functions of convection heat transfer and friction coefficients, obtained thru CFD. A successful fitting was obtained through artificial neural networks (ANN), providing predictions for convective coefficient of relative errors inferior to 12% for approximately 80% of cases and inferior to 15% for approximately 70% of cases for friction coefficient. It was concluded an overcome accuracy of the ANN's predictions shown, compared to the most fitted literature's model considered, for convective heat transfer coefficient.

Index

Table Index

Figure Index

Nomenclature

Variable	Name	Units
h_c	Convective heat transfer coefficient	W/(m^2.K)
f	Friction coefficient	-
f_{FN}	Fanning friction factor	-
q	Power	W
A	Area section/surface	m^2
T_s	Surface temperature	K
T_∞	Fluid temperature	K
Nu	Nusselt number	-
L	Characteristic length	m
k	Thermal Conductivity	W/(m.K)
T_{bulk}	Bulk temperature	K
τ_w	Wall shear stress	Pa
ρ	Volumetric mass density	kg/m^3
U	Mean velocity	m/s
ΔP	Pressure loss	Pa
D_h	Hydraulic diameter	m
H'	Height	m
Re	Reynolds number	-
Pr	Prantl number	-
μ	Fluid's dynamic viscosity	N.s/m^2
μ_{wall}	Wall's dynamic viscosity	N.s/m^2
$\tilde{x}$	Normalized dimension	-
x^+	Normalized dimension	-
γ'	Normalized dimension	-
γ	Normalized dimension	-
ΔT	Temperature gradient between inlet and wall	°C
C_p	Specific Heat	J/(kg.K)
T	Static temperature	K
Gr	Grashof number	-
g	Gravity	m/s^2
β	Thermal expansion coefficient	K^{-1}
Ra	Rayleigh number	-
tk	Thickness	mm
H	Height	mm
Q	Heat flux	W/m^2
v_in	Inlet velocity	m/s
p_{op}	Operating pressure	Pa
R_s	Specific gas constant	J/(kg.K)

Int_turb	**Intensity of turbulence**	-
Ri	**Richardson number**	-
x1, x2, x3	**Normalized dimensions**	-
T_exte_wall	**Wall temperature 1**	°C
T_out	**Mean outlet temperature**	°C
v_out	**Mean outlet velocity**	m/s
T_Air_Center	**Air temperature at duct's center**	°C
T_inte_wall	**Wall temperature 2 (near core)**	°C
T_exte_adja	**Adjacent temperature to external wall**	°C
T_inte_adja	**Adjacent temperature to internal wall**	°C
ΔT_Internal_wall	**Temperature gradient between inlet and outlet (respective to Wall temperature 2)**	°C
ΔT_External_wall	**Temperature gradient between inlet and outlet (respective to Wall temperature 1)**	°C
hc_External_wall	**Convective heat transfer coefficient (Point estimation respective to Wall temperature 1)**	$W/(m^2.K)$
hc_Internal_wall	**Convective heat transfer coefficient (Point estimation respective to Wall temperature 2)**	$W/(m^2.K)$
T_max_wall	**Maximum wall temperature**	°C
tk_n	**Thickness normalized**	-
H_n	**Height normalized**	-
Q_n	**Heat flux normalized**	-
v_bulk_n	**Bulk velocity normalized**	-
v_bulk	**Bulk velocity**	m/s
h_{CFD}	**Convective heat transfer coefficient for CFD simulations**	$W/(m^2.K)$
h_{NET}	**Convective heat transfer coefficient for ANN's predictions**	$W/(m^2.K)$
f_{CFD}	**Friction coefficient for CFD simulations**	-
f_{NET}	**Friction coefficient for ANN's predictions**	-
$h_{MORELLI}$	**Convective heat transfer coefficient for literature's model**	$W/(m^2.K)$
$f_{MORELLI}$	**Friction coefficient for CFD for literature's model**	-
Q_1, Q_2	**Heat flux 1 and 2**	W/m^2
int_turb_in	**Intensity of turbulence at inlet**	-
int_turb_out	**Intensity of turbulence at outlet**	-
p_{in}	**Pressure inlet**	Pa
p_{out}	**Pressure outlet**	Pa

1. Introduction

This work consists on a convection heat transfer study within cooling ducts of a dry-type transformer. The main purpose stands for the definition of descriptive functions of the mean convective heat transfer (h_c) and friction (f) coefficients for natural/free (AN – air natural) and forced (AF - air forced) convection within a specified duct type – vertical annular cylindrical. Both coefficients provide important information to acknowledge the effects of the transformer's operation that outcome from its design.

1.1 Problem Contextualization

Above certain power level, or if required by the client, transformers must be subjected to heat run tests. An economical way to perform this test is by dividing it in a twostep procedure test – defined as No Load Heat run test and the Load heat tests. As for the first one, only magnetic core losses are present, while for the second the losses are regarding the coil's windings. After measurement of the referred temperatures, for both tests, the global final temperature is determined through IEC 60076-11 [1]. Therefore, while on the transformer pre-design phase some preview calculations must be done in order to predict the results. Given the technological evolution of this time this can be done through CFD (Computational Fluid Dynamics) simulations for example. Note that, the most reliable approach would be through experimental results or investigation. However, some detailed measurements are costly and time-consuming, and others can't even be made with a proper precision or even can't be made at all. This explains the main importance role of numerical methods [2].

1.2 Thesis Scheme

This work is divided in four parts. First, an initial introduction providing basic knowledge concerning the studied system and required tools to achieve the defined objective – some transformer's and heat transfer basic concepts and the corresponding modelling tool to study this system (ANSYS® *Fluent* through CFD simulations) and other to numerically fit the obtain results (MATLAB®). Secondly, the development concerning the application of the CFD simulations, according to some defined conditions, escorted by several test's procedures to better construct and implement the CFD model (i.e. independence mesh test, fluid-dynamic model selection), ending with the implementation of the parametric study to the defined CFD model. Thirdly, a previous result's analysis accompanied by the corresponding result's modelling through non-linear data fitting with MATLAB. Ending with result's analysis and discussion followed by conclusions and future possible improvements and ongoing suggestions for this theme.

1.3 Company Introduction

Figure 1. Efacec's logo [3].

Efacec is a Portuguese company specialized in several areas such as energy products, systems and electric mobility, with 70 years of brand, having a strong export focus with presence in more than 65 countries. Its origin, with more than 100 years of history dates to the founding, in 1905, of the "A Moderna" Sociedade de Serração Mecânica. After a few years, "A Moderna" gives rise to Electro Moderna, Lda., a company whose focus would already be the production of electric motors, generators and transformers. Efacec always favoured technological development as a main factor to ensure competitiveness and high quality of its transformers [3]. For instances, Efacec has also developed an Integrated Management System of all the required information for the design and manufacture of Power Transformers. This system includes all the specific software for electric and magnetic field as well as overload and short- circuit analysis, providing multiple solutions, thus allowing a selection of the most reliable and competitive design. Its policy, together with the continuous development in quality and technical product upgrading, has led Efacec Power Transformers to prestige and excellence among its worldwide customers [4]. More recently, in 2015, Efacec's majority capital was acquired by Winterfell Industries company. Today, Efacec is one of the largest industrial companies in Portugal, thanks to its high innovation and adaptability capacity for new challenges of the future [3].

2. Theoretical Fundamentals – Equipment and Phenomenon in Study

2.1 Transformers

Transformer's main purpose stands for the adjustment of electrical voltage levels. In other words, they can link circuits that have different voltages, enabling a universal use of the alternating current system for the transmission and distribution of electrical energy [5]. Therefore, they provide proper operating conditions to several electrical appliances which explains its industrial importance in nowadays society. The following figure demonstrates the previously concepts by showing how an electric source (generator) can provide the needed voltage for different appliances.
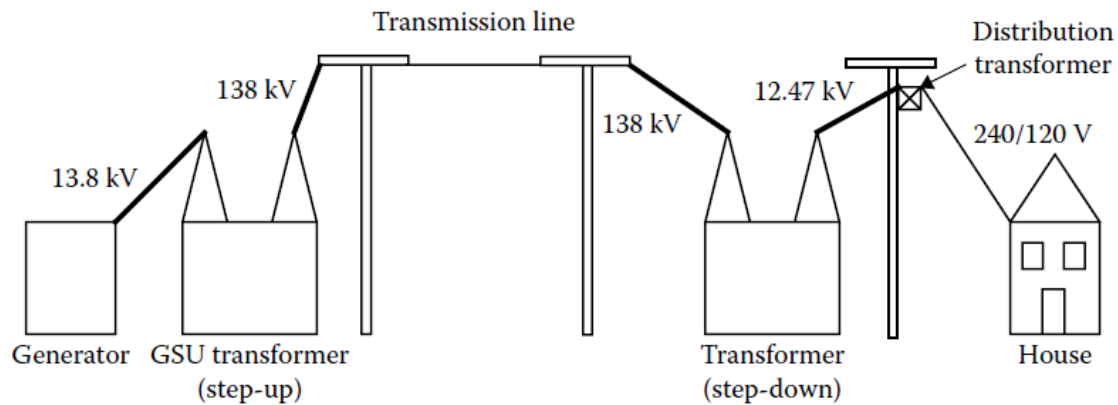
Figure 2. Schematic drawing of a power system [6].

The operation principle of a transformer is based on a magnetic field, generated by electric current, and on the electromagnetic induction, generated by its variation. The heating phenomenon within the transformer occurs by Joule effect (conversion of electric energy into thermal energy, within a conductor) caused by the existence of eddy currents (induced electric current within a conductive material, when subjected to a magnetic field) [7].

Industrially there are several different types of transformers. Its differences are explained by its applications (i.e. requiring a higher or lower power) and regards essentially for; the number of coils - basic unit mainly composed by a core and low and high voltage windings; cooling type and corresponding fluid – the more commonly used are oils and air which can be used, combined or not, through forced or natural convection within the cooling ducts of the transformer.

The studied transformer is of dry type - uses air as a cooling system. It is defined as a three-phase transformer, encapsulated in epoxy resin. These transformers consist of; a core (grounded i.e. with potential 0V); a low voltage winding, layer winding – composed by turns of alternating aluminium and polyester foils, where there are several cooling ducts; and one high tension winding, disk winding – same constitution, also by turns, where the high-tension winding is present, this last winding is coated with a glass mesh and encapsulated with epoxy resin. The use of polyester, glass mesh and epoxy resin have the same purpose – electrical insulation – in order to prevent electrical discharges and short-circuits.
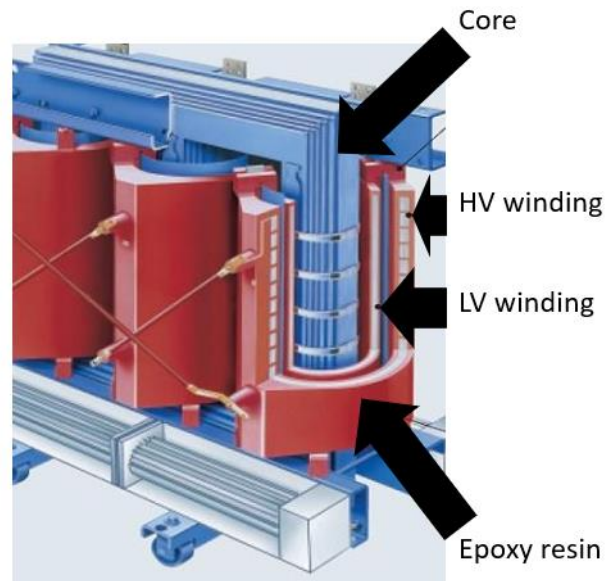
Figure 3. Dry-Transformer[8] .

Dry-type transformers have some advantages such as being environmentally green, with no fluid to leak and degenerate over time [9]. Besides, they are primarily used for indoor applications in order to minimize fire hazards. Concerning its design, nowadays computers can work out several designs (by varying flux density, core diameter, current density, etc.) and come up with an optimum design. One of the major benefits of computers is in the area of analysis. Using commercial 2-D/3-D field computation software, any kind of engineering analysis (electrostatic, electromagnetic, structural, thermal, etc.) can be performed to optimize the design of transformers or to enhance their reliability [5].

The lifetime, reliability, performance and design of the transformer depend and outcome from studies concerning mainly both windings and core heating rate [10]. Within these transformers, heat transfer takes place through three methods, conduction, radiation and convection. These phenomenon's, regarding the transformer windings and the cooling ambient, are threated separately. So, in this work the studied phenomenon stands for convection within the mentioned transformer.

2.2 Heat Transfer - Convection

Heat transfer phenomenon occurs given temperature gradients, resulting on a heat flux from a heated body to a colder one. Convection can be defined by the movement of a fluid to the macroscopic scale in the form of circulation currents. Concerning natural convection, these currents outcome from the heat transfer process between them, while for forced convection the circulation is caused by an external agent.

4

Natural convection manifests itself essentially due to temperature gradients, explained by density differences in the fluid, that translates into its upward and downward movement. In a more extensive and practical manner, the heat flow, applied on the walls, can be converted to wall temperatures which, being higher than the temperature of the fluid, create a temperature gradient. Due to this gradient a heat transfer occurs from the walls to the fluid which increases its own temperature. This temperature rising directly affects the properties of the fluid, more specifically its density, that will decrease. This decrease in air's density causes its upward movement. However, as this upward movement occurs, its temperature decreases so that its density increases again, producing its downward movement. The recurrence of this phenomenon is called natural convection, also known as buoyancy forces. When, any type, of ventilation fan is turned on at the base of the transformer, a force is applied to the fluid, causing a given input velocity. In this case there is forced convection type, since the movement of the fluid is induced by an imposed velocity at the entrance of the duct. This difference between phenomenon's translates into a large amount of transferred heat for this last explained one. In this work the heat transfer will be analysed for both natural convection and forced convection. However, as simplification, for natural convection a low inlet velocity value was assumed, accordingly to its corresponding wall heat flux, as to higher heat flux values a higher velocity value is expected.

Convective Heat Transfer Coefficient (h_c)

The transferred heat by convection is commonly defined through a gradient of temperature, between a surface and a fluid through a given area surface, which might be intern or extern translated by an internal or external flux, given a certain convection heat transfer resistance – inverse of a heat transfer pellicular coefficient. It can also be referred as the transferred convective heat flux between a surface and a fluid, per surface area. This designation is illustrated by Newton's Law, equation 1 [11], and this coefficient is described in the film zone, close to the surface well known as boundary layer, where the resistance to convection heat transfer exists. Theoretical it is known that this coefficient can be determined according to the non-dimensional number of Nusselt, equation 2 [11]. Note that the fluid temperature is generally described by the average temperature of the inlet and outlet fluids (T_{bulk} – bulk's temperature).

$$q = h_c . A(T_s - T_\infty) \tag{1}$$

$$Nu = \frac{h_c . L}{k} \tag{2}$$

About equation (1), potency/power (q) is defined through the product between the convective coefficient (h_c), area section/surface (A) and temperature gradient between surface (T_s) and fluid (T_∞).

For equation (2), the Nusselt number (*Nu*) is described through the quotient between the product of h_c by the characteristic dimension (*L*) through the conductivity (*k*) – according to fluid's properties.

Friction Coefficient (*f*)

The friction coefficient (*f*) is an important parameter in heat transfer since it is directly related to the heat transfer coefficient and mainly with the pressure loss (*ΔP*) along the duct, which is correlated with the power requirements of a pump or fan [12]. It can also be referred to as the existent motion resistance between a surface and a fluid. This parameter can also be known as *Fanning* friction factor (*f_Fn*) and it can be described by the surface/wall shear stress (τ_w), density (ρ) of the fluid and it's mean velocity (*U*), equation 3 [13]. The wall shear stress can be defined as the friction between the fluid and a surface, duct's walls. Therefore, the friction coefficient can also be translated by the pressure drop in the duct, taking in account it's hydraulic diameter (*D_h*), equation 4 [13]. Other way of describing this coefficient is by Moody's diagram (only valid for pipes), where Reynolds number and the relative roughness of the duct are taking in account, Figure 4 [14].

$$f_{Fn} = \frac{\tau_w}{\frac{1}{2}.\rho.U^2} = 4f \tag{3}$$

$$4f = \frac{\left(\frac{\Delta P}{H_l}\right).D_h}{\frac{1}{2}.\rho.U^2} \tag{4}$$
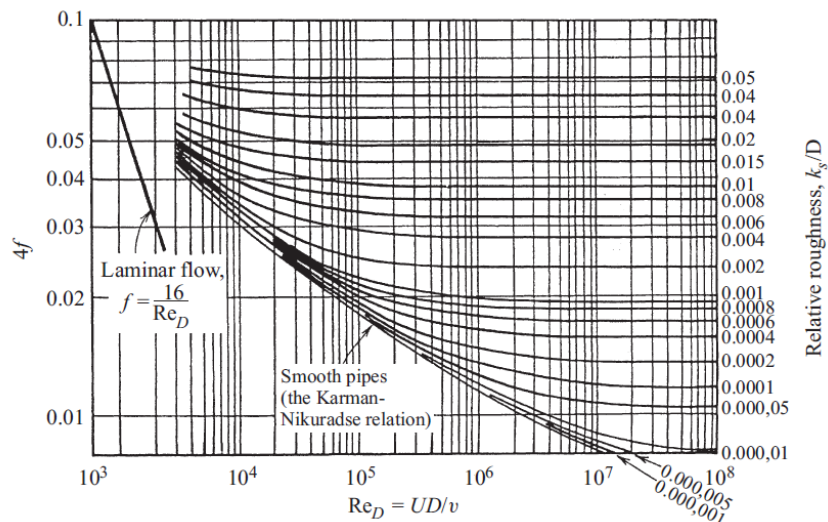
Figure 4. Moody's diagram - Friction factor for duct flow [14].

The most suitable model, considering its identical purpose – "Network based cooling models for Dry Transformers" [15]- will be presented concerning the determination of the convective and friction

6

coefficients. Morelli et al.[15] presents a cooling duct network model for dry transformers (coupling thermal and pressure networks) which was verified and validate by comparing the results with CFD simulations [15]. Later, a comparison between this model and this work results will be performed.

$$
Nu(Re) \begin{cases} 8.235 + \frac{0.024.(\tilde{x})^{-1.14}}{1+0.0358.Pr^{0.17}.(\tilde{x})^{-0.64}} \,,\ \tilde{x} = \frac{L/D_h}{Re.Pr} & Re \leq 2300 \\[3mm] 0.027.Re^{0.8}.Pr^{1/3}.\left(\mu/\mu_{wall}\right)^{0.14} & Re \geq 10000 \\[3mm] (1-\gamma).Nu(2300) + \gamma.Nu(10000), \gamma = \frac{Re-2300}{10000-2300} & 2300 < Re < 10000 \end{cases}
$$

$$(5)\ [15]$$

$$
f(Re) \begin{cases} 4.(x^+).\frac{3.44}{(x^+)^{0.5}} + \frac{24+\frac{0.674}{4.x^+}-\frac{3.44}{(x^+)^{0.5}}}{1+\frac{0.00029}{(x^+)^{-2}}} \,,\quad x^+ = \frac{L}{Re.D_h} & Re \leq 4000 \\[3mm] 0.5072.Re^{-0.3} & Re \geq 10000 \\[3mm] (1-\gamma').f(4000) + \gamma'.f(10000)\,,\ \gamma' = \frac{Re-4000}{10000-4000} & 4000 < Re < 10000 \end{cases}
$$

$$(6)\ [15]$$

Here, for the convective coefficient calculation, equation (5), the Nusselt number (Nu) is resorted, while for the friction coefficient the Reynolds number (Re) was used. Equation (5) also relies on fluid's (μ) and wall's (μ_w) viscosity and other non-dimensional numbers, such as Reynolds number (Re) and Prantl number (Pr). Also, for both equations, some specific normalized dimensions were defined, such as $\tilde{x}$, x^+, γ and γ'. The first (equation 5) and second one (equation 6), depend on the characteristic length and hydraulic diameter, while the last ones are according to the Reynolds number.

Another literature's model[16] was point out for further comparations, concerning the presented equation (7).

$$h_c = 2.17 \times \Delta T^{0.25} \tag{7}$$

Dimensionless Numbers

Some non-dimensional numbers should be referred since they are essential for theoretical determination of the convective heat transfer coefficient. The most important one is, as already

indicated, the Nusselt number. The determination of this one requires the knowledge of others, such as Reynolds (*Re*) and Prandtl (*Pr*) numbers – there's also, Grashof (*Gr*) and Rayleigh (*Ra*) numbers. Acknowledged that these non-dimensional numbers were posteriorly calculated with the temperature values/results, obtained by the CFD simulations. Accordingly, a brief explanation follows.

Reynolds; The Re number can be defined as the ratio between the inertia force to viscous or friction force and interpreted as the ratio of dynamic pressure to shearing stress, as the following equation 8 shows. Note that L corresponds to the characteristic length/dimension, i.e. for intern flux this dimension corresponds to the hydraulic diameter [17].

$$Re = \frac{\rho.U.L}{\mu} \tag{8}$$

Prantl; The Pr number mainly depends on the fluid properties and is translated by the approximation of the ratio of momentum diffusivity (kinematic viscosity) to thermal diffusivity and it can be expressed by equation 9 [18]. Here, C_p stands for the specific heat.

$$Pr = \frac{c_p.\mu}{k} \tag{9}$$

Grashof; The Gr number represents the ratio between the buoyancy force due to spatial variation in fluid density (caused by temperature differences) to the restraining force due to the viscosity of the fluid. This is expressed by equation 10 [19]. Here, g stands for gravity and the thermal expansion coefficient is represented by β (approximation by the inverse of the mean temperature).

$$Gr = \frac{g.\beta(T_S - T_\infty)L^3}{\left(\mu/\rho\right)^2} \tag{10}$$

Rayleigh; The Ra number is simply defined as the product of the *Gr* number, which describes the relationship between buoyancy and viscosity within a fluid, and the *Pr* number, which describes the relationship between momentum diffusivity and thermal diffusivity. Resuming, is used to express heat transfer in natural convection. The magnitude of the Rayleigh number (*Ra*) is a good indication as to whether the natural convection boundary layer is laminar or turbulent [20].

$$Ra = Pr.Gr \tag{11}$$

2.3 Modelling Tool – CFD & *ANSYS® 19.2*

In a real fluid, viscosity introduces resistance to motion. This can be explained by shear or friction forces between fluid particles and, between these and boundary walls. The derivation of the Euler equations can be modified to include the shear stresses in a real fluid in addition to the normal stress or pressure already included there. The result is a set of nonlinear, second-order partial differential equations, called the Navier-Stokes equations. Unfortunately, given its complexity level, few useful analytic solutions to these equations have been found. Therefore, the engineer must be resort to experimental results, semi-empirical methods, and numerical simulations to solve problems [21].

Software Introduction

Computational Fluid Dynamics (CFD) can be explained as the science and methodology for fluid flow prediction by solving mass, energy and movement equations by means of a numerical algorithm and essential empirical models. CFD was made possible with the creation of computers and is continually benefited by increased processor speeds and memory allowance [22].

ANSYS software can be described as an engineering tool, used to design products and create correspondent simulations to solve complex structural engineering problems of fluid dynamic, electromagnetic, etc [23]. *ANSYS FLUENT* consists in a CFD software. In this work *ANSYS® 19.2* version was used.

There are three main components to the implementation of CFD methodology: grid generation, algorithm development, and turbulence / empirical modelling. Grid generation refers to segregating the flow domain into individual cells or elements. The grid is used to calculate derivatives and fluxes for the numerical algorithm. The numerical algorithm corresponds to how the derivatives and fluxes are calculated i.e. central differenced or up-winded and order of accuracy etc. Different fluid dynamic models are used to reduce computational requirements (such as processor speed and memory) [22].

Mathematical Approach – Solver Algorithm

The *Fluent* solver option can be pressure-based or density-based. The pressure-based solver (PBS) is applicable for a wide range of flow regimes from low speed incompressible flow to high-speed compressible flow. Allows flexibility in the solution procedure and requires less memory (storage). The density-based solver (DBS) is applicable when there is a strong interdependence between density, energy, momentum and/or species.

The pressure equation is derived from the continuity and the momentum equations in such a way that the velocity field, corrected by the pressure, satisfies the continuity equation. The solution process involves iterations wherein the entire set of governing equations is solved repeatedly until the solution converges. As a variation of PBS, and presenting a superior performance, there is also the

pressure-based-coupled solver (PBCS), which is applicable for most single-phase flows and only requires 1.5-2 times more memory than the PBS. The PBCS algorithm solves a coupled system of equations comprising the momentum and the pressure correction equations, while the PBS has a segregated solution algorithm [24]. This is represented by Figure 5.
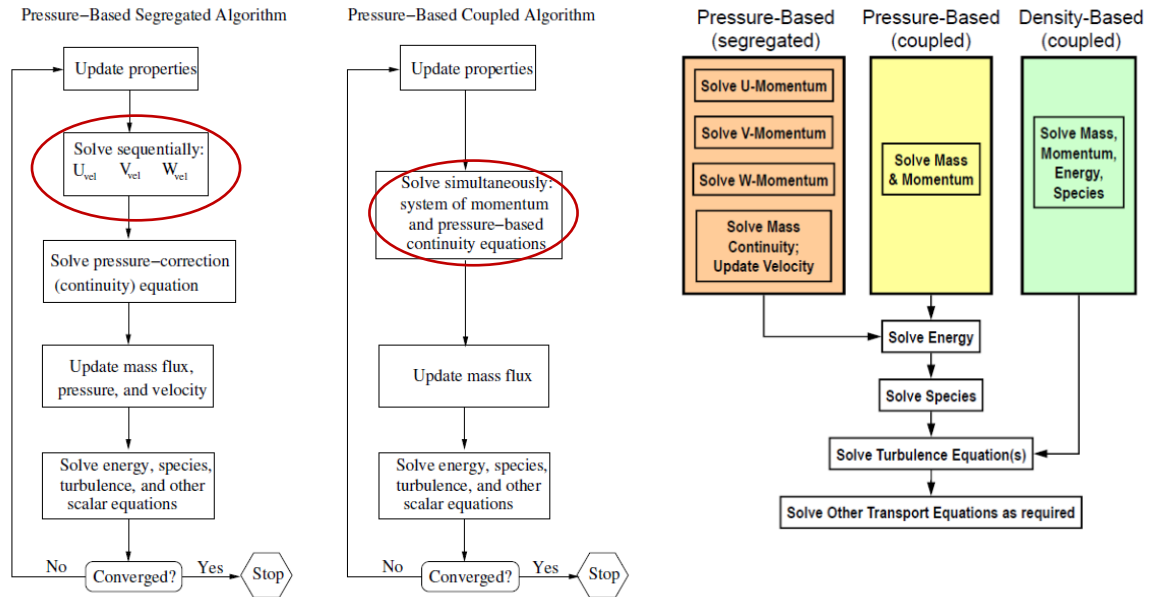
Figure 5. Solver algorithm approaches – PBS, PCBS and DBS [25],[24].

Fluid Dynamic Models – *Fluent*

Fluent provides comprehensive modelling capabilities for a wide range of incompressible and compressible, laminar and turbulent fluid flow problems. Steady-state or transient analyses can be performed. In *Fluent*, a broad range of mathematical models for transport phenomena (like heat transfer and chemical reactions) is combined with the ability to model complex geometries [26].

Turbulence Models

Some of the approaches of turbulence modelling are the followed: 1) Direct Numerical Simulation (DNS) – this first approach does not embody the *Fluent* program; 2) Large Eddy Simulation (LES) - Like DNS, a 3D simulation is performed over many timesteps, however only the larger "eddies" are resolved; and 3) Reynolds Averaged Navier-Stokes solution (RANS). The most commonly used by engineers is the RANS approach, where equations are solved for time-averaged flow behaviour and the magnitude of turbulent fluctuations [27]. The turbulence models available in *Fluent* are presented in Figure 6.
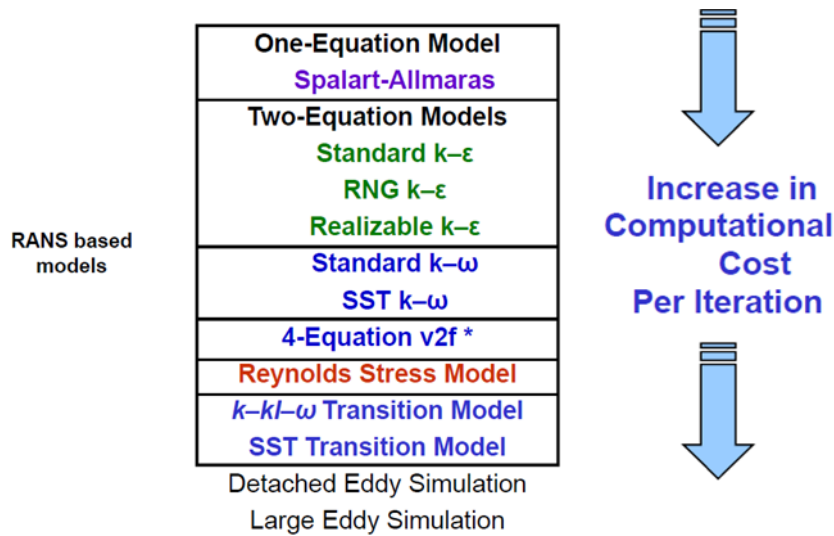
Figure 6. Turbulence Models available in Fluent [27].

k-ε model; The *k-epsilon* model is one of the most common turbulence models. It is a two-equation model, which means, it includes two extra transport equations to represent the turbulent properties of the flow. This allows a two-equation model to account for effects like convection and diffusion of turbulent energy. The first transported variable is turbulent kinetic energy, k. The second transported variable in this case is the turbulent dissipation, ε. It is the variable that determines the scale of the turbulence, whereas the first variable, k, determines the energy in the turbulence [22].

Realizable k-ε model; The Realizable k-epsilon is one of the models that will be presented on the study. This model differs from the standard k-ε model by containing an alternative formulation for the turbulent viscosity and a modified transport equation for the dissipation rate, ε, has been derived from an exact equation for the transport of the mean-square vorticity fluctuation. The term "realizable" means that the model satisfies certain mathematical constraints on the Reynolds stresses, consistent with the physics of turbulent flows [22].

Some of the benefits comparing with standard k-epsilon model are that the Realizable model accurately predicts the spreading rate of both planar and round jets and it is likely to provide superior performance compared with the standard k-epsilon model for flows involving rotation, boundary layers under strong adverse pressure gradients, separation, and recirculation [27].

Standard k-omega model; A two-transport-equation model solving for k and ω, the specific dissipation rate (ε / k) based on Wilcox (1998). This is the default k–ω model. Superior performance for wall-bounded boundary layer, free shear, and low Reynolds number flows.

11

Suitable for complex boundary layer flows under adverse pressure gradient and separation (external aerodynamics and turbomachinery). Can be used for transitional flows. Separation is typically predicted to be excessive and early [27].

SST k-omega model; Corresponds to a variant of the standard k–ω model. Combines the original Wilcox model for use near walls and the standard k–ε model away from walls using a blending function. The transition and shearing options are borrowed from standard k–ω. The k–ω model has many good attributes and performs much better than k–ε models for boundary layer flows. Wilcox' original k–ω model is overly sensitive to the free stream value of ω, while the k–ε model is not prone to such problem. Most two-equation models, including k–ε models, over-predict turbulent stresses in the wake (velocity-defect) regions, which leads to poor performance in predicting boundary layers under adverse pressure gradient and separated flows. The basic idea of SST k–ω is to combine standard k–ω model in the near-wall region with standard k–ε model in the outer region [27].

Transition SST model; The transition SST model is based on the coupling of the SST k-ω transport equations with two other transport equations, one for the intermittency and one for the transition onset criteria, in terms of momentum-thickness Reynolds number. An *ANSYS* proprietary empirical correlation (*Langtry and Menter*) has been developed to cover standard bypass transition as well as flows in low free-stream turbulence environments [28].

Wall functions for turbulence models

Some models can rely on wall function equations. These are based on an analytical solution of the transport equations combined with experimental data fitting. Consequently, there's a computational time decreasing and a relatively accurate representation of the occurrences within the boundary layer, regarding its derivative conditions.

2.4 Mathematical Modelling – Artificial Neural Network (ANN) with MATLAB®

The neural network system had an increasing developing through time. It has been widely used in many industries such as Finance, Food, Energy, Medical, Science and Engineering, Transportation and Communication, etc [29].

Neural network systems have a great advantage in dealing with problems in which many factors influence the process and result. Given the level of complexity and difficulty on defining the descriptive function for the referred coefficients in this study, this modelling tool was considered.

The basic concept of ANN lies on constructing a neural network and train it to recognize patterns. The term neural network (NN) typically refers to an artificial neural network (ANN). An ANN attempts to simulate the biological NN contained in the brains of all animals. ANN were first introduced in the 1950's and its development was improved through time.

NN are composed by neurons forming layers. Input is presented to the layers of neurons. If the input to a neuron is in within the range that the neuron has been trained for, then the neuron will fire. When a neuron fires, a signal is sent to the layer of neurons to which the firing neuron is connected. The connections between neurons are called synapses – regions of input and output; interface between a program and a NN. Each connection is assigned a connection weight, i.e. no connection expresses a zero weight. These weights determine the NN output, so connection weights form the memory of the NN. Besides this neuron attribute, another one is to be considered: threshold. Resuming, the incoming signal will be amplified or de-amplified by its weight as it crosses the incoming synapses. If the weighted input exceeds the threshold, then the neuron will fire – a new analogue signal is transmitted to other neurons. Note that the NN results from neuron's combination, so the fire action occurs regarding the given combination. These two parameters (weights and biases/threshold) are normally stored in matrix form, as NN processes matrix mathematical. The connection weights assigned process its's defined as training. Most training algorithms begin by assigning random numbers to a weight's matrix. Then the validity of the NN is examined. Next, the weights are adjusted based on how well the NN performed and the validity of the results. The most commonly used category training method is defined as supervised. It is accomplished by giving the NN a set of sample data along with anticipated outputs from each of these samples. NN is taken through a given number of iterations or epochs, until the output of NN matches the anticipated output, with a reasonably small rate of error. Each epoch is pass through the training samples. This process is repeated until the validation error is within an acceptable limit, in order to make the created NN use possible [30].

The MATLAB's Neural Net Fitting app (*nftool*) provides the construction of this type of network (involving all training, validation and testing sets) and its corresponding analysis. Figure 7 represents a schematic example of the used NN.
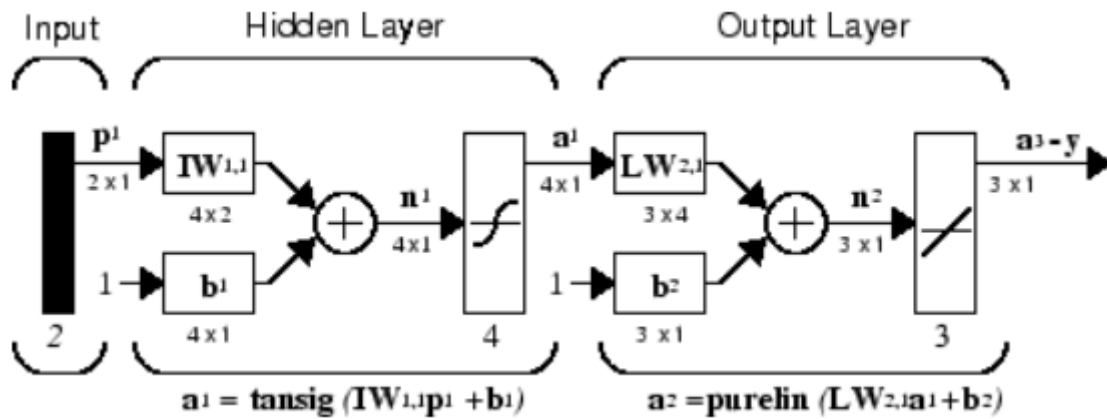
Figure 7. Neural network for MATLAB's nftool [31] .

The hidden layer is affected by an active function, known as *sigmoid* function. It is noticeable the existence of the previously mentioned weights – $IW_{1,1}$ and $LW_{2,1}$ - and biases (same in concept as threshold) – b_1 and b_2. So, in a simple manner, there's an input matrix which will be affected by a sigmoid transfer function, regarding for the defined (through training, validation and testing) weights and biases. The output from this layer corresponds to the input for the output layer which is similarly affected, however with a *purelin* function, which stands for a linear transfer function. This network can be used as a general function approximator. It can approximate any function with a finite number of discontinuities arbitrarily well, given sufficient number of neurons in the hidden layer [31].

3. Modelling

3.1 Description of the System Conditions and Input Parameters

The study system consists in one of the presented cooling duct types (cooling fluid - air), existent in the transformer. All ducts have a vertical cylindrical geometry, distinguishing themselves from each other by the type of corresponding within flow - external, internal and annular. This description can be explained by the transformer profile schematic 2D – Figure 8.
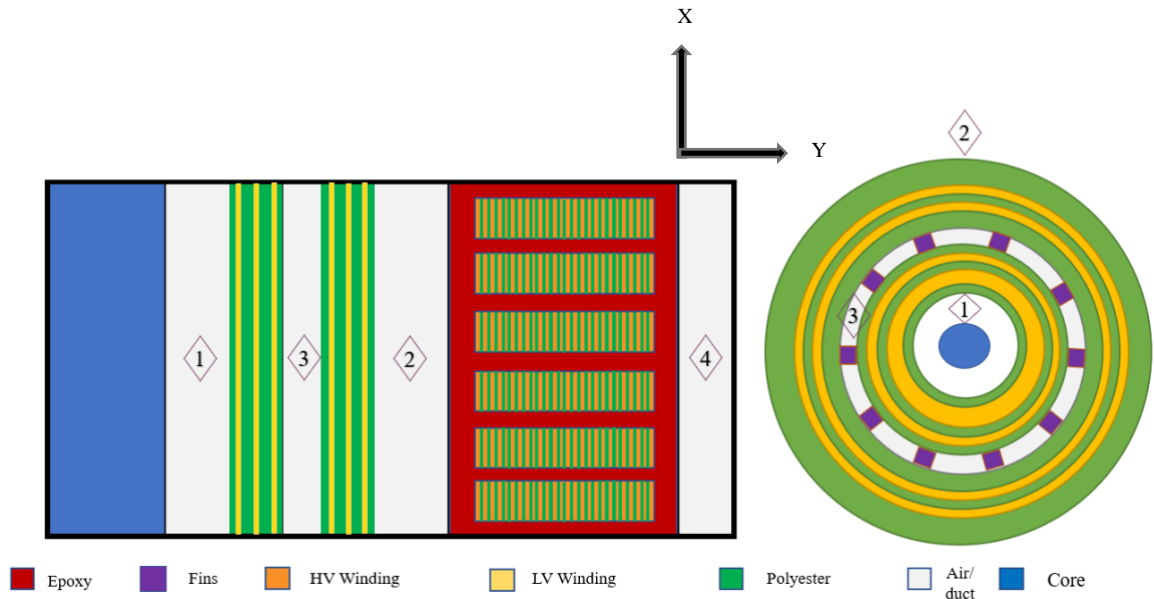
Figure 8. Transformer's 2D profile schematic.

At Figure 8, in the presented axis, X stands for the fluid's direction which is opposite to gravity's vector. In general, it shows the existence of several internal ducts and two vertical annular cylindrical ducts, besides the external one (case 4 - in contact with the exterior environment and the HV winding). The internal duct type (case 3) is located internally of the LV winding and these ducts were created by fins/ribs implementation between the winding. As for the annular ducts, the first one (case 1) is situated between the core and the LV winding, while the second (case 2) is between the LV and the HV winding. About these last two duct's types, an upper scheme view, of the LV winding and core, was also presented for better perception and comprehension of the importance of annular duct, given its mainstream dimension and existence. The duct in study is vertical annular cylindrical type and its analysis will be performed accordingly to a 2D axisymmetric study.

3.2 CFD - Initiation

Before initiate the study, is of most importance to understand some of the fundamentals of the main tool – *ANSYS Fluent* program. The analysis through this program relies on finite elements method, which divides in three steps: pre-processing, processing(analysis) and post-processing. Pre-

processing relies on defining the geometry, analysis type, mesh, material properties and boundary conditions. For the processing the analysis type should be configurated (as linear and non-linear equations, and other configurations) as to obtain the nodal dislocations. At the post-processing, is where the results, such as heat flux, convergence, and others are obtained.

Simplifying, the software is composed by several programs that allow from the definition and construction of the system in study and its conditions, to its very own fluid dynamic simulation and corresponding results. Some of these programs are, i.e., of geometry construction – *Design Modeler* and *Space Claim* – of Mesh construction – *Meshing* – and fluid dynamic simulation – *Fluent*. For this case, the procedure was the following: *Design Modeler* → *Meshing* → *Setup / Fluent*.

The achievement of the descriptive function regarding the convective heat transfer coefficient rely on the variation of some input parameters, which are relevant to mention. The duct's height can be described as total coil's height. Here the radius, in simulation terms describes the distance between the core's central axis and analysed duct and its variation was subject to an independence test, for attesting its independence relatively to h_c. Note that this last parameter differs from the hydraulic diameter, which is commonly defined as the cross-sectional area of the duct divided by the wetted perimeter (which includes all surfaces acted upon by shear stress from the fluid) [14]. The assumption made for this parameter was equivalent to twice the duct's thickness [14]. The thickness corresponds to the duct's own dimension (duct's diameter) since the study case relies on internal flux analysis. The heat flux, potency/power by area unit, which was defined as uniform and on the duct's lateral walls. Roughness, a characteristic wall parameter, which is non-take in account for Laminar and SST models, while for turbulent models a constant value was defined according to literature. Also, for turbulent models the intensity of turbulence (also known as turbulence level), parameter dependable of the Re number, was defined according to an expected Re value (afterwards explained). The velocity, an absolute value was imposed at the duct's inlet, with gravity's opposite direction. For last, initially the operating density was defined according to the inlet temperature and an outlet maximum expected. As for this type of transformer the maximum limit for the increase of the temperature in the winding is of 100ºC, this translates in a half increase order for the duct. Therefore, a mean value was considerate regarding the 40ºC, inlet temperature, and the 90ºC, maximum temperature rising in the duct. However, afterwards was found that this parameter had an automatic calculation mode in *Fluent*, which was used for independence mesh and radius tests and for the final parametric study. In order to normalize the process of the simulations, the input parameters were parameterized in the program.

Accounting these input parameters, aiming the descriptive functions for convective and friction coefficients, the following inputs combinations were considered.

Table 1. Input parameters.

tk (mm)	H (mm)	Q (W/m^2)	AF v_in (m/s)	AN v_in (m/s)
3	250	50	1	0.05
6	600	200	2	0.10
10	1000	500	3.5	0.20
14	1500	800	6.5	0.30
20	2200	1200		0.43
28		1600		0.57
40		2200		0.77
65		3200		1.10
100				

The first and second columns correspond to the duct's thickness and height, respectively. This match a total of 45 possible geometry designs. For simplicity, hereafter all geometric combinations will be indicated in the form: tk x H (mm).

Note that for natural convection (AN), a linear correlation was made based on the assumptions made for the velocity inlet values for the extreme cases of heat flux. This relation is presented by Figure 9 and corresponding Table 2.

Table 2. Heat flux and corresponding inlet velocities for AN.

Q (W/m^2)	v_in (m/s)
50	0.05
200	0.10
500	0.20
800	0.30
1200	0.43
1600	0.57
2200	0.77
3200	1.1
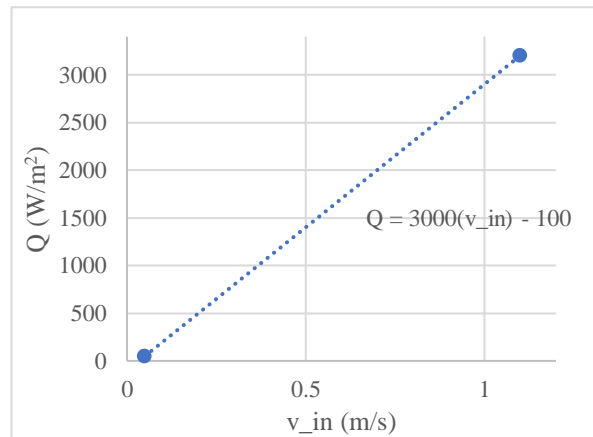
Figure 9. Linear correlation between heat flux and inlet velocity.

Relying on the limit cases assumptions, 0.05 m/s for 3200 W/m^2 and 1.1 m/s for 50 W/m^2, this correlation was defined accordingly. The mentioned assumptions were defined accounting the criteria that for natural convection the velocity value should be lower than for forced convection(AF).

3.3 Geometry – *Design Modeler*

A simple 2D geometry was drawn – rectangle. Concerning an axisymmetric analysis, the geometry was created on the XY plan, where X corresponds to the axisymmetric axe. For simplicity, an edge named selection was done. The inlet zone was defined as "entr", the outlet zone as "said" and walls as "pare_inte" and "pare_exte", where the "pare_inte" refers to the interior wall (located radius distance from the X axe) and "pare_exte" refers to the exterior wall (located radius plus thickness distance from the X axe). Here, the geometry was specified as a fluid body.
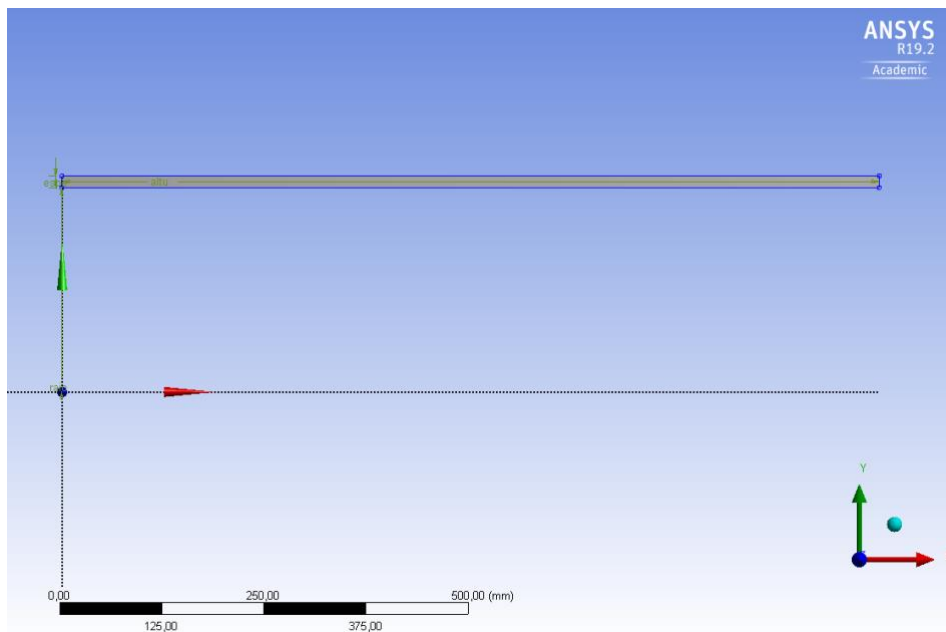
Figure 10. Geometry example for 14x1000 (Design Modeler).

3.4 Mesh – *Meshing*

For the mesh construction the *Edge Sizing* function was used, according to the following parameters:

- Division type: *Number of divisions/ First Element size*
- Progression Option: *Smooth Transition (Growth rate < 1.2) /Bias factor*
- Progression Type: *Circular/Linear*

The *Edge Sizing* function was applied on pairs of existents edges, one edge size function for "entr" and "said" – corresponding to the duct's thickness -, and another for "pare_inte" and "pare_exte" – corresponding to the duct's height. As in this study the wall-nearing analysis is mainly important, a circular growing type mesh was chosen describing smaller elements in this zone and consequently larger elements in the centre zone. Aiming for a more uniform mesh (square elements) the minimum element size of one edge was forced to the other. Recalling the circular progression, this can also be intended as by defining the same *First element size* for each edge, and the middle element for each

edge has approximately the same dimension. A conversion of *First Element size* to *Number of divisions* was made, through a provided routine (*Macros* file), so that the last one was introduced on the *Meshing* program. Concerning *Meshing* tolerance, the *adaptive sizing* function was required and applied, and therefore, the tolerance was set by defining a "*defeatured dimension*", as the minimum element dimension - minimum element size. Also, the function *Face meshing* was enabled with the method *Quadrilaterals*, since in general, for simple geometries it is recommended the quadrilaterals/ hexahedral meshing [32].

Some *Meshing* descriptive tables are shown below, regarding one mesh example – with 107913 Elements.

Table 3. Mesh description example (1).

Model (B3) > Mesh

Object Name	*Mesh*
State	Solved
Display	
Display Style	Use Geometry Setting
Defaults	
Physics Preference	CFD
Solver Preference	Fluent
Element Order	Linear
Element Size	7,9e-004 m
Export Format	Standard
Export Preview Surface Mesh	No
Sizing	
Use Adaptive Sizing	Yes
Resolution	2
Mesh Defeaturing	Yes
Defeature Size	1,29e-004 m
Transition	Slow
Span Angle Center	Fine
Initial Size Seed	Assembly
Bounding Box Diagonal	1,0001 m
Average Surface Area	1,4e-002 m²
Minimum Edge Length	1,4e-002 m
Quality	
Check Mesh Quality	Yes, Errors
Target Skewness	Default (0.900000)
Smoothing	Medium
Mesh Metric	None

Inflation	
Use Automatic Inflation	None
Inflation Option	Smooth Transition
Transition Ratio	0,272
Maximum Layers	2
Growth Rate	1,2
Inflation Algorithm	Pre
View Advanced Options	No
Assembly Meshing	
Method	None
Advanced	
Number of CPUs for Parallel Part Meshing	Program Controlled
Straight Sided Elements	
Number of Retries	Default (0)
Rigid Body Behavior	Dimensionally Reduced
Triangle Surface Mesher	Program Controlled
Topology Checking	Yes
Use Sheet Thickness for Pinch	Yes
Pinch Tolerance	Based on Sheet Thickness
Generate Pinch on Refresh	No
Sheet Loop Removal	No
Statistics	
Nodes	110720
Elements	107913

Table 4. Mesh description example (2).

Model (B3) > Mesh > Mesh Controls

	Edge Sizing	Face Meshing	Edge Sizing 2
Object Name	*Edge Sizing*	*Face Meshing*	*Edge Sizing 2*
State		Fully Defined	
Scope			
Scoping Method		Geometry Selection	
Geometry	2 Edges	1 Face	2 Edges
Definition			
Suppressed		No	
Type	Number of Divisions		Number of Divisions
Number of Divisions	39		2767
Mapped Mesh		Yes	
Method		Quadrilaterals	
Constrain Boundary		No	
Advanced			
Behavior	Hard		Hard
Bias Type	_ ___ _____ ___ _		_ _ ___ _____ _
Bias Option	Smooth Transition		Bias Factor
Bias Growth Rate	1,1		
Specified Sides		No Selection	
Specified Corners		No Selection	
Specified Ends		No Selection	
Bias Factor			5,56
Reverse Bias			1 Edge

3.5 Fluid Dynamic Program Setup – *Fluent*

Double precision was chosen here for better precision. The starting point of this phase is described by selection of the following options:

1. Select solver: ***pressure based*** */ density based;*

2. Select Time option: *Transient /* ***Steady*** → ***Pseudo-Transient;***

3. Select symmetry: *Planar /* ***Axisymmetric*** */ Axisymmetric Swirl;*

4. Enable *Gravity*: **X = -9.81 m/s²**;

5. Enable *Energy;*

6. Select Model: Turbulent (k-Ω; k-ε) / Laminar/ SST;

Note that other models exist, however these were the only ones explored.

Relying on the assumption that each model is the most proper one according to the operating regime, i.e. Laminar model for cases operating under laminar regime conditions and Turbulent models for cases operating under turbulent regime conditions; in order to choose it correctly it is necessary to know the operating regime. Its determination is done by Reynolds number calculation. However, this dimensionless number also depends on the obtained simulations results, such as temperature and velocity, mainly bulk temperature in order to define fluid's properties. Consequently, it is possible to determine the regime mistakenly a priori. Theoretically it is known that density and viscosity (Reynolds variables) depend on temperature, more specifically, it is known that a decrease in temperature causes an increase in Reynolds number. Therefore, it is known that Reynolds takes its maximum value when the temperature is minimum. This allows to determine cases of Reynolds limit / maximum for a minimum value of temperature (inlet temperature). However, the model selection process was not so simple. For the parametric study only one model was elected, in order to easily proceed with correlated data for the descriptive functions of the convective heat transfer and friction coefficients. To select the *Fluent* model (or fluid dynamic model), a group of series of simulations were performed. As to, the conditions were the same as used for the mesh test, however regarding a higher velocity range – capable to englobe all types of possible flow regimes.

3.5.1 Physical and Chemical Fluid Properties - Air

The fluid (Air) properties were defined in *Fluent* program, such as density which was defined regarding the assumption of an incompressible ideal gas, according to equation 12; specific heat and thermal conductivity rely on polynomials, as described in equations 13 and 14, respectively; viscosity which was defined according to *Sutherland's* law, equation 15. Note that, only for 2 files (2 geometry

designs - 80 simulations), for the parametric study, the specific heat was described by piece-wise polynomial with 2 ranges, taking in account the polynomial of equation 13, for temperatures inferior to 1800 K, and a constant mean value of 1.2715×10^3 J/(kg.K) for temperatures values till 3500 K [33].

$$\rho = \frac{p_{op}}{T_{bulk}.R_s} = \frac{p_{op}}{T_{bulk} \times 287.058} \tag{12}$$

In equation 12, density (ρ) is determined directly by the operating pressure (p_{op}) and depending on bulk's temperature (T_{bulk}) and specific air constant (R_s).

$$\begin{aligned} C_p = & -6.80369080045432 \times 10^{-17}.T_{bulk}{}^6 \\ & + 3.70906105579783 \times 10^{-13}.T_{bulk}{}^5 \\ & - 6.44284823514227 \times 10^{-10}.T_{bulk}{}^4 \\ & + 1.77862056023893 \times 10^{-7}.T_{bulk}{}^3 \\ & + 5.17216815148547 \times 10^{-4}.T_{bulk}{}^2 \\ & - 0.242210250039702.T_{bulk} + 1029.83191000858 \end{aligned} \tag{13}$$

$$k = -1.3707 \times 10^{-8}.T_{bulk}{}^2 + 0.07616 \times 10^{-3}.T_{bulk} + 4.5968 \times 10^{-3} \tag{14}$$

$$\mu = \frac{1.458.T^{1/5}}{T+110.4} \times 10^{-6} \tag{15}$$

3.5.2 Boundary Conditions and Solution Methods

The boundary conditions assumptions were the followed, according to its inputs:

Table 5. Boundary conditions for Fluent program.

	Inlet	Outlet	Wall
Boundary condition	Velocity inlet	Pressure outlet	Wall
Input	Temperature (40 °C) [10] Velocity	Static Pressure (atmospheric)	Uniform Heat Flux

Inlet-outlet motion is described by a guiding force. This guiding force must be implicit in these conditions. In this case the ΔP, between the inlet and outlet's duct, stands for the guiding force. Note that this ΔP is caused by the temperature gradient between the fluid and the duct's wall – the temperature rising results in a fluid's density decrease, which disturbs its corresponding velocity,

directly affecting pressure loss (ΔP) along the duct. These boundary conditions can be illustrated by Figure 11.
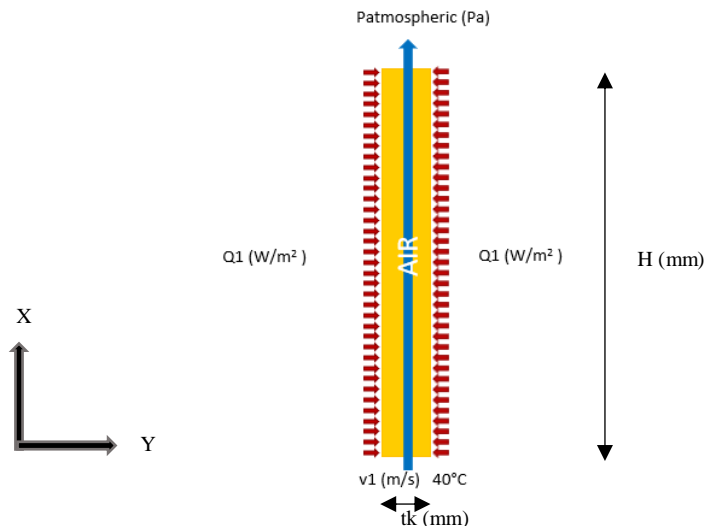
Figure 11. Illustration of Boundary conditions.

Solution Methods

Here is where the solution calculation method is chosen. The concerning parameters associated with the solution method are illustrated in Figure 12 [24].
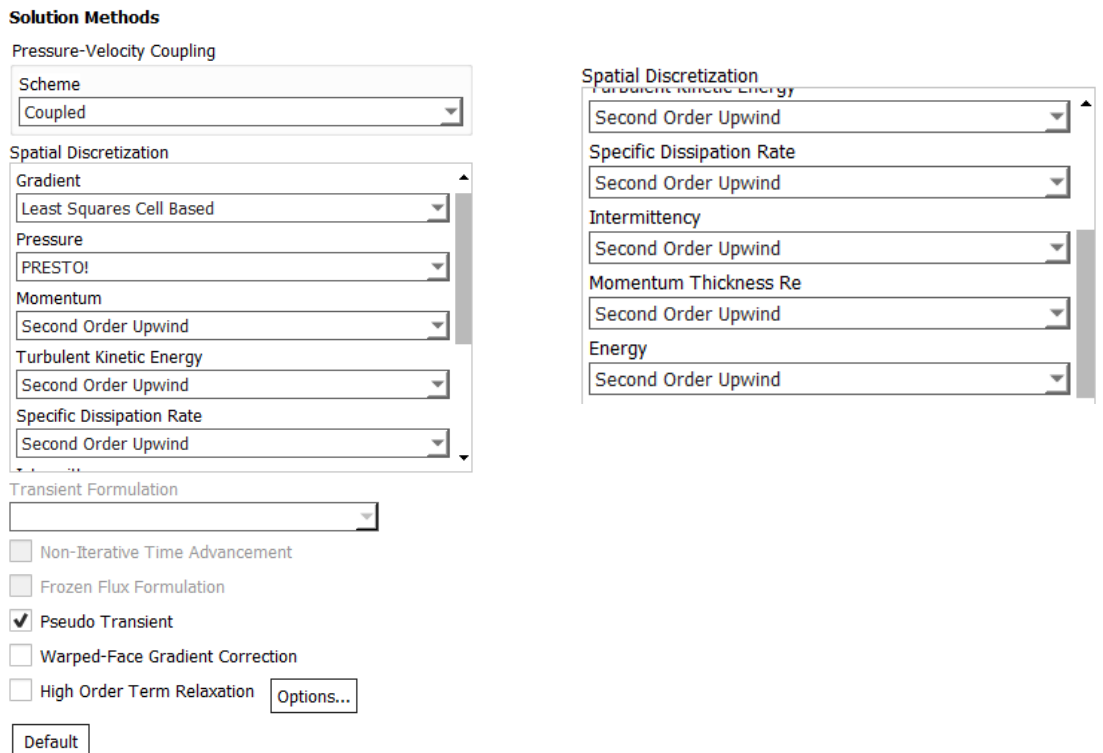
Figure 12. Solution methods - selected options.

Note that all parameters were obtained by second order discretization of the respective equations, i.e. Energy was determined using its second order equation. Also, the time mode option selected was pseudo transient, considering the theoretical knowledge that convection currents are dynamic (non-stationary).

3.5.3 Definition of the Output Parameters

The output parameters were defined accordingly to the study purpose. Therefore, wall temperatures and outlet temperature were the key results for the convective heat transfer coefficient determination. Concerning friction coefficient, inlet and outlet pressures and velocities were the main results. Almost every output was defined as "*Area-Weighted average*" – meaning it was computed by dividing the summation of the product of the selected field variable and facet area by the total area of the surface -, except for the outlet temperature which was defined as "*Mass-Weighted average*" – meaning it was computed by dividing the summation of the product of the selected field variable and the absolute value of the dot product of the facet area and momentum vectors by the summation of the absolute value of the dot product of the facet area and momentum vectors (surface mass flux) [34].

Other output parameters were created to improve the analysis of the simulations, such as, minimum and maximum temperature, velocity and pressure at the inlet and outlet, mean velocity at the inlet, dynamic, static and total pressures at the inlet and outlet. For minimum and maximum results, the respective report was *surface* type, and "*Facet minimum/maximum*".

3.6 Practical Approach – CFD Testing Procedure

3.6.1 Independence Mesh Test

It is noteworthy that an initial sensibility/independence mesh test was performed, in order to improve its adequacy and define the minimum setup – approved mesh by the independence tests, regarding the minimum number of elements in order to economize the simulations time, decreasing it. As this test involves comparing different mesh sizes, a base case was considered. So, in order to obtain an, approximately, hundred thousand element mesh (M1), with a 5.56 *bias factor,* a *First element size* mesh of 0.136 mm was fixated. As strategy, according to the referred mesh, two other correlated situations were considered. Primary M0, a minor size (number of elements) mesh, with a *First element* size corresponding to three times the base case. Secondly M2, a larger size mesh was considered, with a *First element* size, in this case being a third of the initial case. To summarize: Set *bias factor* and vary *First element* size in the ratio of 3. The compared mesh's are presented in Table 6.

Table 6. Mesh's features.

	N.divisions A	N.divisions B	min size	Bias factor (B)	First Element size	N.Elements
M0	21	923	0.40617	5.56	0.408	19383
M1	39	2767	0.1290	5.56	0.136	107913
M2	59	8365	0.0447	5.56	0.045	493535

In this Table 'N.divisions' corresponds to the number of divisions made in each dimension, 'A' and 'B'. 'A' stand for the duct's tk, while 'B' for the duct's H. Note that the minimum and maximum element size corresponds to the minor division/dimension – A. Resuming the comparison will be between a coarse mesh M0 with size of 19383 elements, an intermedia mesh M1 with size of 107913 elements, and a fine mesh M2 with size of 493535 elements. However, note that the mesh refinement level matters given the boundary layer treatment importance. Recall, that some CFD *Fluent* models, specific turbulence models, already have wall functions incorporated. These wall functions allow the near wall interpretation behaviour discarding the highly needing for a very refined mesh. Nevertheless, this study was performed in order to not depend on those conditions. A section of these meshes are presented by Figures 13, 14 and 15.
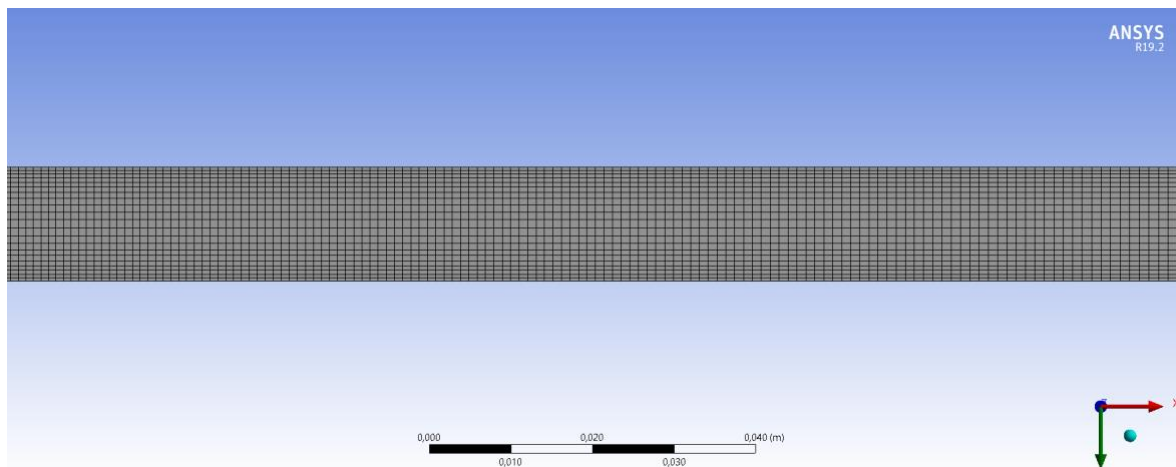
Figure 13. Mesh M0 with 19383 elements.
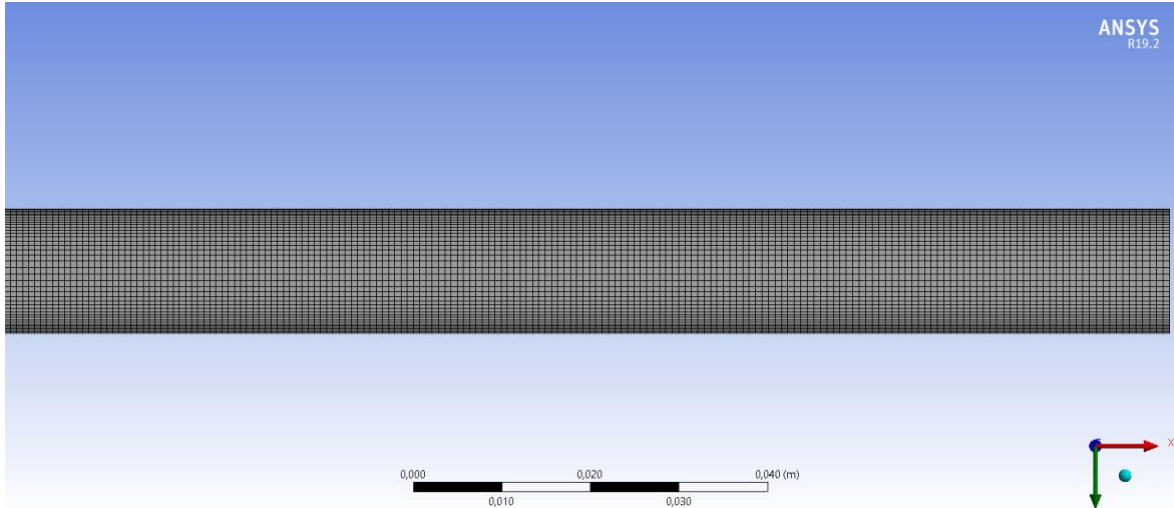
Figure 14. Mesh M1 with 107913 elements.
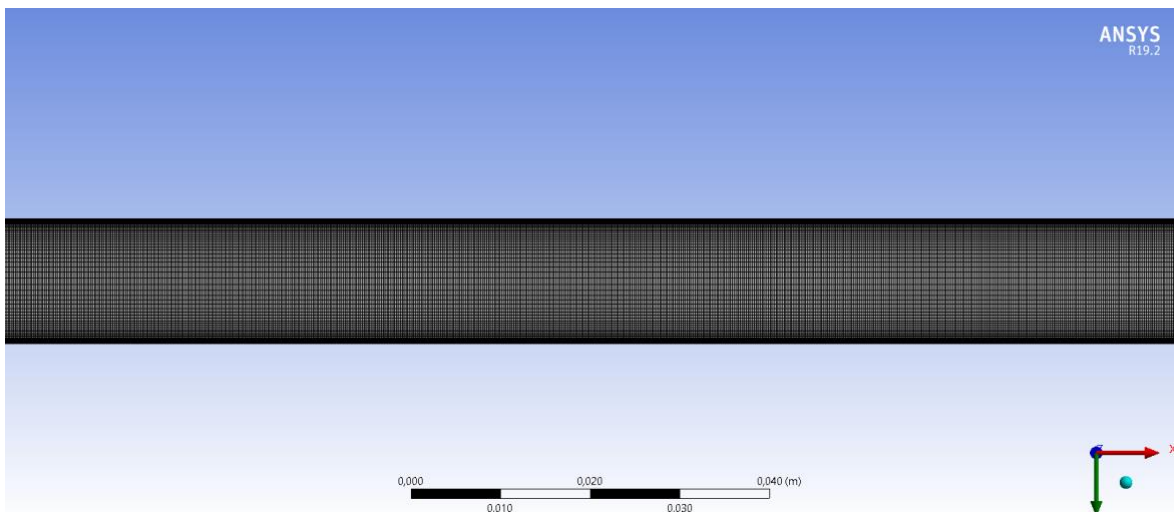
Figure 15. Mesh M2 with 493535 elements.

At this point the fluid dynamic model has not yet been chosen and so, the mesh tests were done for the following considerable models: Laminar, Realizable k-epsilon, k-omega and Transition SST (from now on only referred as SST). The input difference between the models is that for turbulence models a roughness coefficient (1.5×10^{-5} m) and a turbulence intensity value was considered. This last parameter was determined according to equation 16 and considering an inlet Re value (determined with inlet velocity and temperature).

$$int\_turb = 0.16.Re^{-\frac{1}{8}} \tag{16}$$

The independence test was performed taking in account the percentage deviations of the main output variables – outlet's and wall's temperature, pressure drop (between the ins and outlet section) and

outlet velocity. The selection of the most suitable mesh would be based on these results, regarding the deviations between each mesh outputs and accounting for the computational effort.

3.6.2 Fluid Dynamic Model Selection Tests

In order to select the *Fluent* flow model a comparative study was performed. As to, several simulations were performed, as to graphically represent the results to better observe and analyse. The comparing models were Laminar, Realizable k-epsilon, k-omega and SST. For better assessment, it was required to obtain results across all possible regimes - Laminar, Transient and Turbulent. Therefore, 5 different inlet velocities (one more besides the already mentioned) and 2 different wall heat fluxes were simulated for all the 4 models, giving a total of 40 simulations. The considered geometry for these tests was 14x1000. Besides a comparative graphic analysis, a literature's model was considered – Morelli et al. [15]. Given that in the referred model, SST was the fluid dynamic used model, an approximate comparison was possible. As to, the same geometry dimensions and literary referred inputs were applied to the previously SST model. For low velocities the Laminar model was also tested for comparison. This test, if with identical results, would allow to give some credibility to the performed CFD simulations. Note that given the different geometry design an adaptation of the used mesh was performed, again by trying to approximate the minimum element size to the base case mesh. This adaptation is presented by Table 7. Although it isn't mentioned in literature, for this test Re number was determined given the outlet velocity and the fluid properties were calculated accounting for bulk temperature (mean temperature between wall and fluid temperatures).

Table 7. Mesh adaptation for Morelli et al. [15] model.

Mesh	N.divisions A	N.divisions B	min size	Bias factor (B)	N.Elements
M1	39	2767	0.129	5.56	107913
M$_{Morelli}$	45	4153	0.132	5.56	186885

3.6.3 Independence Radius Test

An independence radius test was performed, aiming to reduce the variables number for the parametric study. The expected would be the confirmed independence, once this parameter does not affect the distance between the located two relevant temperatures (wall and fluid centre temperatures) neither the uniform heat flux applied on both duct's walls.

The test was performed for two different geometries, 14x250 and 14x2200, for a heat flux of 200 and 2200 W/m^2. The tested radius values were of 100, 250 and 600 mm for an inlet velocity of 1 m/s.

This test was already performed for the selected *Fluent* flow model – SST. Identically for this test, it was registered the percentage deviations of the main output variables. Once this test was performed concerning different geometries, another mesh adaptation was necessary. Once more, the minimum element size was fixated. The adapted mesh's are presented in Table 8.

Table 8. Mesh adaptation for different geometry designs for independence radius test.

Geometry	N.divisions A	N.divisions B	min size	Bias factor (B)	N.Elements
14x250	39	693	0.129	5.56	27027
14x1000	39	2767	0.129	5.56	107913
14x2200	39	6088	0.129	5.56	237432

3.6.4 Preview Simulation Test

A preview test simulation was performed in order to pre-evaluate the temperature's profiles, more specifically both wall temperatures and theirs corresponding adjacent temperatures, so as the fluid temperature at the centre of the duct. Theoretical, the expected temperature's profiles should have higher temperatures wall-nearing and minimum temperature at the duct's centre described by a non-linear decay.

The specifications for this test were of an 800 W/m^2 heat flux, inlet velocity of 1 m/s for a geometry of 14x1000. The results were obtained for, the same, previously referred *Fluent* options and exported to an excel file. Besides the main outputs, the following temperatures, along the duct's position (H), were reported: wall temperatures, adjacent wall temperatures and fluid centre temperature. Then the temperature gradient was calculated in order to make possible the h_c calculation. Note that here this calculation was locally performed with the fluid temperature at the centre of the duct and wall temperatures.

3.7 Parametric Study

Finished all the mentioned tests, it is possible to initiate the parametric study. As to, all the previously referred geometry designs were considered, and so 44 mesh adaptations were required. Again, the *First element size* was fixated, as 0.136 mm, while for tk division (A) the *Smooth growth* rate of 1.1 was used, whereas *bias factor* of 5.56 for the H division (B). The adapted mesh's features are presented in Table 9, and its respective number of elements in Table 10.

Table 9. Mesh's features for all design geometries.

tk (mm)	N.divisions A	min size	max size	H (mm)	N.divisions B
3	16	0.131	0.256	250	693
6	25	0.130	0.410	600	1660
10	33	0.130	0.601	1000	2767
14	39	0.129	0.790	1500	4153
20	45	0.132	1.079	2200	6088
28	51	0.134	1.462		
40	58	0.134	1.941		
65	68	0.132	3.075		
100	77	0.130	4.886		

Table 10. Parametric study's Mesh sizes

H mm \ tk mm	3	6	10	14	20	28	40	65	100
250	11088	17325	22869	27027	31185	35343	40194	47124	53361
600	26560	41500	54780	64740	74700	84660	96280	112880	127820
1000	44272	69175	91311	107913	124515	141117	160486	188156	213059
1500	66448	103825	137049	161967	186885	211803	240874	282404	319781
2200	97408	152200	200904	237432	273960	310488	353104	413984	468776

For the formerly mentioned CFD, or *Fluent* program conditions and selected model, 45 files were created. Each file corresponding to one geometry design. To each file, the referred parameters were added, which corresponds to 40 simulations, 8 of AN and 32 of AF. This represents a total of 1800 simulations for the parametric study. A residual monitorization was performed for all simulations. It was established a 1×10^{-9} convergence criterion for the Energy equation and 1×10^{-6} for all remaining ones. A minimum residual's decrease by three orders of magnitude indicates at least qualitative convergence [24].

The results were exported from *Fluent* through *.csv* files. Those were read and printed to *Excel* thought *VBA* (*Macros* file). Also, this program automatically calculated the remaining output parameters, such as bulk temperature, pressure gradient, fluid properties at bulk temperature (equations 12 to 15), dimensionless numbers (equations 8 to 11) and both friction (equation 4) and convective (equation 1) coefficients. Note, anew, that for the mentioned equations, the characteristic dimension corresponds to the hydraulic diameter – 2 times the duct's thickness.

In order to proceed with the mathematical modelling, first an analysis concerning all results was made. This analysis simply consisted on evaluate the simulation's outputs, according to some criteria, in order to accept their validation. The used criteria rely on the theoretical knowledge that by increasing the duct's thickness, for the same conditions of heat flux, velocity inlet and height, the temperature should decrease. This wasn't only applied for bulk temperature but also concerning for the minimum and maximum outlet temperature, once these last ones are local results (point determined) which provides higher numerical error level. So, the simulations cases which are not in agreement with this concept were point out. To better observe and analyse this concept, a comparative example was performed regarding the wall temperature, pressure drop and respective coefficients (h_c and f) outputs for different duct's thickness, maintaining all other input variables constants. Once determination of convective coefficient lies on the assumption of fully developed profile, the longitudinal entrance correspondent was determined for all cases. This calculation was performed given that longitudinal entrance region corresponds to ten times the hydraulic diameter [14]. Another comparison was performed, for a specific design and heat flux characteristics, with the presented literature equation (equation 11 [16] in SI units) to determine convective heat transfer coefficient.

3.8 Mathematical Modelling

Aiming for the descriptive function for the referred coefficients, the dependent variables considered was duct's height and thickness, the uniform wall's heat flux and air's mean velocity (bulk velocity). Part of this work purpose was that these descriptive functions only depend on the mentioned variables in their raw form. In order to improve fitting accuracy, a normalization of these variables was performed. Some of the normalization methods were considered, such as *zscore*, *norm*, *scale*, *range* and *center*. The first one (*zscore*) consists on centring and scale each variable data to have a zero mean and standard deviation of 1. The second one (*norm*), normalize by positive numeric scalar. The third (*scale*), consists on scaling each variable data by the respective standard deviation, median absolute deviation, first element or by numeric data value. The fourth one (*range*), normalize each variable data between 0 and 1. The fifth one (*center*), consists on centre each variable data so its centre has mean or median of 0 [35].

The selected normalization method was similar to *range* method, by respective variable data maximum. This, in a practical approach means that every thickness, height, heat flux and velocity data will be normalized by its corresponding maximum value, this can be translated by the followed presented MATLAB's command – equation 17.

$$tk_n = tk()./\max(tk) \tag{17}$$

Initially a nonlinear fitting was tried through a MATLAB's function termed *lsqcurvefit*. This function solves nonlinear curve-fitting (data fitting) in least-squares sense [36].

The concept lies on finding the local minimums of a model function (user-defined), that minimizes the error (mean square error) returning a coefficient's vector. So, the user's inputs are the input and output data, a model function and an initial coefficient's vector. In order to provide some sort of a feasible initial coefficient's vector, MATLAB's *cftool* was resorted. The fitting coefficients obtained, regarding each isolated variable data fitting with the provided output coefficient, were the ones introduced at the initial vector. Several tests were performed:

- Relating all data and by testing several model function's combinations, i.e. considering power, exponential, polynomial and logarithmic form.
- Dividing the data into ranges by meaningful dimensionless numbers, i.e. by means of Re according to the operating flow regime; Gr and Ri (Richardson number – combination of Gr and Re numbers) once these are representative numbers of convection phenomenon – natural, forced or combined.
- Considering scientifically recognized normalized dimensions, i.e. x1, x2 and x3 following presented.

$$x1 = \frac{H}{2 \times tk \times Re \times Pr} \; ; \; x2 = \frac{H}{2 \times tk \times Re} \; ; \; x3 = \frac{H}{2 \times tk}$$

Note that besides relative errors, a large amount of statistic data was withdrawn for all tests, such as relative and absolute standard deviation, correlation coefficients (between errors and the input variables – *corrcoef*(x) in MATLAB), skewness, kurtosis number, and even its corresponding plots. However, the obtained relative errors confirmed the lacking accuracy of the model. So, a least conventional method was considered – ANN (Artificial Neural Network). Acknowledge that this method can have higher performance even when with dispersed or noised data.

The neural network construction, through MATLAB's *nftool*, stands for the definition of the neuron/nodes number followed by a testing procedure defined as training, testing and validation of the neural network. Concerning the number of nodes there's several thumb rules, although they're not very scientifically recognized, such as; this number should be comprised between the input and output size, i.e. (number of output's variables) $1 < N_{nodes} < 4$ (number of input variables); or correspond to 2/3 times the input size plus the output size, i.e. equals to 4 times 2/3 and plus 1 resulting in a number of 4 nodes; and this number of nodes should by lesser than 2 times the input size, i.e. 2 times 4 equals to a number of 8 nodes [30]. Given these thumb rules, the considered number of nodes was from 3 to 8. This definition step is of great importance given it could prevent

for a possible network problem, known as under or overfitting. This stands for the concept that node's number should be minimum, still able to provide a sufficiently accuracy prediction, in order that the correspondent network does not became a "memory bank". This equal saying that this overfitting condition provides perfect prediction for the data which it was used as training, but very poor for intermediate data (not contained in training process) [30]. The neural network learning/training procedure, through which weights and biases are defined, is performed by a second order optimization algorithm – *Levenberg-Marquart*. This algorithm determines the mentioned parameters by several iterations, given the provided input and output (target) data and by minimizing the mean square error (between the output and target). The data was divided, randomly (program's default option), in 70% for training tests and for testing and validation tests 15% each. The network evaluation was performed in two steps. First, through observation of the corresponding regressions obtained from each test (training, testing and validation). Secondly, by testing the obtained network providing all data and representing a correspondent histogram, regarding the relative percental errors (between simulation's results and the network's predictions – explained by equation 18).

$$relative\ error = \frac{output_{CFD} - output_{NET}}{output_{CFD}} \tag{18}$$

The initial obtained results showed poor accuracy, however accounting for the vast range of convective heat transfer coefficient an alternative fitting sort thought. If we consider only the dry-transformer operating domain (given the fluid – air's convective properties and the limited operating temperature) this corresponds only to convective coefficients lower than 20 W/m^2.K. The neural networks, for predicting the pretended coefficients, according to this condition ($h_c < 20$ W/m^2.K) were sort through and the correspondent relative errors were again represented by respective histograms.

Concluding, a final comparison between the obtained results through CFD, literature model (Morelli et al. [15] model – as it represents the most fitted model for this study) and predicted by neural network's was performed.

4. Results and Discussion

Starting with mesh's analysis, the used geometry for this study was 14x1000 and the supported conditions were the following: a heat flux of 500 W/m^2 and 2200 W/m^2, velocities inlet of 2 m/s and 6.5 m/s and a 250 mm radius. The results of the percentage deviations of the main output variables (mean external wall and outlet temperature, pressure loss and mean outlet velocity) between the considered meshes, for Laminar, k-epsilon, k-omega and SST models are following presented. Note that all the compared meshes are orthogonal well structured, as explained in the previously chapter.

Table 11. Mesh's comparison for Laminar model.

		% Deviation			
Q (W/m^2)	Compared Mesh's	T_exte_wall (K)	ΔP (Pa)	T_out (K)	v_out (m/s)
500	M0 and M1	8.48E-03	1.87E+01	4.35E-05	8.95E-04
2200		3.39E-02	1.46E+01	6.55E-04	3.34E-03
500	M1 and M2	2.34E-03	6.25E-01	2.90E-05	2.68E-04
2200		9.01E-03	5.31E-01	1.98E-04	1.05E-03

Table 12. Mesh's comparison for Realizable k-epsilon model.

			% Deviation			
	Q(W/m^2)	Compared Mesh's	T_exte_wall (K)	ΔP (Pa)	T_out (K)	v_out (m/s)
Re > 1000	500	M0 and M1	6.13E-01	2.43E+01	2.48E-05	2.58E-04
	2200		2.06E+00	2.09E+01	3.43E-04	1.38E-03
	500	M1 and M2	5.21E-02	3.26E+00	9.29E-06	1.06E-04
	2200		9.73E-02	1.69E+00	5.62E-05	3.91E-04
Re < 1000	500	M0 and M1	7.37E-02	4.20E+00	6.38E-05	8.04E-04
	2200		1.71E-01	4.31E-01	4.15E-04	3.15E-03
	500	M1 and M2	1.16E-01	3.47E+00	6.67E-05	3.27E-04
	2200		3.88E-01	3.65E+00	1.91E-04	1.11E-03

Table 13.Mesh's comparison for k-omega model.

	Q(W/m²)	Compared Mesh's	% Deviation			
			T_exte_wall (K)	ΔP (Pa)	T_out (K)	v_out (m/s)
Re > 1000	500	M0 and M1	6.79E-01	1.14E+01	3.10E-06	2.37E-04
	2200		2.40E+00	1.09E+01	2.16E-04	8.52E-04
	500	M1 and M2	1.23E-02	7.67E-02	6.19E-06	1.10E-04
	2200		1.14E-02	3.22E-01	6.47E-05	4.09E-04
Re < 1000	500	M0 and M1	1.25E-02	8.88E-01	5.80E-05	8.36E-04
	2200		3.13E-01	1.52E+00	1.32E-03	4.16E-03
	500	M1 and M2	1.29E-02	6.26E-01	4.35E-05	3.13E-04
	2200		3.49E-02	4.94E-01	6.01E-04	1.55E-03

Table 14.Mesh's comparison for SST model.

	Q(W/m²)	Compared Mesh's	% Deviation			
			T_exte_wall (K)	ΔP (Pa)	T_out (K)	v_out (m/s)
Re > 1000	500	M0 and M1	3.86E-02	7.87E-01	1.22E-04	9.68E-04
	2200		9.21E-02	8.66E-01	2.31E-04	2.71E-03
	500	M1 and M2	2.95E-03	5.95E-01	2.61E-05	2.86E-04
	2200		8.37E-03	4.04E-01	1.55E-04	9.38E-04
Re < 1000	500	M0 and M1	1.34E+00	2.62E+01	6.19E-06	1.85E-04
	2200		4.11E+00	1.63E+01	9.19E-04	1.37E-04
	500	M1 and M2	2.19E-02	3.68E-01	9.29E-06	1.22E-04
	2200		5.13E-01	2.27E+00	4.47E-04	8.17E-04

It is observed that most of the percental deviations are lower between M1 and M2. Once the deviation between M1 and M2 are lower than 5% and that for M1 the computational effort is much lower (less time per simulation) we can assume the mesh independence and that M1's mesh is sufficient as the minimum setup to represent. Consequently, this combination was the base case for other mesh's construction for the parametric study.

Regarding the comparative study for the fluid dynamic model selection, the same geometry of 14x1000 was used for this test, based on a 107913-size mesh (M1). The results are presented by the following Figures 16, 17, 18 and 19 and corresponding Tables 15 and 16. Note that Laminar range corresponds to a Re inferior to 2600, while for Turbulent Re is greater than 10000 (these intervals were represented by the followed vertical black lines). Also, this dimensionless number was

determined according to the outlet velocity result for each simulation. Table 15 and 16 are sorted by Re number for all models.

Table 15. Results for a 500 W/m² wall heat flux.

Model	T_exte_wall (°C)	ΔP (Pa)	Re	v_in (m/s)
Laminar	122.1	2.17	1.38E+03	1.0
k-omega	122.1	2.17	1.38E+03	6.5
SST	119.7	2.20	1.39E+03	1.0
k-epsilon	115.1	2.26	1.40E+03	10
k-epsilon	95.23	3.53	1.47E+03	0.5
Laminar	103.1	4.39	2.85E+03	2.0
k-omega	103.1	4.39	2.85E+03	10
SST	99.02	4.51	2.88E+03	2.0
k-omega	85.08	5.42	2.98E+03	0.5
k-epsilon	72.14	2.20	3.08E+03	1.0
Laminar	90.90	8.48	5.10E+03	3.5
SST	81.82	9.03	5.22E+03	3.5
k-omega	69.40	12.3	5.39E+03	1.0
k-epsilon	60.86	21.3	5.51E+03	2.0
Laminar	79.62	18.7	9.71E+03	6.5
SST	60.22	29.2	1.02E+04	6.5
k-omega	58.07	32.9	1.03E+04	2.0
k-epsilon	53.09	54.0	1.04E+04	3.5
Laminar	73.04	33.1	1.52E+04	10
SST	53.17	65.4	1.60E+04	10
k-omega	52.68	68.0	1.60E+04	3.5
k-epsilon	49.62	102.4	1.61E+04	6.5

Figure 16. Graphic representation of T_exte_wall output in order to Re number, for a 500 W/m² wall heat flux, for all considered models.

Starting, as expected, for all models a Re increasing decodes into a wall temperature decreasing. Likewise, for low Re's it is easily perceptible the obtained high wall temperatures. Analysing Figure 16, it's noticeable, for a laminar regime, that SST and Laminar models are approximately identical, obtaining roughly similar wall temperature results. Along the increase of the regime's turbulence there is an intensification of the deviation between these two models, more perceptive for higher Re numbers. However, note that while the mentioned deviation increases, it decreases the one related to the turbulence models (k-epsilon and k-omega). As expected, the k-epsilon model gives the most deviated results, once this model performs poorly for wall-bounded boundary layer, contrarily to the k-omega model.

Figure 17. Graphic representation of ΔP output in order to Re number, for a 500 W/m² wall heat flux, for all considered models.

Before analysing Figure 17, it is important to acknowledge that wall temperature is directly related with the pressure loss, i.e. by increasing wall temperature, through heat transfer, it will affect the fluid density, decreasing it and consequently resulting in a pressure decrease. So, also as theoretical expected, Figure 17 corroborates the notion that a wall temperature rising results on a pressure loss decreasing.

Concerning the global pressure loss (between the duct's inlet and outlet), at Figure 17 the similarity now exists between the SST and k-omega model along all regimes range. The Laminar and k-epsilon model's deviation substantially increases entering the turbulent regime. Again, as pressure loss is related to the wall temperature result, the poorly performance of the k-epsilon model in near-wall treatment is likewise stated, i.e. inflex point in transition zone between laminar and transient regime.

Table 16. Results for a 2200 W/m² wall heat flux.

Model	T_exte_wall (°C)	ΔP (Pa)	Re	v_in (m/s)
Laminar	353.5	4.21	1.00E+03	1.0
SST	287.8	4.2	1.01E+03	1.0
k-omega	246.0	4.2	1.01E+03	1.0
k-epsilon	204.9	5.52	1.12E+03	1.0
Laminar	179.5	7.36	2.09E+03	2.0
SST	347.7	7.39	2.13E+03	2.0
k-omega	275.6	7.69	2.24E+03	2.0
k-epsilon	226.9	2.88	2.54E+03	2.0
Laminar	140.0	12.7	3.79E+03	3.5
SST	100.8	12.9	3.93E+03	3.5
k-omega	278.2	15.1	4.35E+03	3.5
k-epsilon	181.7	25.1	4.76E+03	3.5
Laminar	181.7	25.4	7.44E+03	6.5
SST	98.0	30.7	8.55E+03	6.5
k-omega	82.4	36.6	8.89E+03	6.5
k-epsilon	350.10	60.1	9.42E+03	6.5
Laminar	246.3	42.8	1.19E+04	10
SST	175.2	68.6	1.43E+04	10
k-omega	122.8	72.3	1.44E+04	10
k-epsilon	98.02	111.1	1.50E+04	10
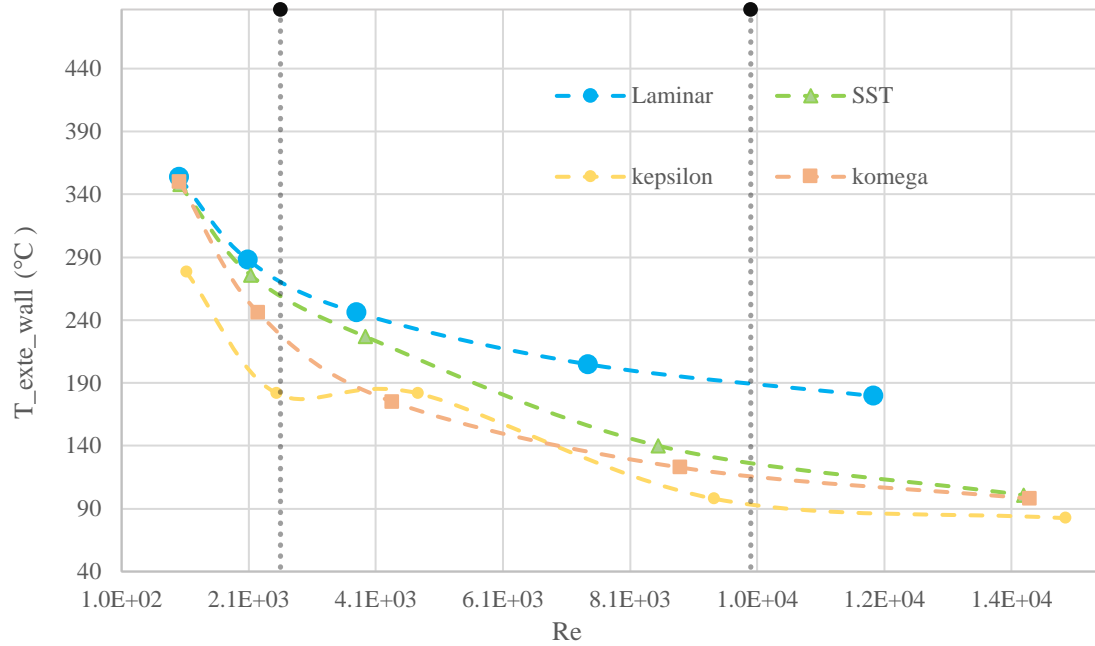
Figure 18. Graphic representation of T_exte_wall output in order to Re number, for a 2200 W/m² wall heat flux, for all considered models.

The analysis here is identical to the one made for Figure 16. However, in this case note the existence of an inflex point in k-epsilon model curve. Once more, this fact questions the accuracy of this model for this study case, concerning the same previously mentioned reasons.
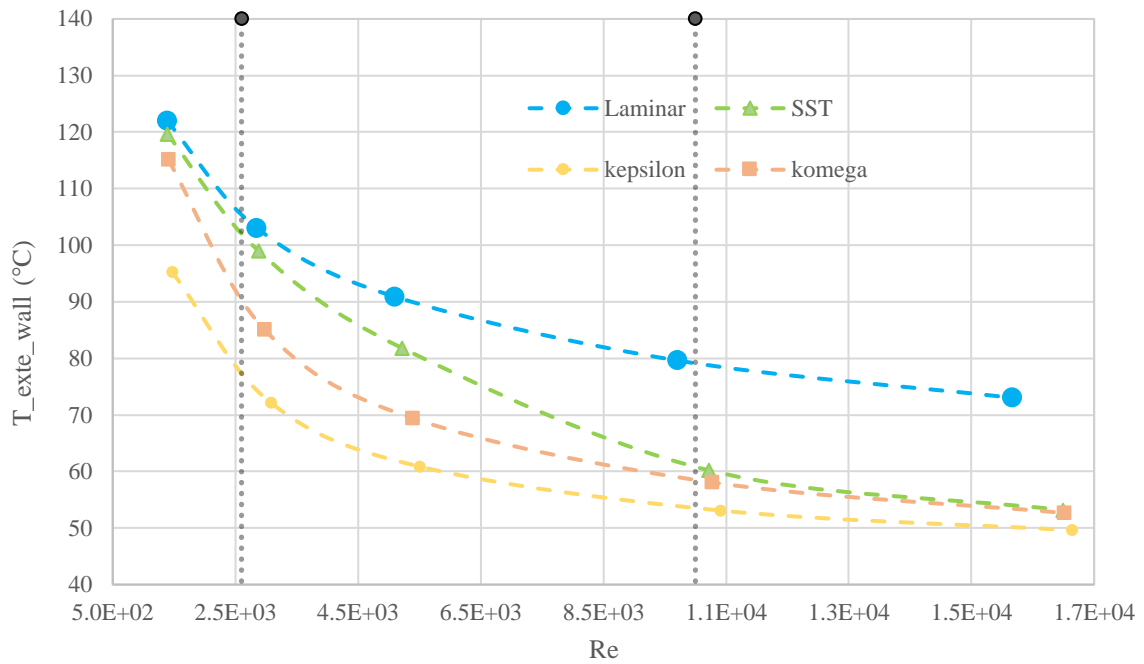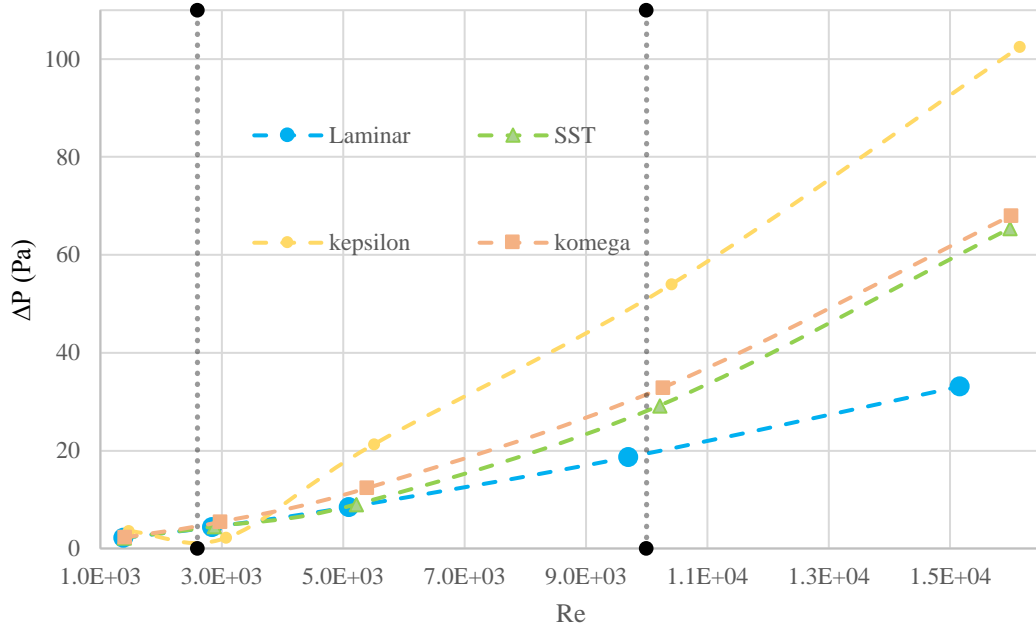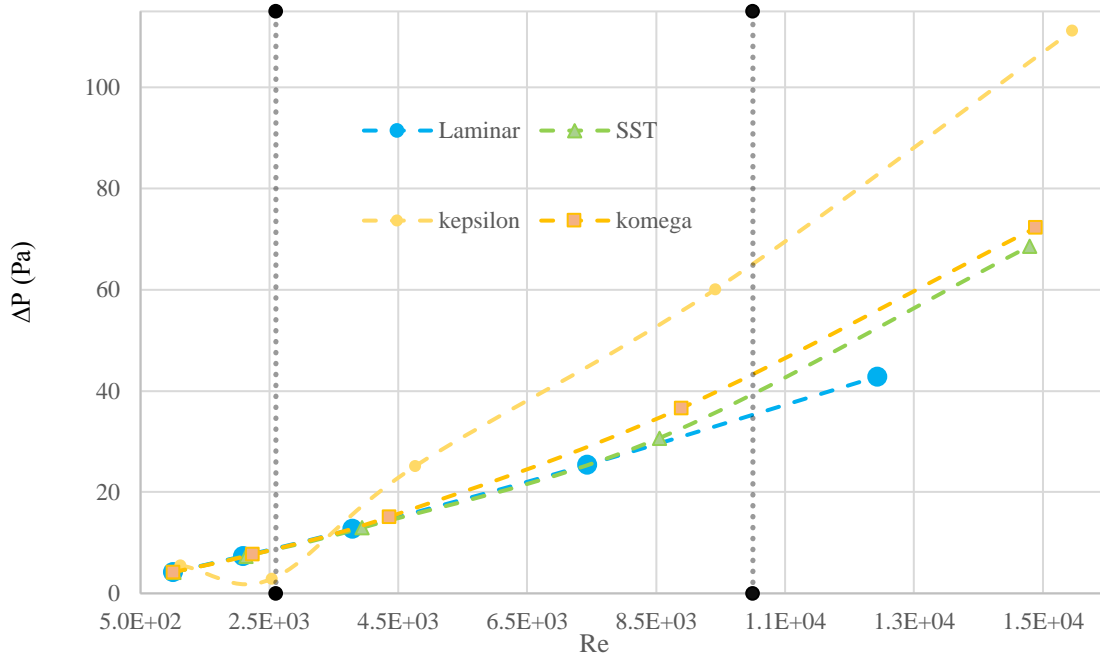
Figure 19. Graphic representation of ΔP output in order to Re number, for a 2200 W/m² wall heat flux, for all considered models.

Comparing both wall temperature representations, for 500 and 2200 W/m², the difference stands for the increasing of wall temperatures given the increasing wall heat flux. As already mentioned, the same goes for the pressure loss representation.

For the literature CFD comparison (Morelli et al.[15]) test, the features specified in the article, were a thickness of 20 mm, a height of 1500 mm, a diameter of 320 mm, and a wall heat flux of 199 W/m² for the exterior wall, and 177 W/m² for the inner wall. For velocities of 0.5 m/s and 1m/s the Laminar model was also presented below. For the adapted mesh ($M_{Morelli}$) the following results were presented in Table 17.

Table 17. Simulation Results for Morelli's conditions.

	radius	tk	H	v_in	T_exte_wall	ΔT	v_out	T_out	ΔP	Re
	mm	mm	mm	m/s	K	°C	m/s	K	**Pa**	
SST	160	20	1500	0.5	359.24	**46.09**	0.576	360.54	**0.898**	1.07E+03
	160	20	1500	1	346.22	**33.07**	1.076	336.87	**1.77**	2.18E+03
	160	20	1500	2	337.54	**24.39**	2.076	325.02	**3.90**	4.44E+03
	160	20	1500	5	325.05	**11.90**	5.076	317.90	**15.4**	1.15E+04
Laminar	160	20	1500	0.5	359.58	**46.43**	0.576	360.54	**0.899**	1.07E+03
	160	20	1500	1	347.08	**33.93**	1.076	336.87	**1.75**	2.18E+03

The compared output parameters were ΔT (between inlet and wall temperatures) and ΔP (between inlet and outlet pressures), accounting for Re number. These values were compared with the ones presented by Morelli et al [15].

The obtained results are approximate to the previously mentioned, presenting deviations only for low Re values. One explanation for its deviations is that they may derivate from the Re calculation mode, for instances, as it is not mentioned, i.e. Re can be determined using a mean or input velocity. As the main deviation was figured for extreme regime situations, more specific for very low Re, some simulations were performed for Laminar model. However, as shown by the obtained results, the difference, between the SST results, was minor. Another justification might be that the respective boundary conditions were not specified by Morelli et al.[15] , this possible difference should affect the obtain results.

The selected model was SST. This choice was made given its similarity to the Laminar model, within the laminar regime domain and analogously observation within the turbulent model, similarity to the turbulent model k-omega. Regarding the inexistent experimental results, note that there's no scientific incontestable justification for this selection once, for instances, the same model would be used for all parametric study, disregarding for the operating regime (as it depends on the output temperature's results as already mentioned). If it was possible, another choice would be the usage of each different model, according to its operating regime. However, this may outcome as a problem, if the mathematic modelling weren't done by ranges, divided by the existing regimes. Every model has high complexity and are composed by several normal and complex parameters, which its management requires some background understanding. Therefore, given this last statement, the Laminar model would be the simpler one to use, once it involves fewer and less complex parameters (fewer number of parameters and corresponding complexity). Then again, recalling the Figures 16, 17, 18 and 19 shown for model comparison, for turbulent regime this model shows a high deviation from other models, though it can't be assertively considered as the wrong model. Although, one of the tested models can be completely disregard, k-epsilon model. Given its stated behave, inflexion curve zones corresponding to a non-conformity with theoretical knowledge. Specifying, theoretically an inlet velocity rising corresponds to a mass flow increasing which should promote the heat transfer between wall and fluid, translated by a wall temperature decreasing. Also, recall that a wall temperature decrease causes a pressure rising (by increasing the fluid's density), another k-epsilon model non-conformity. So, in order to at least have one approximately eligible comparison model (Morelli et al. [15]) for final results, the SST model was used.

For the radius independence test, the resulted percentage deviations are presented in Table 18.

Table 18. Percentage output's deviation regarding diameter variation.

Geometry	Compared Radius (mm)	Q (W/m2)	% Deviation			
			T_exte_wall (K)	ΔP (Pa)	T_out (K)	v_out (m/s)
14x250	100 and 250	200	4.53E-02	3.12E-04	3.13E-06	9.80E-06
		2200	3.01E-01	2.85E-03	1.28E-04	7.38E-05
	100 and 600	200	6.46E-02	5.50E-04	3.13E-06	1.27E-04
		2200	4.29E-01	3.40E-03	1.49E-04	1.89E-04
	600 and 250	200	1.93E-02	2.38E-04	0.00E+00	1.18E-04
		2200	1.28E-01	5.49E-04	2.92E-04	2.38E-05
14x2200	100 and 250	200	1.49E-01	1.24E-03	8.14E-06	8.50E-06
		2200	5.46E-01	5.23E-04	2.25E-04	1.30E-04
	100 and 600	200	2.12E-01	1.37E-03	1.09E-05	5.10E-05
		2200	7.82E-01	8.41E-04	2.65E-04	1.40E-04
	600 and 250	200	6.30E-02	1.27E-04	2.71E-06	5.95E-05
		2200	2.31E-01	3.17E-04	4.03E-05	1.05E-05

In the previous table it is shown that, for the same tk x H geometry design, all percentage deviations are inferior to 1%. Even for 2200 W/m^2 the higher deviation value goes to 0.782%. So, the diameter independence is evident as expected.

As for the preview test, the obtained results were graphically represented in Figure 20.
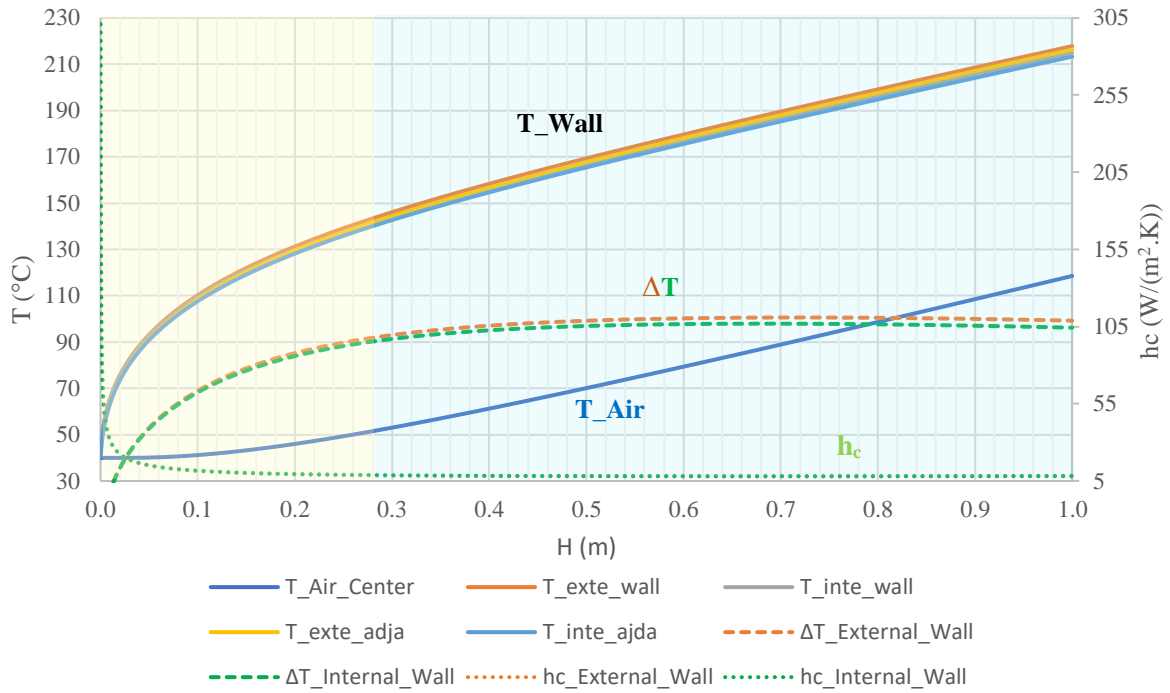
Figure 20. Temperature representations along the duct's height.

The righthand Y axe stands for the ΔT while the left one is respecting local temperatures. The exported *Fluent* data file contained 2775 position points. The wall's temperature profiles were as expected. External and internal wall take similar temperature values, as foreseen. Also, its corresponding adjacent temperatures were represented and curiously, were very proximate to theirs corresponding wall. Given the proximity of the wall's temperatures the same is expectable and obtained for the respective convection coefficient. Note that this last calculation should have been done according to an average fluid temperature (average temperature for all tk positions with the same H position). So, these h_c will be lower than the obtained in the final parametric study. Between both temperatures, wall and fluid centre, it is noticeable the linearization of its increasing from a given position point. From this point on, approximately 0.28 m, it is very likely to evidence the fully developed flow profile. The necessary length for fully developed profile was determined according to literature references [14]. It was confirmed that this length corresponds to 0.28 m, confirming the observations. Another noteworthy observation from this test, is related to the temperature gradient between the wall and the fluid at the centre of the duct. This gradient becomes practically constant after the referred fully development is achieved, this settles the theory – Considering an uniform heat flux applied on the wall, when flow reaches the fully developed state, the temperature gradient between wall and fluid will became constant [14]. Given that the lower temperature profile within the duct will, in theory, correspond to its centre, while the higher one to its wall, we can expect that

its bulk temperature (average motion temperature of the fluid) profile will be contained within these limits. However, once the obtained profile incorporates non-fully developed flow results, presumably the calculation for the convective coefficient will be affected. In order to approximate the final convective coefficient results to its fully developed flow state, the considered bulk temperature will be defined at the final section area (outlet section), since it presents higher probability of acquiring the referred state. Given all these observations, it can be assumed that for the parametric study, the temperature gradient that will be considered for the determination of h_c will be the difference between wall's local outlet temperature and the fluid's average outlet temperature.

As the previous part shows more evidentially the temperature profiles, some velocity plots were also exported from *Fluent* for better monitoring and analysis. The following Figures are also respective to 14x1000 simulation case, with a wall heat flux of 800 W/m², however, for a velocity inlet of 2 m/s.
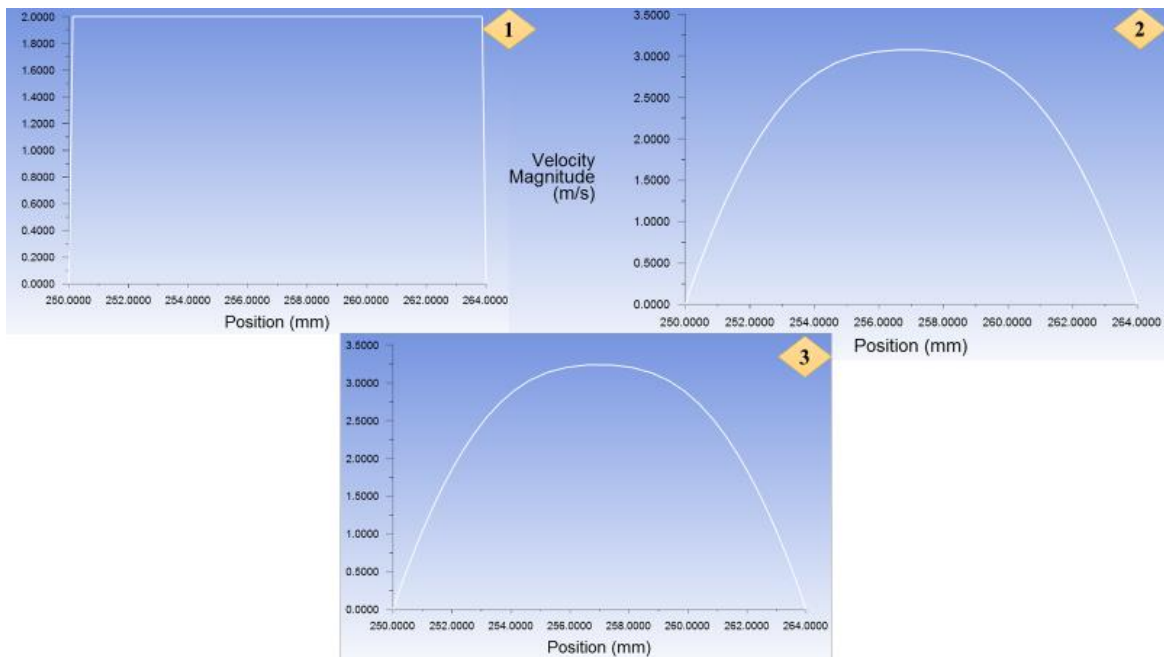
Figure 21.Velocity plots for a H position.

Concerning Figure 21, case 1 corresponds to the inlet section (H position equals to zero). Case 2 resembles to the duct's centre section (H position equals to 500 mm). Case 3 corresponds to the outlet section (H position equals to 1000 mm). Initially, as expected for an imposed velocity inlet the front velocity has the presented form, uniform front. However, along the heat transfer phenomenon occurs, this velocity increases along its duct position and acquires a different front profile, as shown by case 2. This profile was also expected, regarding for the existence of the well-known friction coefficient.

In a simplified manner, this last parameter decreases velocity near walls, so the higher velocity will occur at the centre of the duct, providing a parabolic front appearance. At the outlet section, case 3, this parabolic front is intensified, translated by a greater velocity vector at the centre of the parabolic front.

Entering the parametric study results, an initial comparison was performed with Blume's [16] literature model. This model only concerns a geometry between 20-28x1000 and an inlet velocity of 1 m/s. The obtained results were compared in Table 19.

Table 19. Convection coefficient results obtained by CFD simulations and literature's model.

tk (mm)	H (mm)	Q (W/m2)	v_bulk (m/s)	h_{CFD} (W/(m^2.K))	h_{BLUME} (W/(m^2.K))	Relative error (%)
20	1000	50	1.01	6.32	3.84	39.2%
28	1000	50	1.01	5.21	4.00	23.2%
20	1000	200	1.04	6.71	5.36	20.1%
28	1000	200	1.03	5.59	5.57	0.3%
20	1000	500	1.07	7.34	6.61	9.9%
28	1000	500	1.05	6.14	6.86	-11.7%
20	1000	800	1.11	7.83	7.33	6.4%
28	1000	800	1.08	6.53	7.62	-16.6%
20	1000	1200	1.17	8.37	7.99	4.5%
28	1000	1200	1.12	6.93	8.33	-20.2%
20	1000	1600	1.22	8.83	8.49	3.9%
28	1000	1600	1.16	7.25	8.88	-22.4%
20	1000	2200	1.31	9.48	9.04	4.6%
28	1000	2200	1.22	7.66	9.51	-24.2%
20	1000	3200	1.44	10.49	9.70	7.5%
28	1000	3200	1.32	8.29	10.25	-23.5%

As shown by Table 19, exactly half of the presented cases have a relative error inferior to 15%. As for a 28x1000 geometry, only for a heat flux of 200 W/m^2, this model shows some proximity to the simulation's results. It can be verified that this literature's model only presents good results, according to these simulations, for a geometry of 20x1000, disregarding for low heat fluxes values, specifying less than 200 W/m^2.

As for the comparative example for different duct's thickness, the conditions for this example were a duct's height of 1000 mm, an inlet velocity of 1 m/s and a heat flux of 500 W/m². The obtained results were followed presented, from Figure 22 to 29.
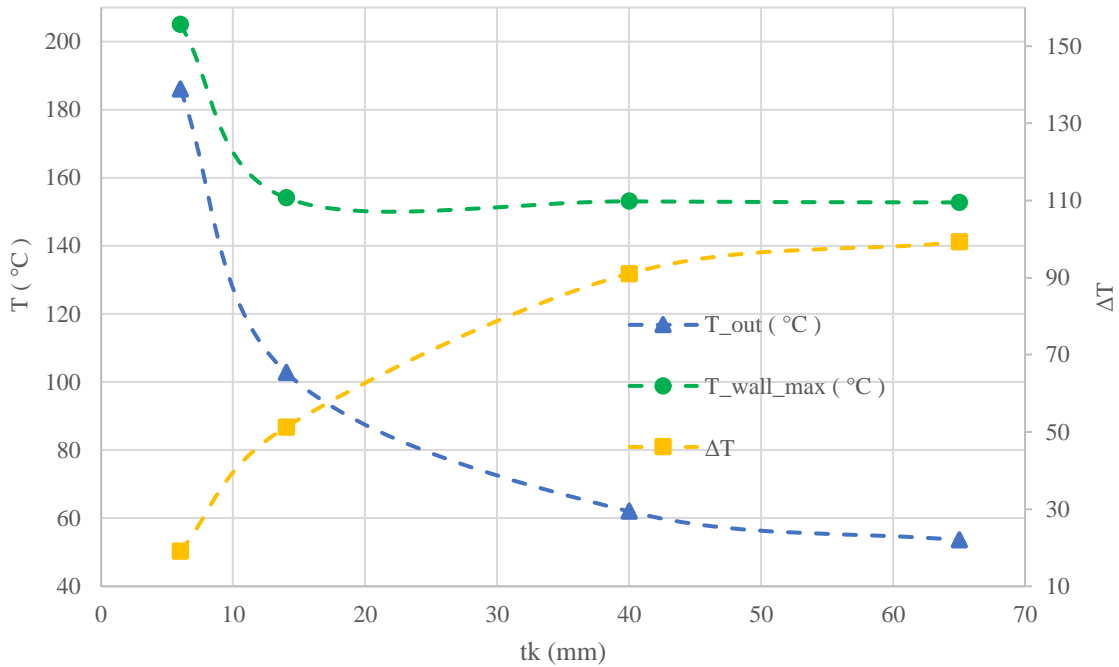
Figure 22. Temperatures and respective variation in order to the duct's thickness.

The presented temperatures are refer to the outlet section (considered for convective coefficient calculation) – wall and fluid – in order to different thicknesses and its corresponding difference curve (yellow curve). According to the mentioned criteria, as the duct's thickness increases a decreasing wall temperature is observable. However, this stagnates approximately at 14 mm. From this thickness on the wall's temperature is approximately constant. Yet, the fluid temperature continues to decrease but only until approximately 40 mm. Recall that convective coefficient depends on the difference between both temperatures. Accordingly, to the cooling process within the transformer, this wall's temperature stagnation indicates, in a practical manner, a minimum duct thickness for cooling existence. This in terms of convective heat transfer coefficient is following explained by Figure 23.
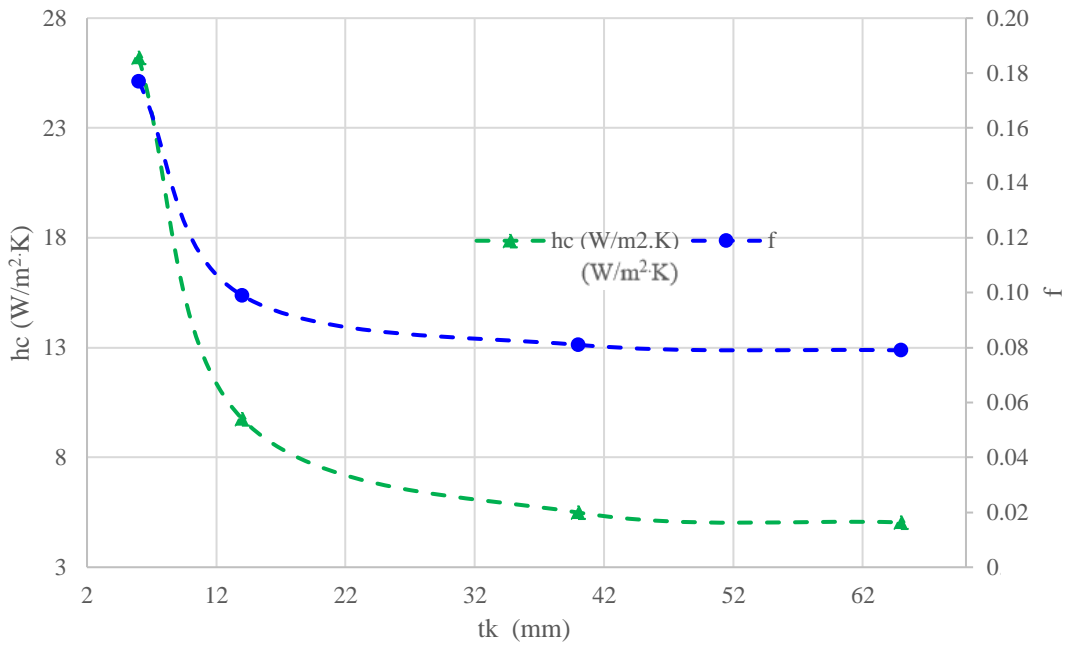
Figure 23. Convection and friction coefficients representation in order to duct's thickness.

As it's noticeable, up until 14 mm, the observed variation on the convective coefficient is much higher. For higher thicknesses the decreasing level is much lower, until approximately 40 mm both coefficients stagnate, corresponding in Figure 22 to both, wall and fluid's, temperature stabilization. This indicates, for this example that the minimum duct's thickness in order to achieve an approximately constant coefficient, in this case of 5 $W/m^2.K$, is of 40 mm.
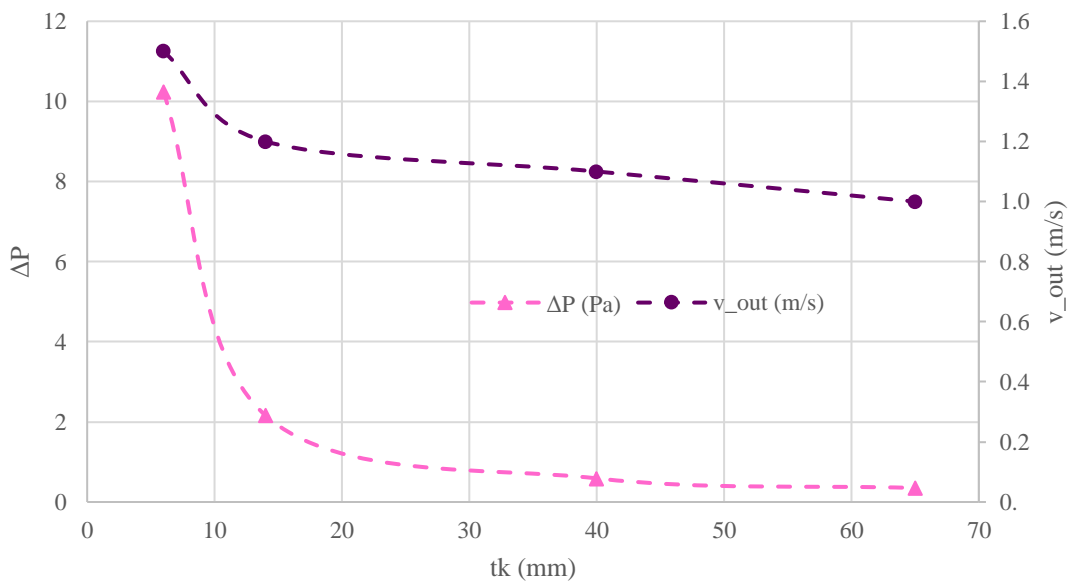
Figure 24. Pressure drop and outlet velocity representation in order to duct's thickness.

About Figure 24 the observations repeat themselves. It's observable an initial slowing at 14 mm and, from 40 mm, a stagnation of the friction coefficient's dependent variables – outlet velocity and pressure drop.

For a more extensive analysis some of the corresponding velocity profiles were followed presented.
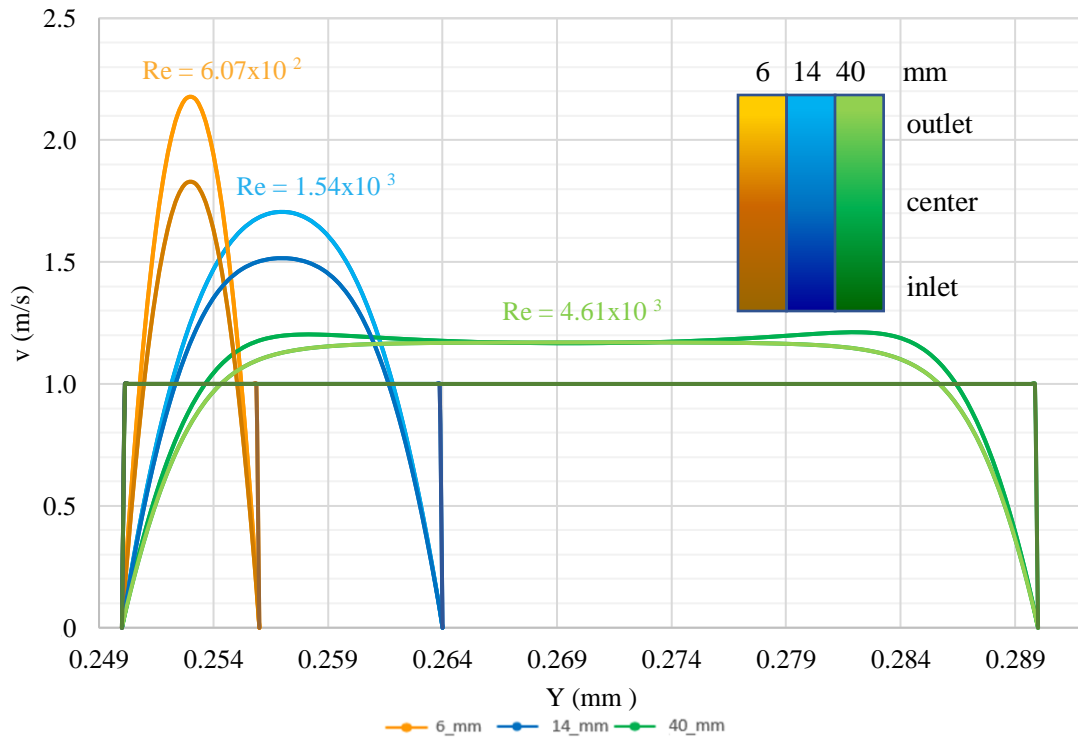
Figure 25. Velocity profiles at the inlet, centre and outlet section.

Figure 25 represents the velocity profiles for thicknesses of 6, 14 and 40 mm, at the inlet, centre and outlet section of the duct. Note that in yy axe the duct's wall corresponds to position 0.250 mm (radius – distance between the core and duct). First, as expected we can observe a rectangular or uniform front corresponding to the inlet section, explained by the imposed inlet velocity. According to the heat transfer phenomenon, the fluid's velocity within the duct will increase, as it is also confirmed by the sequential increasing inlet-centre-outlet. For lower duct's thicknesses higher velocities are observed, also as expected. However, the interesting fact here, is the 40 mm velocity profile. This one does not present a parabolic form. The explanation is very simple, lies on the operating regime's changing, described by Re, and mainly for the velocity zone stagnation, indicating that this zone/area it isn't probably embraced by the boundary layer – where the diffusive and dissipative effects of mechanic energy are contained/felt.
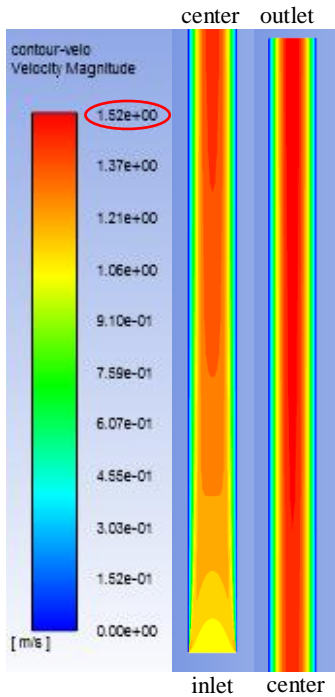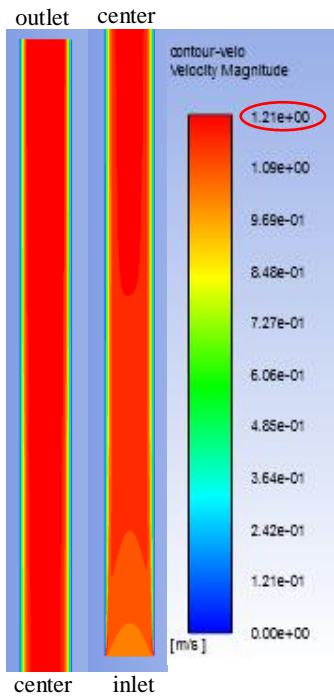
Figure 26. Velocity contour divided in two parts at the duct's center.

As Figure 26 shows, higher velocities are observed for lower thicknesses. Maximum velocity for 14 mm is 1.52 m/s while for 40 mm is only 1.21 m/s.

The corresponding temperature profiles were followed presented in Figure 27.
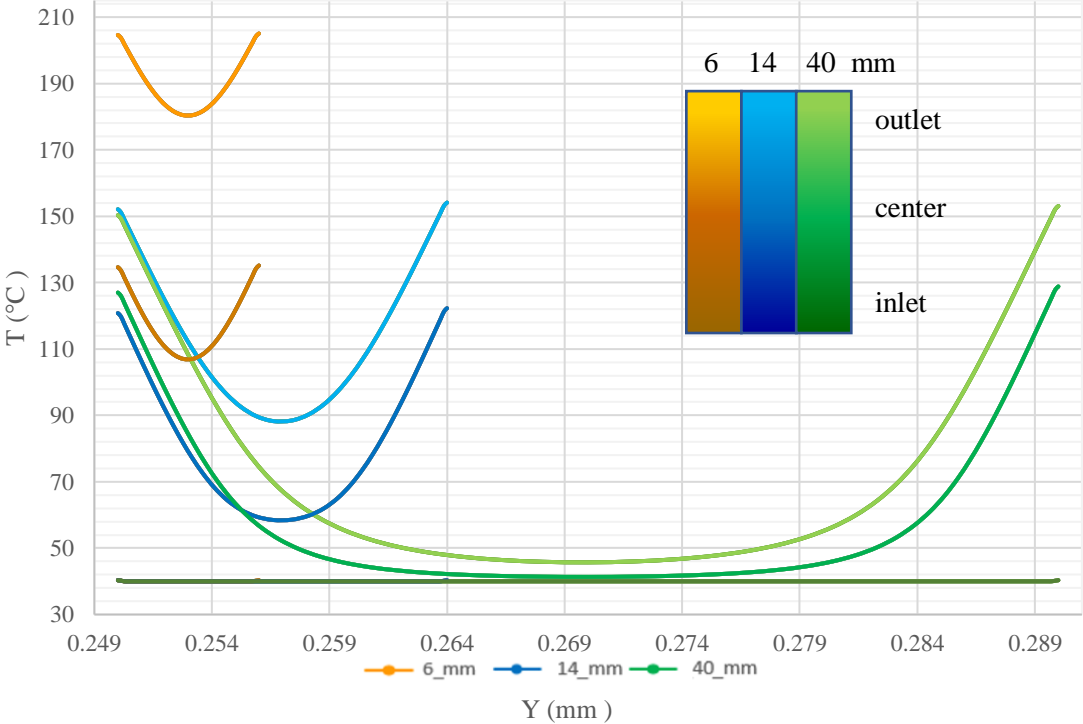
Figure 27. Temperature profiles for inlet, centre and outlet section.

As observable, lower thickness corresponds to higher temperatures. These temperatures are always higher near walls and lower at the duct's centre. As we can observe, a thickness rising is not only escorted by a temperature decreasing but also by the formation of a baseline on the duct's centre, evidenced by 40 mm case. This baseline is limited by the minimum air temperature (40°C), reason why this baseline formation occurs. The beginning position of this baseline is also indicative of the where off the boundary layer effect, in other words, this baseline concerns an approximately stagnated fluid zone were the heat transfer is much limited. The reason why this decrease in temperature is not allowed with increasing thickness (criterion considered) is explained by the formation of this baseline. Theoretically, for low values of thickness is expected a low variation of temperature, between the wall and the centre of the duct. That is, as the duct's thickness increases, this variation will increase. However, above a certain thickness, given the magnitude of the distance between the wall and the centre, the heat transfer effect is minimal so that from this position the temperature will be approximately constant, translating into the formation of this baseline.

This can also be verified by its corresponding temperature contours, presented in Figures 28 and 29.
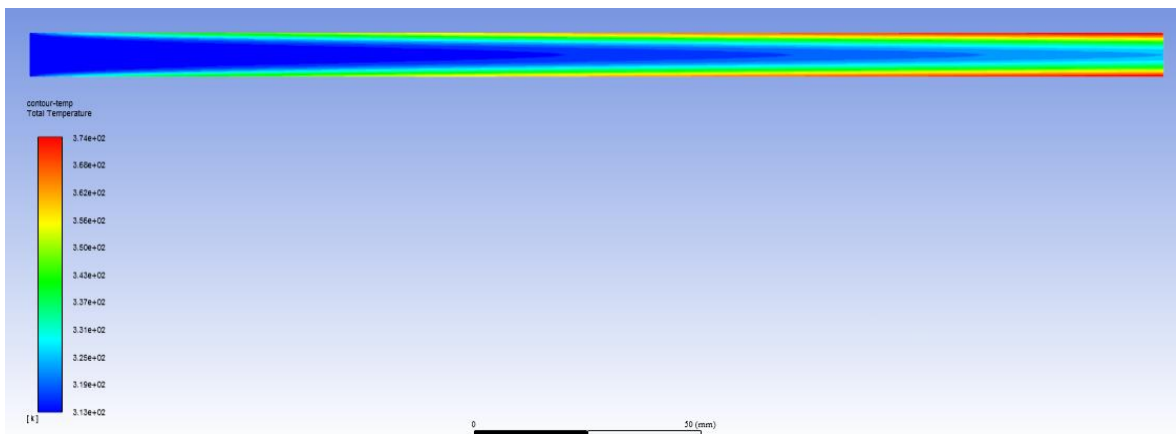
Figure 28. Total temperature contour for 14x1000.
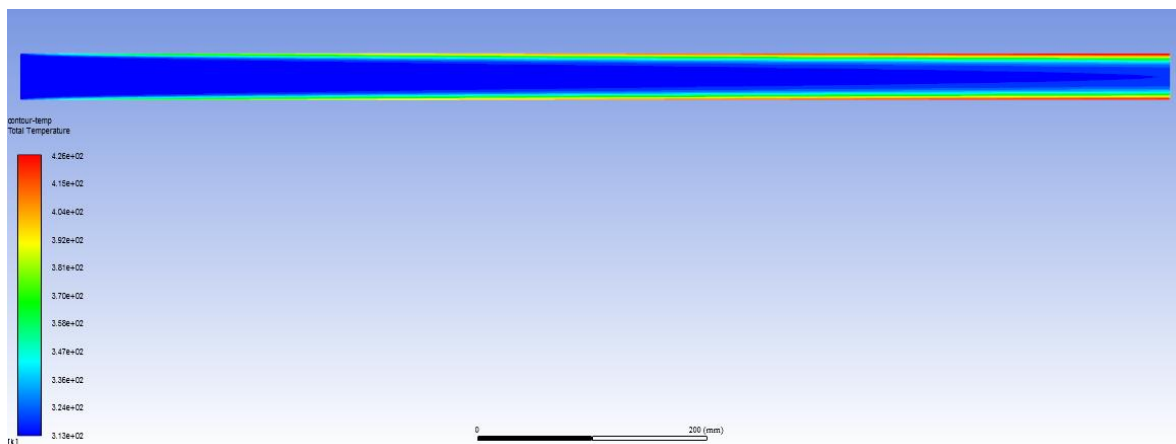
Figure 29. Total temperature contour for 40x1000.

As mentioned, for higher duct's thickness the lower is the heat transfer effect at the fluid's centre. This is verified by Figures 28 and 29. In the first one, for 14 mm a temperature's increasing at the fluid's centre can be observed contrarily to the 40 mm case.

According to the assumption of fully developed flow, it was stated by the previously mentioned criteria, that longitudinal entrance region is ten times the hydraulic diameter. Considering this, only 73.3% of all cases are in conformity. This could outcome as a problem in mathematical modelling, once this may translate into an attempt to correlate uncorrelated data.

Concerning mathematical modelling, as mentioned, the first approach by means of *lsqcurvefit* from MATLAB showed low accuracy. Only an example will be here exposed. On behalf of the corresponding data for turbulent regime (Re > 2900) one of the model function's fitting attempt, for convection coefficient, is followed exemplified in equation 19.

$$modelfun = c0(1) + \left(\frac{tk_n^{c0(14)} \times H_n^{c0(15)} \times Q_n^{c0(16)}}{c0(17) + c0(18) \times Q_n} \right) + \left(c0(2) + c0(3) \times tk_n^{c0(4)} \right)$$
$$+ \left(c0(5) + c0(6) \times H_n^{c0(7)} \right) + \left(c0(8) + c0(9) \times Q_n^{c0(10)} \right)$$
$$+ \left(c0(11) + c0(12) \times v_{bulk_n}^{c0(13)} \right)$$

$$(19)$$

As for the initial coefficient's vector, a vector of ones was considered. However, for adjusting (center the residuals and avoid variables and residual's correlations) the first element, c0(1), was changed to 0.9373. The obtained coefficient's vector was the followed presented in equation 20.

$$
\begin{aligned}
modelfun = \quad & -0.96422686 \\
& + \left(\frac{tk_n^{0.00783495} \times H_n^{-0.00926275} \times Q_n^{0.04919385}}{0.02513875 + 4.05\text{E} - 05 \times Q_n} \right) \\
& + \left(-0.99586743 - 1.96677456 \times tk_n^{0.20120642} \right) \\
& + \left(-0.98732603 + 8.74296343 \times H_n^{0.04025362} \right) \\
& + \left(-1.0842037 - 41.3292824 \times Q_n^{0.04721475} \right) \\
& + \left(-1.08219189 + 0.96687839 \times v_{bulk_n}^{1.88315602} \right)
\end{aligned}
$$

$$(20)$$

Some correspondent statistic obtained results are presented in Table 20.

Table 20. Statistic data for convection coefficient fitting through lsqcurvefit.

p – value (MATLAB's *corrcoef* function)								
tk_n	H_n	Q_n	v_bulk_n	mean (RES)	Std (RES)	Std (rel.error)	kurtosis	skewness
0.7685	0.9841	0.9981	0.8934	-6.3E-06	0.0811	0.283	4.9207	-0.3467

The presented p-values results, in MATLAB's language mean there is no correlation between the independent variables and the obtained residuals (RES), once all values are greater than 0.05. For an ideal gaussian distribution it is known that kurtosis number should be nearby 3 value, while for skewness number it should be 0. Given this, regarding the obtained values, we may predict an approximate gaussian behavior.

The residuals, difference between convective coefficients obtained by the model function and simulations results, were divided by this last (simulation's results) in order to obtain the relative errors. These are represented by the followed histogram in Figure 30.
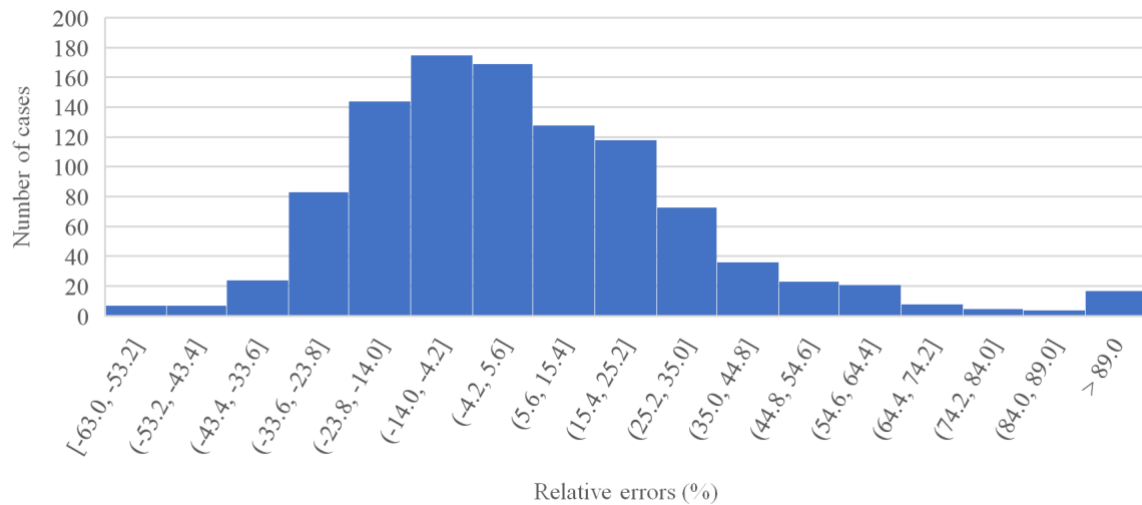
Figure 30. Relative errors (%) histogram for turbulent convection coefficient fit by lsqcurvefit.

It was observed a relative error range of [-15,15] % for 46% of the cases, corresponding to 479 cases of 1042. As not even half of the cases are comprised in this relative error range, very poor accuracy is concluded for this fit.

For the ANN approach, the respective neural networks were evaluated according to its relative errors according to the CFD's results and corresponding network predictions, as presented by the following histograms – number of simulation cases with respective percentage of relative errors.

1. Convection heat transfer coefficient fitting neural network (h_c)
   A) All data
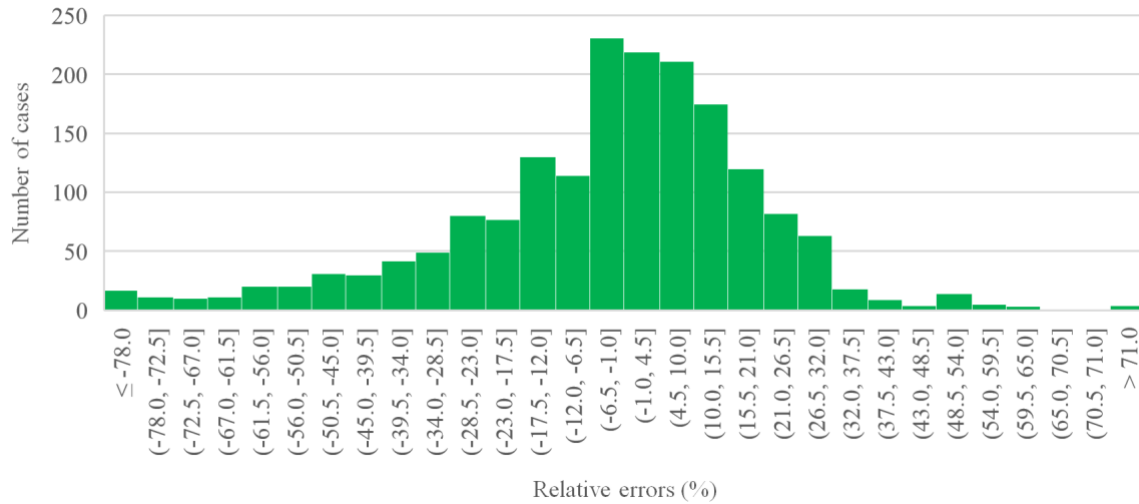
Figure 31. Relative errors histogram for fit case A.

For this case only 56% of all cases, which corresponds to 1102 of 1800, has a relative error comprised in a range of [-15, 15] %. The corresponding standard deviation was of 24.8, which shows the percentage mean deviation of the obtained errors.

This represents a low level of accuracy for the neural network's predictions, once it only fairly good predicts approximately half of the cases, involving all data.

B) Comprising only $h_c < 20$ W/m².K data
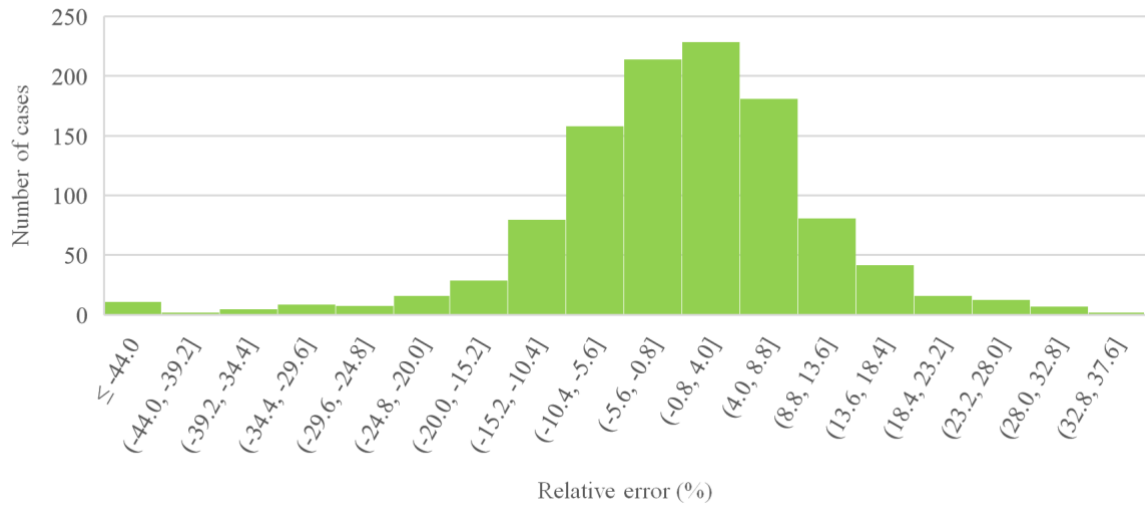
Figure 32. Relative errors histogram for fit B.

For this case 79.8% of all cases, which corresponds to 880 of 1103, has a relative error comprised in a range of [-12, 12] %. The corresponding standard deviation was of 14.1, which shows improvement of the percentage mean deviation of the obtained errors, compared to the previous fit.

2. Friction coefficient fitting neural network (f)

   C) All data
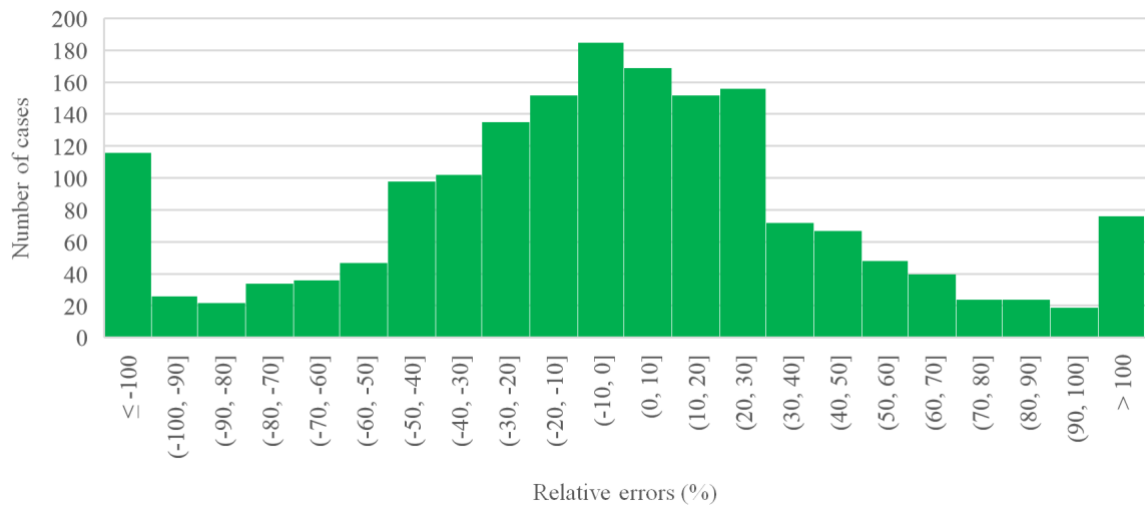
Figure 33. Relative errors histogram for fit C.

For this case 29% of all cases, which corresponds to 522 of 1800, has a relative error comprised in a range of [-15, 15] %. The corresponding standard deviation was of 105.3, which indicates a non-

gaussian behavior for this error curve, and this can be explained by the 116 cases with % relative error higher than 100%.

D) Comprising only $h_c < 20$ W/m^2.K data

Figure 34. Relative errors histogram for fit D.

For this case 69.4 % of all cases, which corresponds to 766 of 1103, has a relative error comprised in a range of [-15, 15] %. The corresponding standard deviation was of 15.9, which shows a massive improvement compared to the previous fit, since for this fit case there's a proximity to a gaussian curve and an acceptable percentage mean deviation of the obtained errors.

Note that for convective coefficient the neural network required only 7 neurons, while 9 were necessary for friction coefficient. This indicates an easier and simpler fit for the convective coefficient. Recalling the previously mentioned thumb rules, as for friction coefficient network the number of nodes necessary was greater than 8, which could indicate overfitting. In order to prove the non-existence of overfitting, tests involving the determination of intermediate points were carried out and are presented in Table 21.

Table 21. Coefficient's results predicted by neural networks (NET) and obtained by simulations (CFD).

tk (mm)	H (mm)	Q (W/m^2)	v_bulk (m/s)	h$_{CFD}$ (W/m^2.K)	h$_{NET}$ (W/m^2.K)	f$_{CFD}$	f$_{NET}$
20	1000	1200	1.2	8.37	8.73	0.113	0.1209
20	1000	1400	1.2	-	8.94	-	0.1288
20	1000	1600	1.2	8.83	9.13	0.124	0.1363

The case presented in Table 21 concerns a 20x1000 geometry duct with a velocity input of 1 m/s. The simulated cases were for heat fluxes of 1200 and 1600 W/m^2. So, the intermediate case here to be observed corresponds to a 1400 W/m^2 heat flux. For the friction coefficient, given it accounts for higher relative errors, 0.1288 is higher than 0.113 but is not lower than 0.124. If we take note that for 1200 W/m^2.K the network predicts 0.1209 while the simulation result was 0.113, the correspondent error is about -7% and for 1600 W/m^2.K the respective error is about -10%. If we apply a mean relative error of -8.5% to the intermediate prediction (1400 W/m^2.K) the corresponding simulation result would be approximately 0.119, which is comprised between 0.124 and 0.113. These results indicate low probability of overfitting. Regarding an analogous procedure for convective coefficient, if the intermediate network's result is affected with an average error of approximately -4% the simulation result would be approximately 8.60 W/m^2.K which is comprised between 8.37 and 8.83 W/m^2.K. Again, this indicates low probability of overfitting.

As for the final illustrative comparison, concerning the neural networks predictions, mentioned literature's model and simulation's results, the corresponding Table 22 is followed presented.

Table 22. Coefficient's results predicted by NN and obtained by simulations and literature's model.

tk mm	H mm	Q W/m^2	v_bulk m/s	h_{CFD} W/m^2.K	h_{NET} W/m^2.K	$h_{MORELLI}$ W/m^2.K	f_{CFD}	f_{NET}	$f_{MORELLI}$
14	1500	500	1.2	10.11	10.9	8.82	0.095	0.1019	0.9625
20	1000	1200	1.2	8.37	8.73	9.97	0.113	0.1209	0.400
20	1000	1600	1.2	8.83	9.13	9.91	0.124	0.1363	0.410
40	600	800	3.7	10.44	12.09	163.9	0.098	0.0375	0.0525
65	2200	2200	2.4	5.65	5.59	155.1	0.119	0.0476	0.1225

For the friction coefficient, the neural networks predictions seem to present a similar accuracy that literature's model, regarding simulation's results, i.e. although for case 20x1000 and 1200 W/m^2.K the network's prediction of 0.1209 better approximates of 0.113 than the literature's model 0.400, we can observe the reverse for case 65x2200. However, for convective coefficient it is evident the overcome of neural network's predictions compared to the literature's model.

5. Conclusions

This study implied the correlation between all 1800 fluid dynamic's simulations and its numerical modelling (fitting). As for the first part, mesh and fluid dynamic (FD) model selection process were the main subjects. A good mesh and FD model choice improves the level of accuracy and reality representation, respectively to the obtained results.

The selected mesh was M1, with 107913 elements, for a specific geometry. Given all compared meshes were created based on the same principles and orthogonal well structured, the choice was concluded for the lower output's deviations and computational time effort. Therefore, M1 was the mesh base case for the parametric study, base for all 44 mesh adaptations (total study of 45 geometries).

Also, as for the external diameter, parameter define as the distance between the duct and core, was proven that it does not affect the main output parameters, given its zero percentage deviations, as expected.

Concerning the FD model selection, the selected model was SST (*Shear Stress Transport Model*). This choice was made accounting for the similarity between SST and Laminar models, while on laminar regime, and likewise when on turbulent regime, similarity between SST and k-omega models. Also, the poor performance near wall, regarding k-epsilon model, was verified. The comparison with Morelli et al.[15] model was useful to increase credibility at the generic SST model's results.

The preview test helped verifying literature's theory (given a uniform heat flux, when fully developed flow is achieved the temperature gradient between wall and fluid will became constant), and more importantly, guide to determine a simpler consideration for the calculation of the convective heat transfer coefficient – as the outlet section evidences higher probability of presenting fully developed flow - ,the gradient of temperature between wall and fluid's at the outlet section of the duct.

The literature's approximate model (Blume [16]) for determination of convective heat transfer coefficients exhibit fitting only for 20x1000 geometry and 1 m/s inlet velocity, through provided low obtained errors (less than 10%) respective to the obtained simulation's results, except for very low heat fluxes (50 W/m^2).

Accounting for the tested theoretical criteria and comparative example (for different thicknesses), that increasing the duct's thickness results in wall and fluid's temperature decreasing, it was stated an earlier/faster stagnation for wall's temperature. So for cooling process, it was concluded that it is possible, for some cases, to define a minimum duct's thickness. This can be considered as a practical useful industry's evaluation.

Regarding the second part – numerical modelling – this consisted on creating a mathematical model that can determine both convective and friction coefficient's by providing the base variables – duct's thickness and height, heat flux and fluid's velocity.

The first problem faced, within this subject, was the difficulty in obtaining a good fit. This may outcome from a non-fully developed profile obtained in some of the studied cases, exactly 26.7%.

For the final numeric modelling, friction's coefficient neural network showed higher fitting difficulty level requiring 9 nodes while for convective's coefficient only 7 nodes were needed. Although, no signs of overfitting have been detected, for both cases. The final fitting results were considering the operating dry-transformer domain, and for convective's coefficient the approximate descriptive function prediction has a relative error inferior to 12% for approximately 80% of all simulation cases, while only inferior to 15% for approximately 70% of the simulation cases, for friction's coefficient. Through final comparison between the more fitted considered (for this study case) literature's model (Morelli et al. [15]), it was concluded an overcome of the obtained model predictions for the convective coefficient corresponding in higher level of accuracy.

6. Future Work Suggestions

There is a series of possible on-going tests for this study and its improvement.

As observed and stated, some simulation cases may not correspond to fully developed flow state, this condition affects the final convection coefficient. Given this, the possibility would be to disregard these simulations (correspondent to a non-fully developed profile) and preform a re-modelling.

Once this study was performed considering a 2D geometry, a group of representative simulations could be repeated considering the real geometry in 3D, through *Fluent* program. This would be significant/noteworthy even if only to compare output deviations, in order to evaluate the accuracy of the 2D results.

Recall, that only homogenous wall heat fluxes were considered, i.e. equal imposed heat flux at both walls, so tests regarding different heat fluxes at each wall could be done. In a practical approach, this last one corresponds to a more realistic point of view. In real cases, there is one wall with higher heat flux than the other, given its proximity to the heat source, for instances.

As for the main follow-up, as previously mentioned, the related transformer's constitution involves other cooling ducts types. An analogous study is required, comprising the remaining ducts (internal and external), in order to enable the complete analysis of convective heat transfer within this dry-type transformer.

7. References

[1]   *International Electrotechnical Comission, Dry-type Transformers -Temperature-rise test (type test). IEC 60076-11*. Geneva, Switzerland, 2004.

[2]   M. P. J.H.Ferziger, *Computacional Methods for Fluid Dynamics*. Springer, 2002.

[3]   'Efacec Web Page'. [Online]. Available: https://www.efacec.pt/en/about-us/. [Accessed: 18-Feb-2019].

[4]   'Efacec Energy Products: Transformers'. [Online]. Available: http://www.efacec.pt/en/wp-content/uploads/2018/01/CS383I1710A1-view.pdf. [Accessed: 18-Feb-2019].

[5]   S. Khaparde and S. Kulkarni, *Transformer Engineering*. Boca Raton, USA: CRC Press, 2012.

[6]   R. Del Vecchio, B. Poulin, P. Feghali, D. Shah, and R. Ahuja, *Transformer Design Principles*. Boca Raton, USA: CRC Press, 2017.

[7]   'Electrical Engineering Portal'. [Online]. Available: https://electrical-engineering-portal.com/what-is-the-eddy-current. [Accessed: 20-Mar-2019].

[8]   'My Electrical Engineering'. [Online]. Available: https://myelectrical.com/notes/entryid/7/aluminium-windings-in-cast-resin-dry-type-transformers. [Accessed: 03-Apr-2019].

[9]   'Electrical Engineering Portal'. [Online]. Available: https://electrical-engineering-portal.com/heating-of-the-dry-type-transformer. [Accessed: 11-Feb-2019].

[10]   J. H. Harlow, *Electric Power Transformer Engineering : Electric Power Engineering Handbook*. Boca Raton, USA: CRC Press, 2007.

[11]   F. Incropera, D. Dewitt, B. T.L, and A. Lavine, *Fundamentals of Heat and Mass Transfer*. New York, USA: J.Wiley, 2011.

[12]   Y. A. Cengel, *Heat Transfer: A Pratical Approach*. New York, USA: McGraw-Hill, 2002.

[13]   W. M. Rohsenow, J. P. Hartnett, and Y. I. Cho, *Handbook of Heat Transfer*. New York, USA: McGraw-Hill, 1998.

[14]   A. Bejan and A. D.Kraus, *Heat Transfer Handbook*. Akron, USA: J.Wiley, 2003.

[15]   E. Morelli, P. Di Barba, B. Cranganu-Cretu, and A. Blaszczyk, 'Network Based Cooling Models for Dry-Transformers', in *Advanced Research Workshop on Transformers*, 2013, pp. 321–326.

[16]   L. Blume, *Transformer Engineering: A Treatise on the Theory, Operation, and Application of Transformers*. New York, USA: J.Wiley, 1951.

[17]   'The Engineering ToolBox'. [Online]. Available: https://www.engineeringtoolbox.com/reynolds-number-d_237.html. [Accessed: 17-Dec-2018].

[18]   'The Engineering ToolBox'. [Online]. Available:
         https://www.engineeringtoolbox.com/prandtl-number-d_1068.html. [Accessed: 17-Dec-2018].

[19]   'Thermopedia'. [Online]. Available: http://www.thermopedia.com/content/824/. [Accessed: 17-Dec-2018].

[20]   'Nuclear Power'. [Online]. Available: https://www.nuclear-power.net/nuclear-engineering/heat-transfer/introduction-to-heat-transfer/characteristic-numbers/what-is-rayleigh-number/. [Accessed: 04-Jan-2019].

[21]   'University of Cambridge lectures'. [Online]. Available:
         http://www2.eng.cam.ac.uk/~jl305/3A1/unFilledLectureNotes.pdf. [Accessed: 20-Feb-2019].

[22]   T. M. Soe and S. Y. Khaing, 'Comparison of Turbulence Models for Computational Fluid Dynamics Simulation of Wind Flow on Cluster of Buildings in Mandalay', *Int. J. Sci. Res. Publ.*, vol. 7, no. 8, pp. 337–350, 2017.

[23]   'ANSYS Web Page'. [Online]. Available: https://www.ansys.com/products/structures. [Accessed: 17-Dec-2018].

[24]   ANSYS Inc., 'Solver Settings: Introduction to ANSYS Fluent'. [Online]. Available:
         https://imechanica.org/files/fluent_13.0_lecture05-solver-settings.pdf. [Accessed: 23-Oct-2018].

[25]   Inc. ANSYS, 'ANSYS Fluent 12.0 Theory Guide', *Software Review*, 2009. [Online]. Available:
         https://www.researchgate.net/file.PostFileLoader.html?id=55e038a95e9d974b798b4568&assetKey=AS:273841442492429@1442300295992. [Accessed: 12-Oct-2018].

[26]   'ANSYS FLUENT 6.3 Documentation'. [Online]. Available:
         https://www.sharcnet.ca/Software/Fluent6/html/ug/node381.htm. [Accessed: 07-Jan-2019].

[27]   ANSYS Inc., 'Turbulence Modeling: Introduction to ANSYS Fluent', *ANSYS Customer Training Material*, 2010. [Online]. Available:
         https://www.researchgate.net/profile/Hocine_Tebbiche/post/Yplus_of_NACA0012/attachment/59d62bed79197b807798a515/AS%3A3450856790302272%401459286245663/download/fluent_13.0_lecture06-turbulence.pdf. [Accessed: 23-Oct-2018].

[28]   'ANSYS FLUENT 12.0 Documentation'. [Online]. Available:
         http://www.afs.enea.it/project/neptunius/docs/fluent/html/th/node73.htm. [Accessed: 04-Jan-2019].

[29]   D. J. Sarma and S. G. Sarma, 'Neural Networks and their Applications in Industry', *DESIDOC Bull. Inf. Technol.*, vol. 20, no. 1&2, pp. 29–36, 2000.

[30]   J. Heaton, *Introduction to Neural Networks with Java*. Chesterfield, USA: Heaton Research, Inc, 2008.

[31]   'MathWorks Support'. [Online]. Available: https://www.mathworks.com/help/deeplearning/ug/multilayer-neural-network-architecture.html?searchHighlight=neural network fitting&s_tid=doc_srchtitle#bss33y1-3. [Accessed: 27-Feb-2019].

[32]   'ANSYS Meshing Documentation'. [Online]. Available: https://www.sharcnet.ca/Software/Ansys/16.2.3/enus/help/flu_ug/flu_ug_choicemeshtypes.html. [Accessed: 30-Oct-2018].

[33]   'Cambridge Appendix E'. [Online]. Available: https://www.cambridge.org/ie/files/9513/6697/5546/Appendix_E.pdf. [Accessed: 08-Jan-2019].

[34]   'ANSYS FLUENT 6.3 Documentation'. [Online]. Available: https://www.sharcnet.ca/Software/Fluent6/html/ug/node1199.html. [Accessed: 18-Feb-2019].

[35]   'MathWorks Documentation'. [Online]. Available: https://www.mathworks.com/help/matlab/ref/double.normalize.html;jsessionid=54c40710da438a6c431b2f965fdc. [Accessed: 22-Mar-2019].

[36]   'MathWorks Documentation'. [Online]. Available: https://www.mathworks.com/help/optim/ug/lsqcurvefit.html. [Accessed: 22-Mar-2019].

8. Appendices

8.1 Impact of the Operating Density Parameter Specification

Table 23. Comparison between two different specified operating density values and one non-specified, under Morelli conditions.

						ρ_{op} 1.049584	ρ_{op} 0.990769	no ρ_{op}
Model	tk (mm)	H (mm)	Q1 (W/m²)	Q2 (W/m²)	v_in (m/s)	ΔP	ΔP	ΔP
SST	20	1500	199	177	0.5	0.8065	1.383	0.8984
SST	20	1500	199	177	1	2.036	2.613	1.766
SST	20	1500	199	177	2	4.386	4.963	3.905
SST	20	1500	199	177	5	16.02	16.60	15.36
Laminar	20	1500	199	177	0.5	0.8389	1.380	0.8985
Laminar	20	1500	199	177	1	2.044	2.586	1.746

As the obtained results in Table 23 verified, the specification of the density operating parameter has observable impact in the output's pressure drop. As there's an automatic mode calculation in the CFD program, this will be utilized.

8.2 Impact of Turbulence Intensity Parameter – Influence Test

This parameter describes the ratio between the floating velocity and the mean velocity. As a used parameter in SST fluid-dynamic model and it must be defined at the inlet and outlet without knowing the velocity outlet à priori, an impact test was performed in order to determine if the assumption of assuming same value for inlet and outlet was feasible. This impact test relies on the observation of the main output's variation.

For this test the conditions were the following: duct's type of 14x2200 (thickness x height - in mm) for 1m/s inlet velocity and 1200W/m² heat flux. The inlet turbulence intensity was defined according to its inlet velocity. Regarding the variation of outlet turbulence intensity six simulation cases were performed:

- int_turb_1 (outlet) = 1.02*int_turb_1 (inlet)
- int_turb_1 (outlet) = 0.98*int_turb_1 (inlet)
- int_turb_1 (outlet) = 1.05*int_turb_1 (inlet)
- int_turb_1 (outlet) = 0.95*int_turb_1 (inlet)

- int_turb_1 (outlet) = int_turb_1 (inlet)
- int_turb_2 (outlet) = int_turb_2 (inlet)

Table 24. Output results for different turbulence intensity values.

tk	H	Q	v_in	int_turb_in	int_turb_out	T_exte_wall	T_inte_wall	p_in	p_out	v_out	T_out
mm	mm	W/m^2	m/s	-	-	K	K	Pa	Pa	m/s	K
14	2200	1200	1	0.0634	0.0834	576.88818	573.05011	9.17994	1.382889	2.0388	638.456
14	2200	1200	1	0.0634	0.0434	576.88818	573.05011	9.17994	1.382889	2.0388	638.456
14	2200	1200	1	0.0634	0.1134	576.88818	573.05011	9.17994	1.382889	2.0388	638.456
14	2200	1200	1	0.0634	0.0134	576.88818	573.05011	9.17994	1.382889	2.0388	638.456
14	2200	1200	1	0.0634	0.0634	576.88818	573.05011	9.17994	1.382889	2.0388	638.456
14	2200	1200	1	0.0600	0.060	577.03268	573.18654	9.178847	1.382892	2.0388	638.456
				Δ (0.0034) int_turb		2.50E-04	2.38E-04	1.19E-04	2.46E-06	0E+00	0E+00

The results show that the manipulation of this parameter at outlet (2% and 5% of the inlet) does not affect at all the outputs – deviation of 0% for every output. The modification of this parameter only affects results if manipulated at the inlet. However, results show that even this modification isn't much significative – a variation of approximately 5% at the inlet (0.0034) causes a maximum output deviation of 0.025%.

8.3 Convergence Difficulties – Particular Simulation Cases

Along the simulation procedure some cases with convergence difficulties were noted. For the majority this problem was solved by changing/adapting the parameter of turbulence intensity, and others by the manipulation of the relaxation factors, by execute commands along the simulation. Mostly convergence difficulties occur regarding low inlet velocities and heat flux (natural convection

cases). One of the most difficult cases was 100x1000 (thickness x height - in mm) for 0.05m/s inlet velocity and 50W/m^2 heat flux, so that's the reason for its followed description.

The following figures describes the velocity magnitude (Figure 36) and total temperature (Figure 35) of the fluid along the duct.
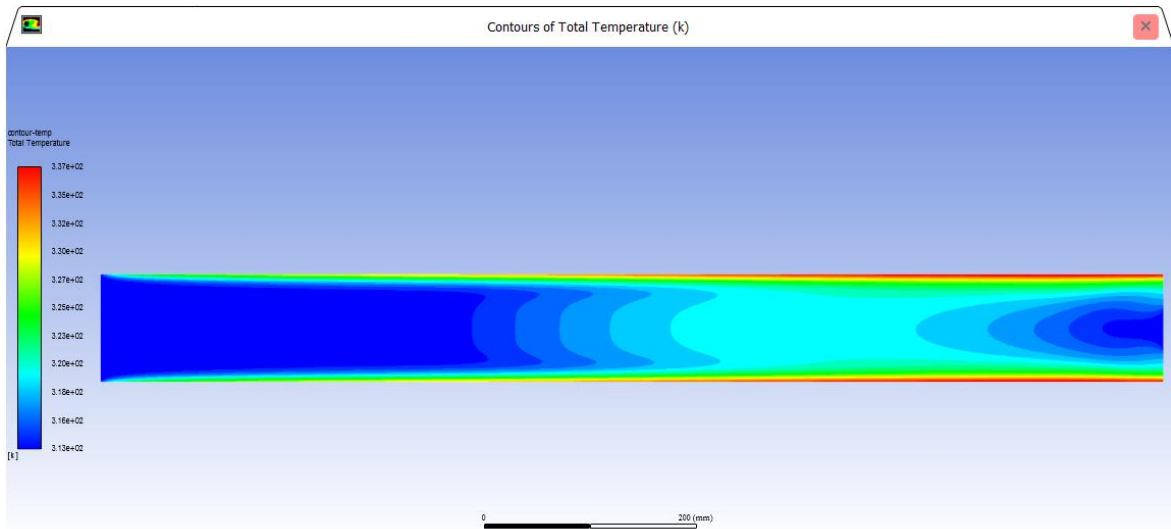
Figure 35. Total Temperature Contour for case 100x1000, 0.05 m/s and 50 W/m^2.
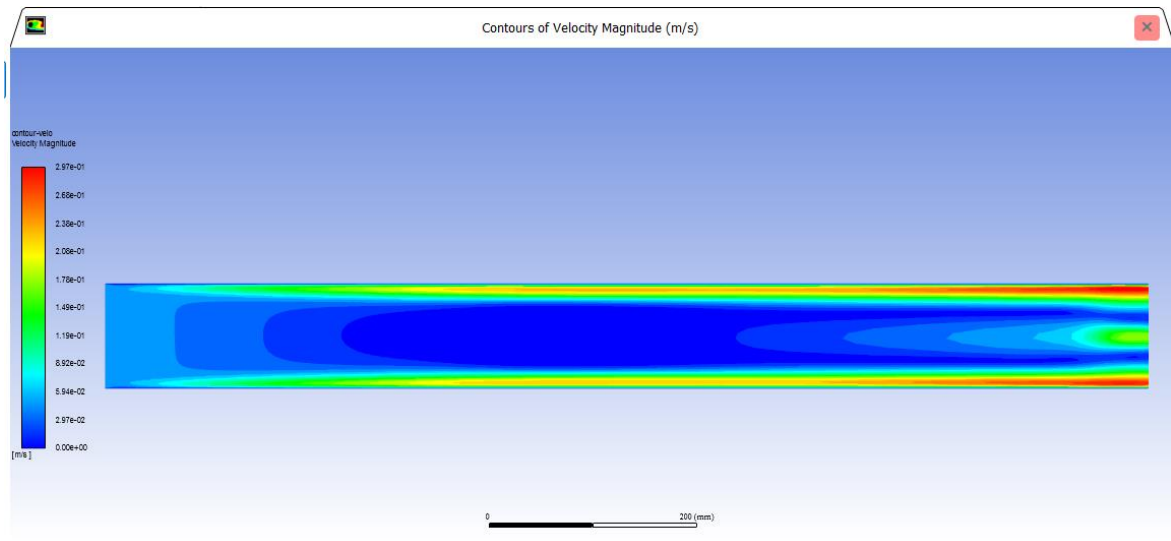
Figure 36. Velocity contour for case 100x1000, 0.05 m/s and 50 W/m^2.

The stated problem, in both figures is the existence of reversed flow, entering through the outlet duct zone. This can be explained by the simplification/assumption made for natural convection simulations, as a low velocity inlet was imposed (although it's a low value, it still is a velocity imposition which is affecting the system). Both profiles show that the imposed velocity is not

sufficiently higher to carry all air through the duct, consequently the needing system will get the lacking velocity through the outlet unaffected air. So, this air flows through the duct, with reverse orientation, until the zone where fluid's velocity is insufficient and add the missing necessary to its outflow. From these particular cases adulterated results can outcome, since the outlet velocity and temperature profile were affected, i.e. the outlet temperature won't be the actual real one, corresponding not to the temperature of the heated fluid but to the fluid's temperature entering this section to provide the lacking required flow. Given this, the most correct approach would be to exclude these cases from the study. However, this would consist on opening and going thought file by file, simulation by simulation to point out all cases, which is not practicable considered and very time-consuming.

8.4 Table Results

Table 25. Laminar mesh test.

radius	tk	H	Q	v_in	Mesh Elements	T_exte_wall	T_out	v_out	ΔP
mm	mm	mm	W/m^2	m/s		K	K	m/s	
250	14	1000	500	2	19383	376.234	344.620	2.201	3.601
250	14	1000	2200	2	19383	561.149	450.548	2.877	4.925
250	14	1000	500	2	107913	376.202	344.620	2.201	4.427
250	14	1000	2200	2	107913	560.959	450.551	2.878	5.766
250	14	1000	500	2	493535	376.193	344.621	2.201	4.455
250	14	1000	2200	2	493535	560.908	450.552	2.878	5.797

Table 26. k-epsilon mesh test.

radius	tk	H	Q	v_in	Mesh Elements	T_exte_wall	T_out	v_out	ΔP
mm	mm	mm	W/m²	m/s		K	K	m/s	
250	14	1000	500	6.5	19383	328.247	322.846	6.701	40.867
250	14	1000	2200	6.5	19383	378.770	355.749	7.384	47.480
250	14	1000	500	6.5	107913	326.246	322.846	6.701	53.987
250	14	1000	2200	6.5	107913	371.129	355.751	7.384	60.048
250	14	1000	500	6.5	493535	326.076	322.846	6.701	55.804
250	14	1000	2200	6.5	493535	370.768	355.751	7.384	61.080
250	14	1000	500	2	19383	345.550	344.633	2.201	8.903
250	14	1000	2200	2	19383	454.121	450.829	2.879	11.985
250	14	1000	500	2	107913	345.296	344.633	2.201	9.294
250	14	1000	2200	2	107913	454.899	450.831	2.879	12.037
250	14	1000	500	2	493535	345.695	344.633	2.201	8.971
250	14	1000	2200	2	493535	456.671	450.832	2.879	11.597

Table 27. k-omega mesh test.

radius	tk	H	Q	v_in	Mesh Elements	T_exte_wall	T_out	v_out	ΔP
mm	mm	mm	W/m²	m/s		K	K	m/s	
250	14	1000	500	6.5	19383	328.998	322.846	6.701	37.231
250	14	1000	2200	6.5	19383	386.552	355.748	7.384	40.498
250	14	1000	500	6.5	107913	331.246	322.846	6.701	33.413
250	14	1000	2200	6.5	107913	396.067	355.747	7.384	36.528
250	14	1000	500	6.5	493535	331.287	322.846	6.701	33.439
250	14	1000	2200	6.5	493535	396.112	355.747	7.384	36.646
250	14	1000	500	2	19383	358.334	344.632	2.201	5.522
250	14	1000	2200	2	19383	521.428	450.762	2.879	6.151
250	14	1000	500	2	107913	358.289	344.632	2.201	5.571
250	14	1000	2200	2	107913	519.799	450.768	2.879	6.246
250	14	1000	500	2	493535	358.243	344.632	2.201	5.606
250	14	1000	2200	2	493535	519.980	450.771	2.879	6.277

Table 28. SST mesh test.

radius	tk	H	Q	v_in	Mesh Elements	T_exte_wall	T_out	v_out	ΔP
mm	mm	mm	W/m²	m/s		K	K	m/s	
250	14	1000	500	2	19383	372.027	344.623	2.201	4.476
250	14	1000	2200	2	19383	548.276	450.603	2.878	7.331
250	14	1000	500	2	107913	372.171	344.624	2.201	4.511
250	14	1000	2200	2	107913	548.782	450.604	2.878	7.395
250	14	1000	500	2	493535	372.160	344.624	2.201	4.538
250	14	1000	2200	2	493535	548.736	450.605	2.878	7.425
250	14	1000	500	6.5	19383	328.901	322.846	6.701	36.863
250	14	1000	2200	6.5	19383	396.170	355.747	7.384	35.692
250	14	1000	500	6.5	107913	333.374	322.846	6.701	29.201
250	14	1000	2200	6.5	107913	413.162	355.744	7.384	30.677
250	14	1000	500	6.5	493535	333.447	322.846	6.701	29.309
250	14	1000	2200	6.5	493535	411.054	355.745	7.384	31.388

Table 29. Fluid-dynamic model selection test data.

	tk	H	Q	v_in	T_exte_wall	ΔP	T_out	v_out
Model	mm	mm	W/m2	m/s	K		K	m/s
Laminar	14	1000	500	1	395.20	2.171	376.01	1.201
	14	1000	2200	1	626.63	4.210	585.36	1.869
	14	1000	500	2	376.20	4.387	344.62	2.201
	14	1000	2200	2	560.96	7.365	450.55	2.878
	14	1000	500	3.5	364.05	8.480	331.14	3.701
	14	1000	2200	3.5	519.15	12.73	391.88	4.380
	14	1000	500	6.5	352.77	18.67	322.84	6.701
	14	1000	2200	6.5	478.01	25.43	355.62	7.381
	14	1000	500	10	346.19	33.10	319.45	10.20
	14	1000	2200	10	452.69	42.83	340.78	10.88
SST	14	1000	500	1	392.81	2.196	376.01	1.201
	14	1000	2200	1	620.83	4.198	585.36	1.869
	14	1000	500	2	372.17	4.511	344.62	2.201
	14	1000	2200	2	548.78	7.395	450.60	2.878
	14	1000	500	3.5	354.97	9.031	331.15	3.701
	14	1000	2200	3.5	500.07	12.95	391.96	4.381
	14	1000	500	6.5	333.37	29.20	322.85	6.701

	14	1000	2200	6.5	413.16	30.68	355.74	7.384
	14	1000	500	10	326.32	65.43	319.45	10.20
	14	1000	2200	10	373.90	68.61	340.86	10.88
k-epsilon	14	1000	500	1	368.38	3.532	376.02	1.201
	14	1000	2200	1	551.37	5.520	585.57	1.870
	14	1000	500	2	345.29	2.201	344.63	2.201
	14	1000	2200	2	454.86	2.879	450.83	2.879
	14	1000	500	3.5	334.01	21.30	331.15	3.701
	14	1000	2200	3.5	405.64	25.14	392.11	4.383
	14	1000	500	6.5	326.24	54.01	322.85	6.701
	14	1000	2200	6.5	371.11	60.07	355.75	7.384
	14	1000	500	10	322.77	102.4	319.45	10.20
	14	1000	2200	10	355.59	111.1	340.86	10.88
k-omega	14	1000	500	1	388.26	2.262	376.01	1.201
	14	1000	2200	1	623.25	4.202	585.37	1.869
	14	1000	500	2	358.23	5.422	344.63	2.201
	14	1000	2200	2	519.41	7.692	450.77	2.879
	14	1000	500	3.5	342.55	12.32	331.15	3.701
	14	1000	2200	3.5	448.32	15.11	392.10	4.382
	14	1000	500	6.5	331.22	32.89	322.85	6.701
	14	1000	2200	6.5	395.94	36.61	355.75	7.384
	14	1000	500	10	325.83	68.03	319.45	10.20
	14	1000	2200	10	371.17	72.26	340.86	10.88

Table 30. Data for comparison example - correspondent data for Figures 22,23 and 24.

H	v_in	Q	tk	v_out	ΔP	Re	T_out	ΔT	T_wall_max	ΔT_{TC}	h_c	f
mm	m/s	W/m^2	mm	m/s	-	-	°C	-	°C	-	W/m^2.K	-
1000	1	500	6	1.5	10.2	6.07E+02	186.0	146.0	205.06	19.10	26.2	0.177
			14	1.2	2.16	1.54E+03	102.9	62.86	154.11	51.25	9.76	0.099
			40	1.1	0.590	4.61E+03	62.02	22.02	153.07	91.05	5.49	0.081
			65	1	0.350	7.56E+03	53.55	13.55	152.76	99.21	5.04	0.079

Table 31. Exported Fluent velocity data for comparison example - 6 mm.

Y	v_in	Y	v_center	Y	v_out	Y
mm	m/s	mm	m/s	mm	m/s	mm
0.25	0	0.256	0	0.25	0	0.25
0.250131	1	0.255869	0.166352	0.250131	0.197968	0.250131
0.250274	1	0.255726	0.330766	0.250274	0.39372	0.250274
0.250433	1	0.255567	0.501585	0.250433	0.597152	0.250433
0.250607	1	0.255393	0.677342	0.250607	0.80653	0.250607
0.250798	1	0.255202	0.855994	0.250798	1.01944	0.250798
0.251008	1	0.254992	1.03481	0.251008	1.23264	0.251008
0.25124	1	0.25476	1.21018	0.25124	1.44183	0.25124
0.251495	1	0.254505	1.37749	0.251495	1.64146	0.251495
0.251775	1	0.254225	1.53082	0.251775	1.8244	0.251775
0.252083	1	0.253917	1.66267	0.252083	1.9816	0.252083
0.252422	1	0.253578	1.76363	0.252422	2.10164	0.252422
0.252795	1	0.253205	1.82198	0.252795	2.17013	0.252795
0.253205	1	0.252795	1.82291	0.253205	2.16897	0.253205
0.253578	1	0.252422	1.76618	0.253578	2.09849	0.253578
0.253917	1	0.252083	1.66649	0.253917	1.97688	0.253917
0.254225	1	0.251775	1.53553	0.254225	1.81859	0.254225
0.254505	1	0.251495	1.38272	0.254505	1.63504	0.254505
0.25476	1	0.25124	1.21556	0.25476	1.43524	0.25476
0.254992	1	0.251008	1.04001	0.254992	1.22626	0.254992
0.255202	1	0.250798	0.860762	0.255202	1.01361	0.255202
0.255393	1	0.250607	0.681444	0.255393	0.801521	0.255393
0.255567	1	0.250433	0.504845	0.255567	0.593176	0.255567
0.255726	1	0.250274	0.333048	0.255726	0.390938	0.255726
0.255869	1	0.250131	0.167561	0.255869	0.196496	0.255869
0.256	0	0.25	0	0.256	0	0.256

Table 32. Exported Fluent temperature data for comparison example - 6 mm.

Y	T_in	Y	T_center	Y	T_out
mm	K	mm	K	mm	K
0.25	313.492	0.256	408.306	0.25	477.753
0.250131	313.347	0.255869	407.329	0.250131	476.893
0.250274	313.171	0.255726	405.182	0.250274	475.008
0.250433	313.152	0.255567	402.84	0.250433	472.956
0.250607	313.15	0.255393	400.306	0.250607	470.742
0.250798	313.15	0.255202	397.595	0.250798	468.38
0.251008	313.15	0.254992	394.739	0.251008	465.902
0.25124	313.15	0.25476	391.792	0.25124	463.356
0.251495	313.15	0.254505	388.838	0.251495	460.819
0.251775	313.15	0.254225	386	0.251775	458.399
0.252083	313.15	0.253917	383.452	0.252083	456.247
0.252422	313.15	0.253578	381.424	0.252422	454.56
0.252795	313.15	0.253205	380.207	0.252795	453.595
0.253205	313.15	0.252795	380.147	0.253205	453.649
0.253578	313.15	0.252422	381.258	0.253578	454.707
0.253917	313.15	0.252083	383.196	0.253917	456.472
0.254225	313.15	0.251775	385.671	0.254225	458.688
0.254505	313.15	0.251495	388.451	0.254505	461.158
0.25476	313.15	0.25124	391.362	0.25476	463.734
0.254992	313.15	0.251008	394.278	0.254992	466.308
0.255202	313.15	0.250798	397.111	0.255202	468.807
0.255393	313.15	0.250607	399.807	0.255393	471.182
0.255567	313.152	0.250433	402.332	0.255567	473.405
0.255726	313.171	0.250274	404.67	0.255726	475.461
0.255869	313.347	0.250131	406.815	0.255869	477.348
0.256	313.492	0.25	407.792	0.256	478.209

Table 33. Exported Fluent velocity data for comparison example - 14 mm.

Y	v_in	Y	v_center	Y	v_out
mm	m/s	mm	m/s	mm	m/s
0.25	0	0.25	0	0.25	0
0.250129	1	0.250129	0.076787	0.250129	0.079119
0.250271	1	0.250271	0.154029	0.250271	0.158932
0.250427	1	0.250427	0.236057	0.250427	0.243944
0.250599	1	0.250599	0.322762	0.250599	0.334121
0.250788	1	0.250788	0.413906	0.250788	0.42932
0.250996	1	0.250996	0.509085	0.250996	0.529259
0.251225	1	0.251225	0.607698	0.251225	0.633486
0.251476	1	0.251476	0.708923	0.251476	0.741355
0.251753	1	0.251753	0.811726	0.251753	0.851997
0.252058	1	0.252058	0.914832	0.252058	0.964287
0.252393	1	0.252393	1.01663	0.252393	1.07679
0.252761	1	0.252761	1.11516	0.252761	1.18773
0.253166	1	0.253166	1.20809	0.253166	1.29499
0.253612	1	0.253612	1.2928	0.253612	1.39606
0.254102	1	0.254102	1.36647	0.254102	1.48811
0.254642	1	0.254641	1.42634	0.254642	1.56799
0.255235	1	0.255235	1.47071	0.255235	1.63238
0.255887	1	0.255887	1.4997	0.255887	1.67818
0.256605	1	0.256605	1.51423	0.256605	1.70276
0.257395	1	0.257395	1.5139	0.257395	1.70243
0.258113	1	0.258113	1.4987	0.258113	1.67718
0.258765	1	0.258765	1.46894	0.258765	1.63067
0.259358	1	0.259358	1.42373	0.259358	1.56556
0.259898	1	0.259898	1.36306	0.259898	1.48501
0.260388	1	0.260388	1.28873	0.260388	1.39239
0.260834	1	0.260834	1.20352	0.260834	1.29087
0.261239	1	0.261239	1.11028	0.261239	1.18332
0.261607	1	0.261607	1.01163	0.261607	1.07223
0.261942	1	0.261942	0.909855	0.261942	0.959722
0.262247	1	0.262247	0.806921	0.262247	0.847561
0.262524	1	0.262524	0.704411	0.262524	0.737164
0.262775	1	0.262775	0.60358	0.262775	0.62964
0.263004	1	0.263004	0.505442	0.263004	0.52584

0.263212	1	0.263212	0.410801	0.263212	0.426392
0.263401	1	0.263401	0.320239	0.263401	0.331732
0.263573	1	0.263573	0.234144	0.263573	0.242125
0.263729	1	0.263729	0.15274	0.263729	0.157702
0.263871	1	0.263871	0.076126	0.263871	0.078486
0.264	0	0.264	0	0.264	0

Table 34. Exported Fluent temperature data for comparison example - 14 mm.

Y	T_in	Y	T_center	Y	T_out
mm	K	mm	K	mm	K
0.25	313.496	0.25	393.961	0.25	425.251
0.250129	313.349	0.250129	392.966	0.250129	424.316
0.250271	313.172	0.250271	390.776	0.250271	422.256
0.250427	313.152	0.250427	388.363	0.250427	419.989
0.250599	313.15	0.250599	385.712	0.250599	417.496
0.250788	313.15	0.250788	382.805	0.250788	414.759
0.250996	313.15	0.250996	379.628	0.250996	411.762
0.251225	313.15	0.251225	376.171	0.251225	408.492
0.251476	313.15	0.251476	372.432	0.251476	404.938
0.251753	313.15	0.251753	368.417	0.251753	401.097
0.252058	313.15	0.252058	364.142	0.252058	396.974
0.252393	313.15	0.252393	359.648	0.252393	392.591
0.252761	313.15	0.252761	355	0.252761	387.987
0.253166	313.15	0.253166	350.303	0.253166	383.233
0.253612	313.15	0.253612	345.706	0.253612	378.437
0.254102	313.15	0.254102	341.411	0.254102	373.758
0.254642	313.15	0.254641	337.666	0.254642	369.415
0.255235	313.15	0.255235	334.704	0.255235	365.695
0.255887	313.15	0.255887	332.669	0.255887	362.925
0.256605	313.15	0.256605	331.635	0.256605	361.435
0.257395	313.15	0.257395	331.726	0.257395	361.613
0.258113	313.15	0.258113	332.935	0.258113	363.424
0.258765	313.15	0.258765	335.148	0.258765	366.488
0.259358	313.15	0.259358	338.288	0.259358	370.467
0.259898	313.15	0.259898	342.202	0.259898	375.031
0.260388	313.15	0.260388	346.649	0.260388	379.892

0.260834	313.15	0.260834	351.374	0.260834	384.835
0.261239	313.15	0.261239	356.178	0.261239	389.705
0.261607	313.15	0.261607	360.911	0.261607	394.399
0.261942	313.15	0.261942	365.473	0.261942	398.85
0.262247	313.15	0.262247	369.799	0.262247	403.024
0.262524	313.15	0.262524	373.853	0.262524	406.901
0.262775	313.15	0.262775	377.62	0.262775	410.481
0.263004	313.15	0.263004	381.095	0.263004	413.768
0.263212	313.15	0.263212	384.284	0.263212	416.774
0.263401	313.15	0.263401	387.198	0.263401	419.515
0.263573	313.152	0.263573	389.852	0.263573	422.009
0.263729	313.172	0.263729	392.263	0.263729	424.274
0.263871	313.349	0.263871	394.451	0.263871	426.329
0.264	313.496	0.264	395.444	0.264	427.262

Table 35. Exported Fluent velocity data for comparison example - 40 mm.

Y	v_in	Y	v_center	Y	v_out
mm	m/s	mm	m/s	mm	m/s
0.29	0	0.25	0	0.25	0
0.289865	1	0.250135	0.057386	0.250135	0.061267
0.289717	1	0.250283	0.115073	0.250283	0.122925
0.289555	1	0.250445	0.176141	0.250445	0.188269
0.289376	1	0.250625	0.240473	0.250625	0.257183
0.289178	1	0.250822	0.307847	0.250822	0.329453
0.288962	1	0.251038	0.377921	0.251038	0.404739
0.288723	1	0.251277	0.450202	0.251277	0.482552
0.288461	1	0.251539	0.524028	0.251539	0.562226
0.288173	1	0.251827	0.598561	0.251827	0.642902
0.287855	1	0.252145	0.672815	0.252145	0.723523
0.287506	1	0.252494	0.745689	0.252494	0.802834
0.287122	1	0.252878	0.815911	0.252878	0.879342
0.2867	1	0.2533	0.882036	0.2533	0.951335
0.286236	1	0.253764	0.942534	0.253764	1.01694
0.285725	1	0.254275	0.995915	0.254275	1.07424
0.285163	1	0.254837	1.04092	0.254837	1.12144
0.284544	1	0.255456	1.07705	0.255456	1.15738

0.283864	1	0.256136	1.1049	0.256136	1.18201
0.283116	1	0.256884	1.12564	0.256884	1.19637
0.282293	1	0.257707	1.14056	0.257707	1.20237
0.281388	1	0.258612	1.15098	0.258612	1.20238
0.280392	1	0.259608	1.15807	0.259608	1.1986
0.279297	1	0.260703	1.16276	0.260703	1.19281
0.278092	1	0.261908	1.1658	0.261908	1.18632
0.276766	1	0.263234	1.16774	0.263234	1.18003
0.275308	1	0.264692	1.16895	0.264692	1.17454
0.273705	1	0.266295	1.16969	0.266295	1.1703
0.27194	1	0.268059	1.17014	0.268059	1.16766
0.27	1	0.27	1.17036	0.27	1.16705
0.268059	1	0.271941	1.17036	0.27194	1.16881
0.266295	1	0.273705	1.17012	0.273705	1.17255
0.264692	1	0.275308	1.16956	0.275308	1.17788
0.263234	1	0.276766	1.16852	0.276766	1.18445
0.261908	1	0.278092	1.16674	0.278092	1.19183
0.260703	1	0.279297	1.16382	0.279297	1.19939
0.259608	1	0.280392	1.15922	0.280392	1.20622
0.258612	1	0.281388	1.15219	0.281388	1.21095
0.257707	1	0.282293	1.14178	0.282293	1.21173
0.256884	1	0.283116	1.12681	0.283116	1.20627
0.256136	1	0.283864	1.10595	0.283864	1.19214
0.255456	1	0.284544	1.0779	0.284544	1.16739
0.254837	1	0.285163	1.04152	0.285163	1.13101
0.254275	1	0.285725	0.996231	0.285725	1.08314
0.253764	1	0.286236	0.942552	0.286236	1.02501
0.2533	1	0.2867	0.881769	0.2867	0.958484
0.252878	1	0.287122	0.815393	0.287122	0.885552
0.252494	1	0.287506	0.744963	0.287506	0.808127
0.252145	1	0.287855	0.671932	0.287855	0.727953
0.251827	1	0.288173	0.597574	0.288173	0.64654
0.251539	1	0.288461	0.522996	0.288461	0.565157
0.251277	1	0.288723	0.449178	0.288723	0.484862
0.251038	1	0.288962	0.376955	0.288962	0.406516
0.250822	1	0.289178	0.306978	0.289178	0.330776
0.250625	1	0.289375	0.239735	0.289376	0.258126

0.250445	1	0.289555	0.175561	0.289555	0.188898
0.250283	1	0.289717	0.114669	0.289717	0.123299
0.250135	1	0.289865	0.057173	0.289865	0.061436
0.25	0	0.29	0	0.29	0

Table 36. Exported Fluent temperature data for comparison example - 40 mm.

Y	T_in	Y	T_center	Y	T_out
mm	m/s	mm	m/s	mm	m/s
0.29	313.485	0.25	400.149	0.25	423.451
0.289865	313.342	0.250135	399.125	0.250135	422.472
0.289717	313.17	0.250283	396.869	0.250283	420.316
0.289555	313.152	0.250445	394.381	0.250445	417.939
0.289376	313.15	0.250625	391.643	0.250625	415.319
0.289178	313.15	0.250822	388.633	0.250822	412.435
0.288962	313.15	0.251038	385.333	0.251038	409.262
0.288723	313.15	0.251277	381.725	0.251277	405.778
0.288461	313.15	0.251539	377.798	0.251539	401.96
0.288173	313.15	0.251827	373.55	0.251827	397.788
0.287855	313.15	0.252145	368.983	0.252145	393.246
0.287506	313.15	0.252494	364.117	0.252494	388.321
0.287122	313.15	0.252878	358.988	0.252878	383.013
0.2867	313.15	0.2533	353.667	0.2533	377.339
0.286236	313.15	0.253764	348.262	0.253764	371.34
0.285725	313.15	0.254275	342.925	0.254275	365.101
0.285163	313.15	0.254837	337.854	0.254837	358.76
0.284544	313.15	0.255456	333.233	0.255456	352.506
0.283864	313.15	0.256136	329.172	0.256136	346.54
0.283116	313.15	0.256884	325.717	0.256884	341.057
0.282293	313.15	0.257707	322.87	0.257707	336.206
0.281388	313.15	0.258612	320.587	0.258612	332.058
0.280392	313.15	0.259608	318.803	0.259608	328.609
0.279297	313.15	0.260703	317.439	0.260703	325.806
0.278092	313.15	0.261908	316.419	0.261908	323.571
0.276766	313.15	0.263234	315.67	0.263234	321.831
0.275308	313.15	0.264692	315.135	0.264692	320.522
0.273705	313.15	0.266295	314.771	0.266295	319.6

0.27194	313.15	0.268059	314.556	0.268059	319.044
0.27	313.15	0.27	314.49	0.27	318.88
0.268059	313.15	0.271941	314.587	0.27194	319.151
0.266295	313.15	0.273705	314.834	0.273705	319.81
0.264692	313.15	0.275308	315.234	0.275308	320.84
0.263234	313.15	0.276766	315.812	0.276766	322.266
0.261908	313.15	0.278092	316.614	0.278092	324.136
0.260703	313.15	0.279297	317.7	0.279297	326.516
0.259608	313.15	0.280392	319.144	0.280392	329.482
0.258612	313.15	0.281388	321.024	0.281388	333.112
0.257707	313.15	0.282293	323.418	0.282293	337.46
0.256884	313.15	0.283116	326.392	0.283116	342.525
0.256136	313.15	0.283864	329.987	0.283864	348.228
0.255456	313.15	0.284544	334.195	0.284544	354.405
0.254837	313.15	0.285163	338.965	0.285163	360.849
0.254275	313.15	0.285725	344.178	0.285725	367.355
0.253764	313.15	0.286236	349.644	0.286236	373.731
0.2533	313.15	0.2867	355.161	0.2867	379.839
0.252878	313.15	0.287122	360.575	0.287122	385.601
0.252494	313.15	0.287506	365.779	0.287506	390.976
0.252145	313.15	0.287855	370.705	0.287855	395.951
0.251827	313.15	0.288173	375.316	0.288173	400.53
0.251539	313.15	0.288461	379.599	0.288461	404.728
0.251277	313.15	0.288723	383.549	0.288723	408.562
0.251038	313.15	0.288962	387.172	0.288962	412.056
0.250822	313.15	0.289178	390.482	0.289178	415.232
0.250625	313.15	0.289375	393.496	0.289376	418.116
0.250445	313.152	0.289555	396.235	0.289555	420.731
0.250283	313.17	0.289717	398.719	0.289717	423.102
0.250135	313.342	0.289865	400.971	0.289865	425.25
0.25	313.485	0.29	401.992	0.29	426.225
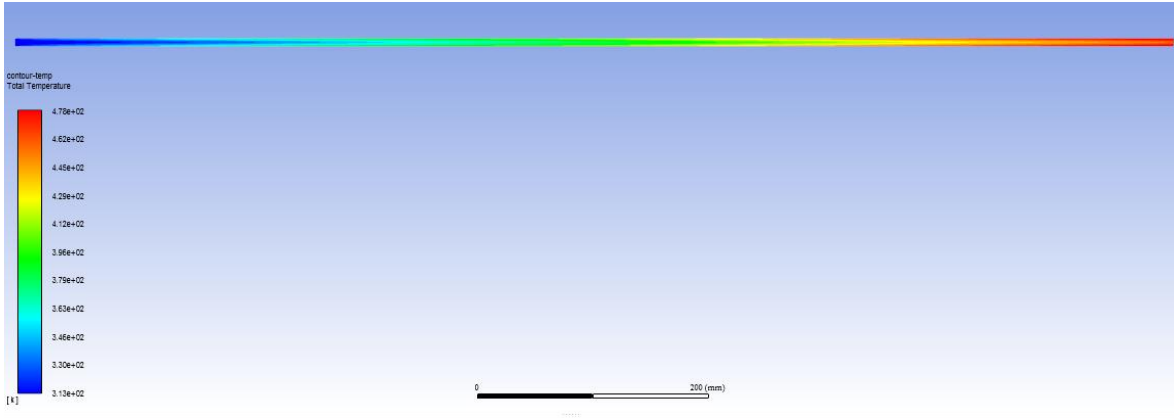
Figure 37. Total temperature contour - comparison example 6 mm.
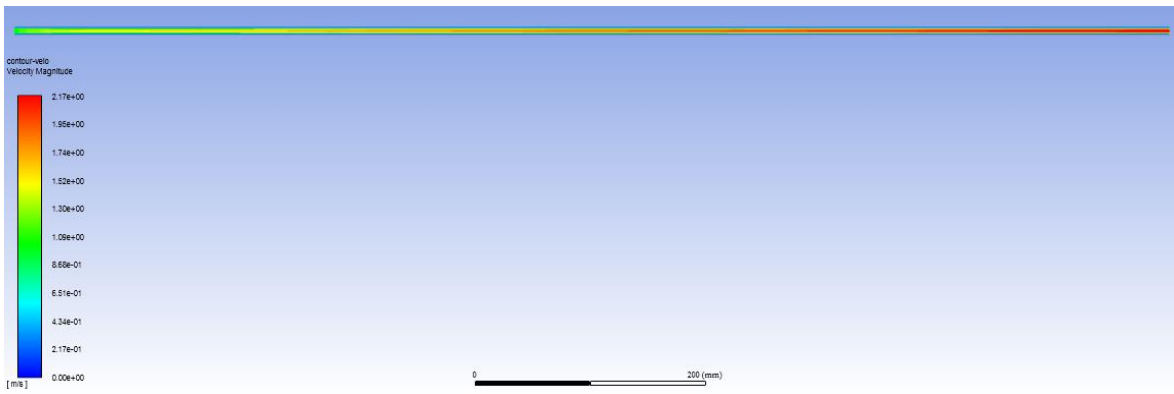
Figure 38. Velocity contour - comparison example 6 mm.
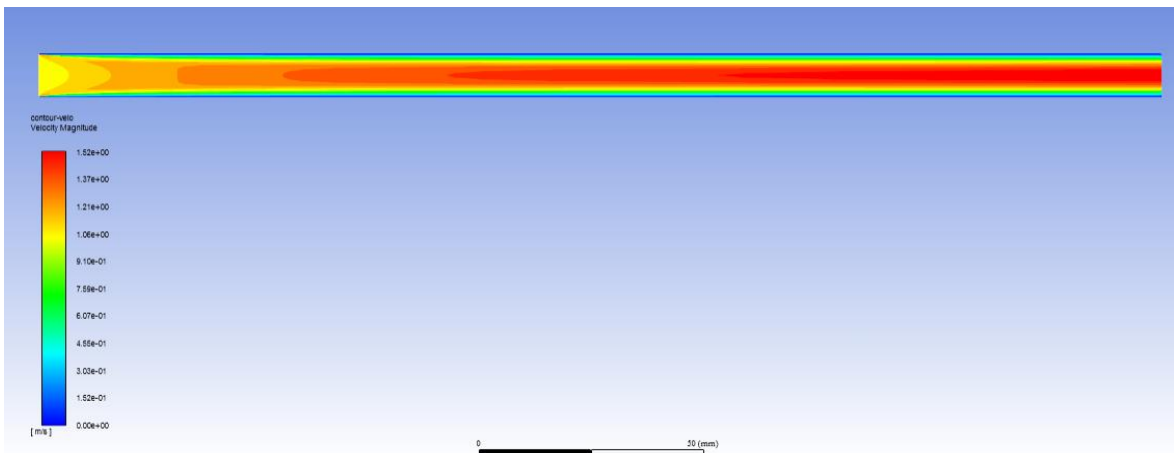
Figure 39. Total temperature contour - comparison example 14 mm.
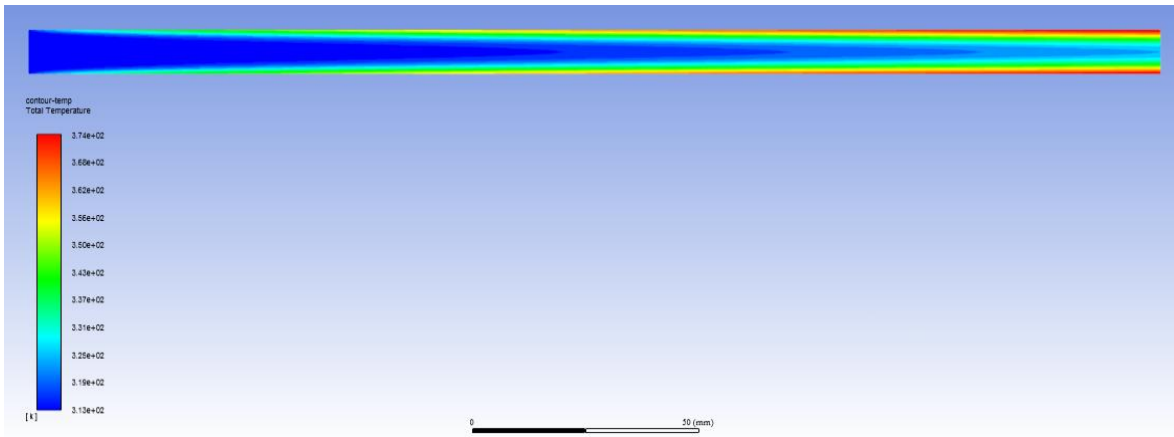
Figure 40. Velocity contour - comparison example 14 mm.
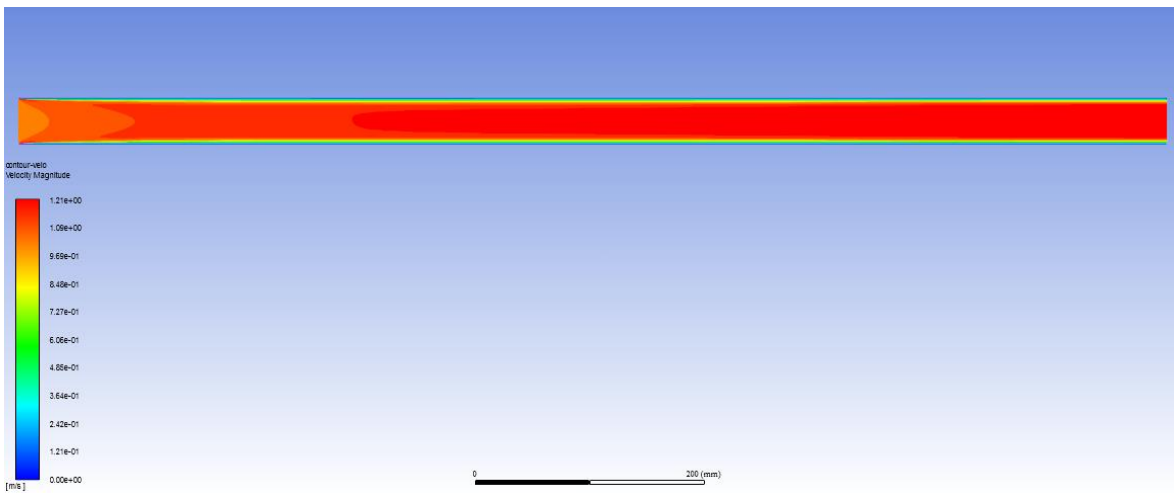
Figure 41. Total temperature contour - comparison example 40 mm.
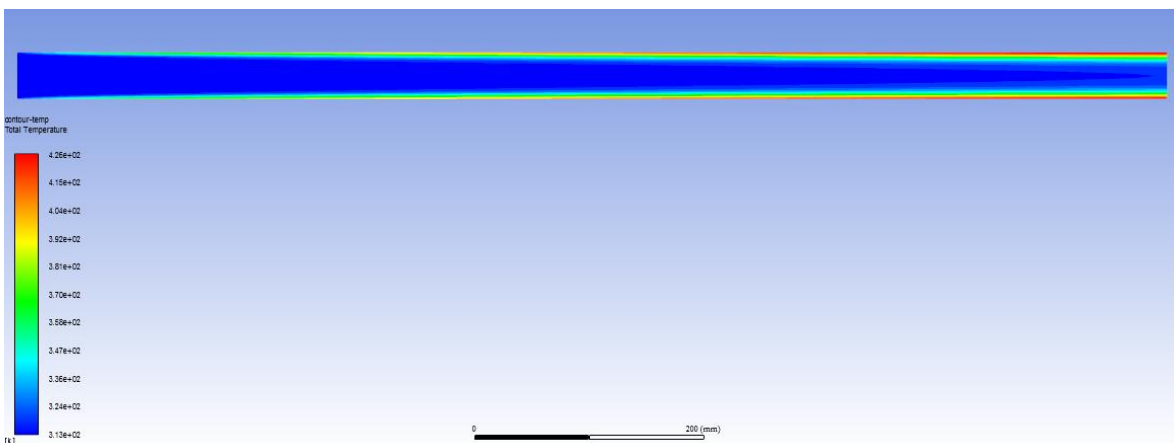
Figure 42. Velocity contour - comparison example 40 mm.

77

A Residual's monitoring example is presented by the following Figure.
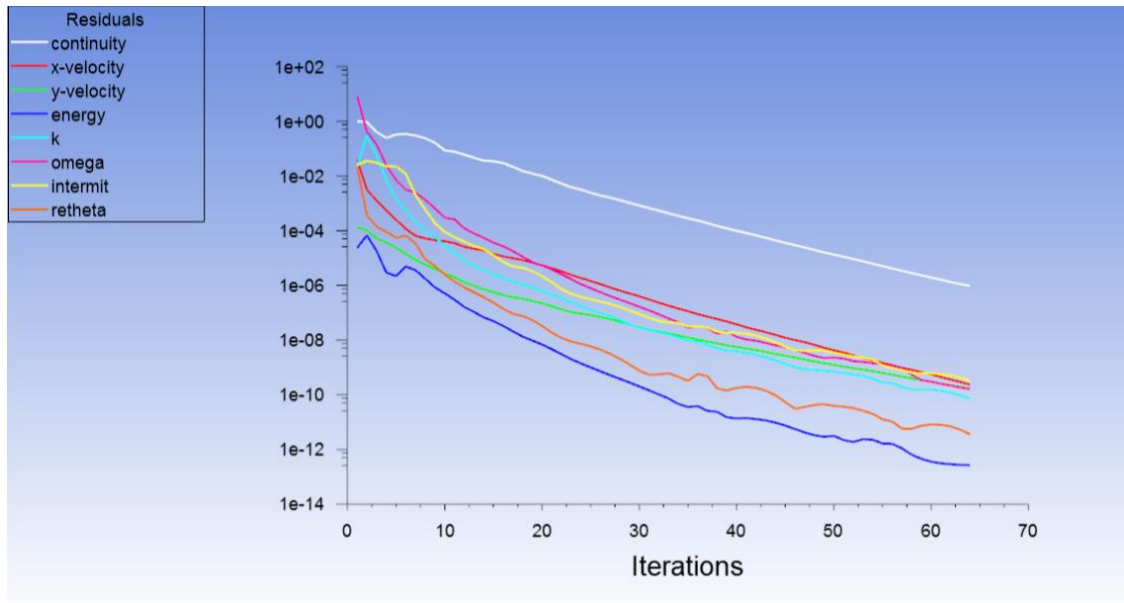
Figure 43. Scaled Residuals (14x1000), for a heat flux of 800W/m² and a velocity inlet of 2m/s.

8.5 MATLAB - Extra Information and Results

An example of the used MATLAB code for *lsqcurvefit* modelling attempt is followed presented (example shown in Result's analysis and Discussion chapter).

```matlab
clear all;clc;
%Load data from excel file
numData= xlsread('test_lsq.xlsx',1) ;

%Define input and output data
tk=numData(:,1);
H=numData(:,2);
Q=numData(:,3);
v_bulk=numData(:,4);
hc=numData(:,5);    % output 1
f=numData(:,6);     %output 2


ndata=numel(tk);    %data number
nparameters=4;      % variable number

%Normalize - method: x/max(x)
tk_n = tk()./max(tk);
```

```matlab
H_n = H()./max(H);
Q_n = Q()./max(Q);
v_bulk_n= v_bulk()./max(v_bulk);
hc_n = hc()./max(hc);
f_n = f()./max(f);

%Preditor's matrix
parameters=[tk_n,H_n,Q_n,v_bulk_n];

%Initial condition's vector
c0=[0.9373;1;1;1;1;1;1;1;1;1;1;1;1;1;1;1;1;1];
%c0=ones(18,1);

%Model Function
modelfun=@(c0,parameters)(c0(1)+(parameters(:,1).^c0(14).*parameters(:,2).^c0(15).*parameters(:,3).^c0(16)./(c0(17)+
c0(18).*parameters(:,3)))+((c0(2)+c0(3).*parameters(:,1).^c0(4))+(c0(5)+c0(6).*parameters(:,2).^c0(7))+(c0(8)+c0(9).*p
arameters(:,3).^c0(10))+(c0(11)+c0(12).*parameters(:,4).^c0(13))));

%Increase limit number of iterations
options=optimoptions('lsqcurvefit','MaxFunEvals',100000,'MaxIter',2000)

%Non-linear regression "lsqcurvefit"
LB=[];
UB=[];
[c,RESNORM,RESIDUAL] = lsqcurvefit(modelfun,c0,parameters,hc_n,LB,UB,options)

%Independent Plot
% scatter(tk_n,A,'-bo')
% scatter(H_n,A,'-yo')
% scatter(Q_n,A,'-ro')
% scatter(v_bulk_n,A,'-go')

% plot(parameters,hc_n,'mo',parameters,modelfun(c,parameters),'bx')
% xlabel('parameters')
% ylabel('h')

%Plot Relative Errors
A=RESIDUAL./hc_n
plot(parameters,A,'ko')
xlabel('parameters')
ylabel('RESIDUAL / h(CFD)')
```

```
%Statistic Data
RES_std=std(RESIDUAL)
RES_mean=mean(RESIDUAL)
RES_sk=skewness(RESIDUAL)
RES_kt=kurtosis(RESIDUAL)
RESh_std=std(A)

%Check correlation RES vs parameters
[c_tk,P]=corrcoef(tk_n,RESIDUAL)
[c_H,P]=corrcoef(H_n,RESIDUAL)
[c_Q,P]=corrcoef(Q_n,RESIDUAL)
[c_v_bulk,P]=corrcoef(v_bulk_n,RESIDUAL)
```

Some ANN's extra reports are followed presented.

1. Convection heat transfer coefficient fitting neural network

   A) All data
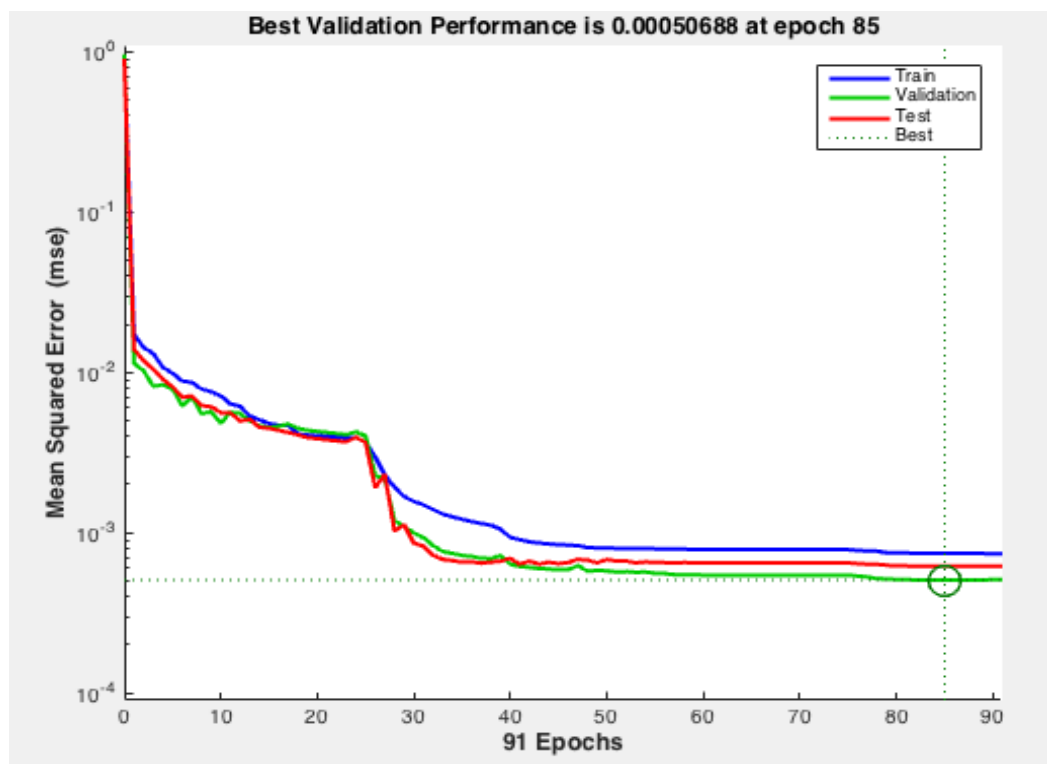
Figure 44. Performance report for convection coefficient fit.
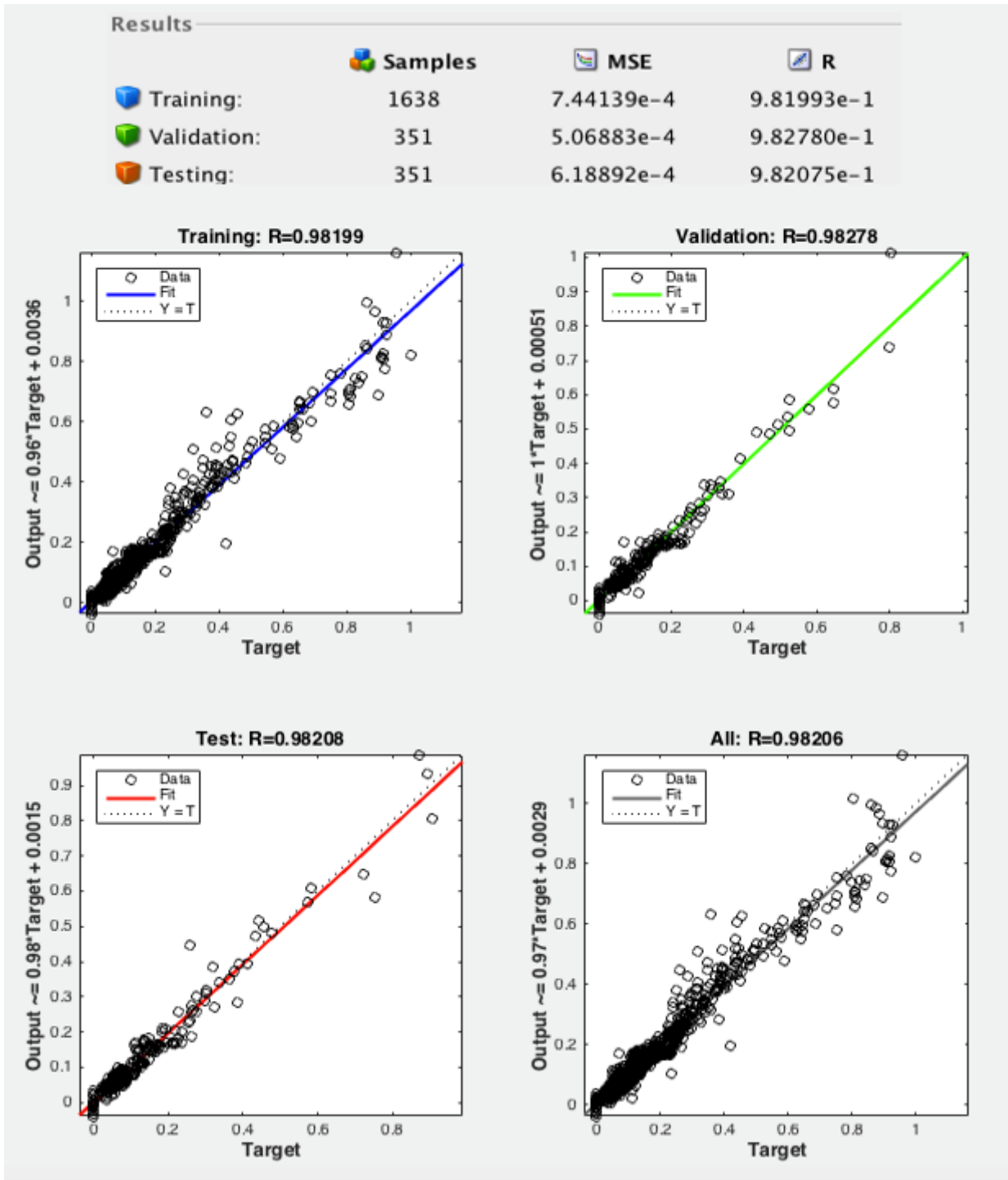
Figure 45. Neural network fit for convection heat transfer coefficient.

B) Comprising only $h_c < 20$ W/m^2.K data
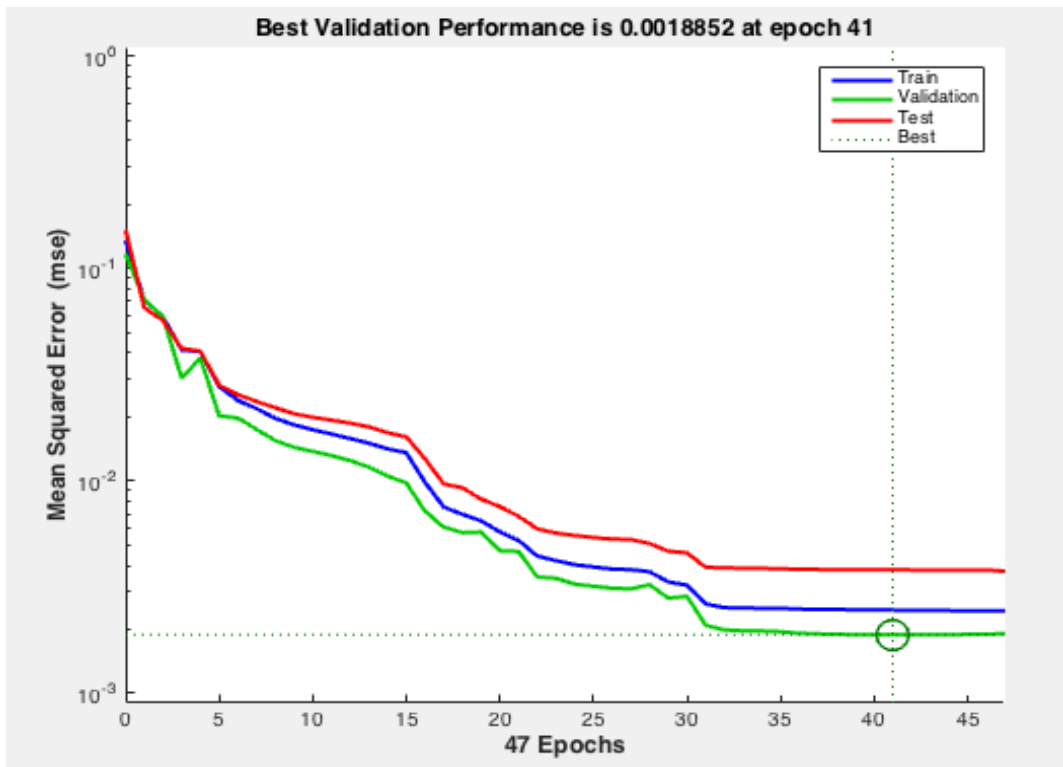
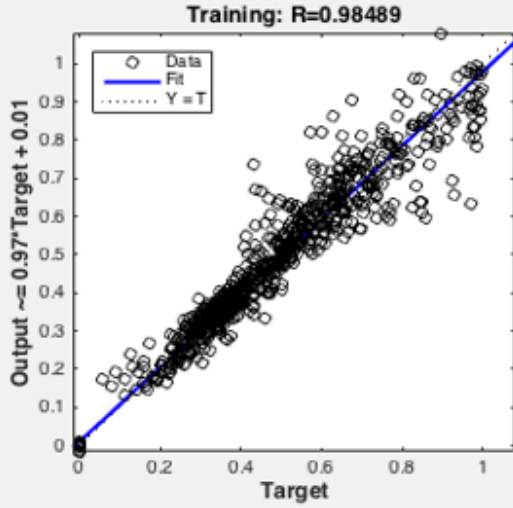*Figure 46. Performance report for convection coefficient lower than 20 W/m^2.K fit.*

Figure 47. Neural network fit for convection heat transfer coefficient lower than 20 W/m².K.

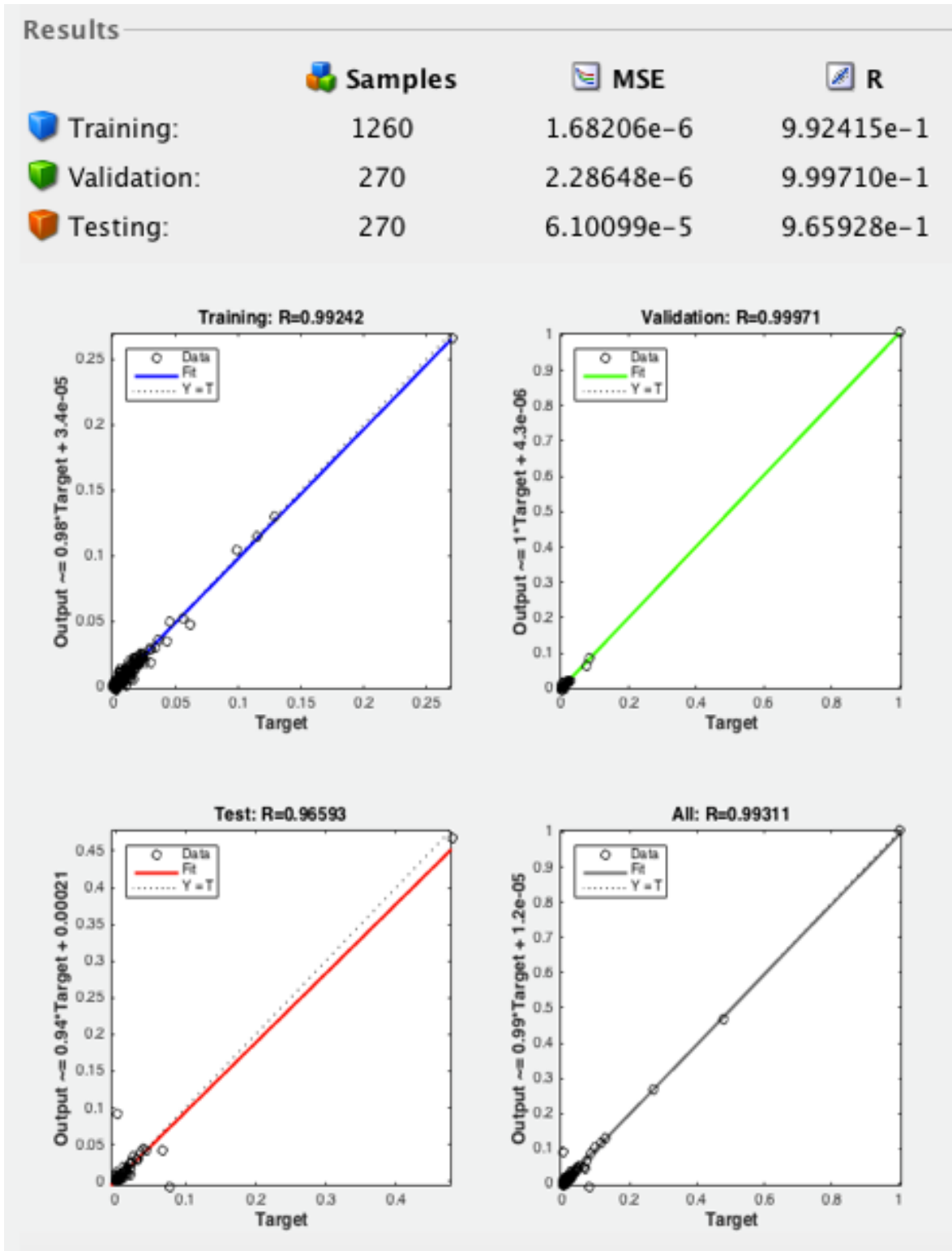2. Friction coefficient fitting neural network

   C) All data

Figure 48. Neural network fit for friction coefficient.
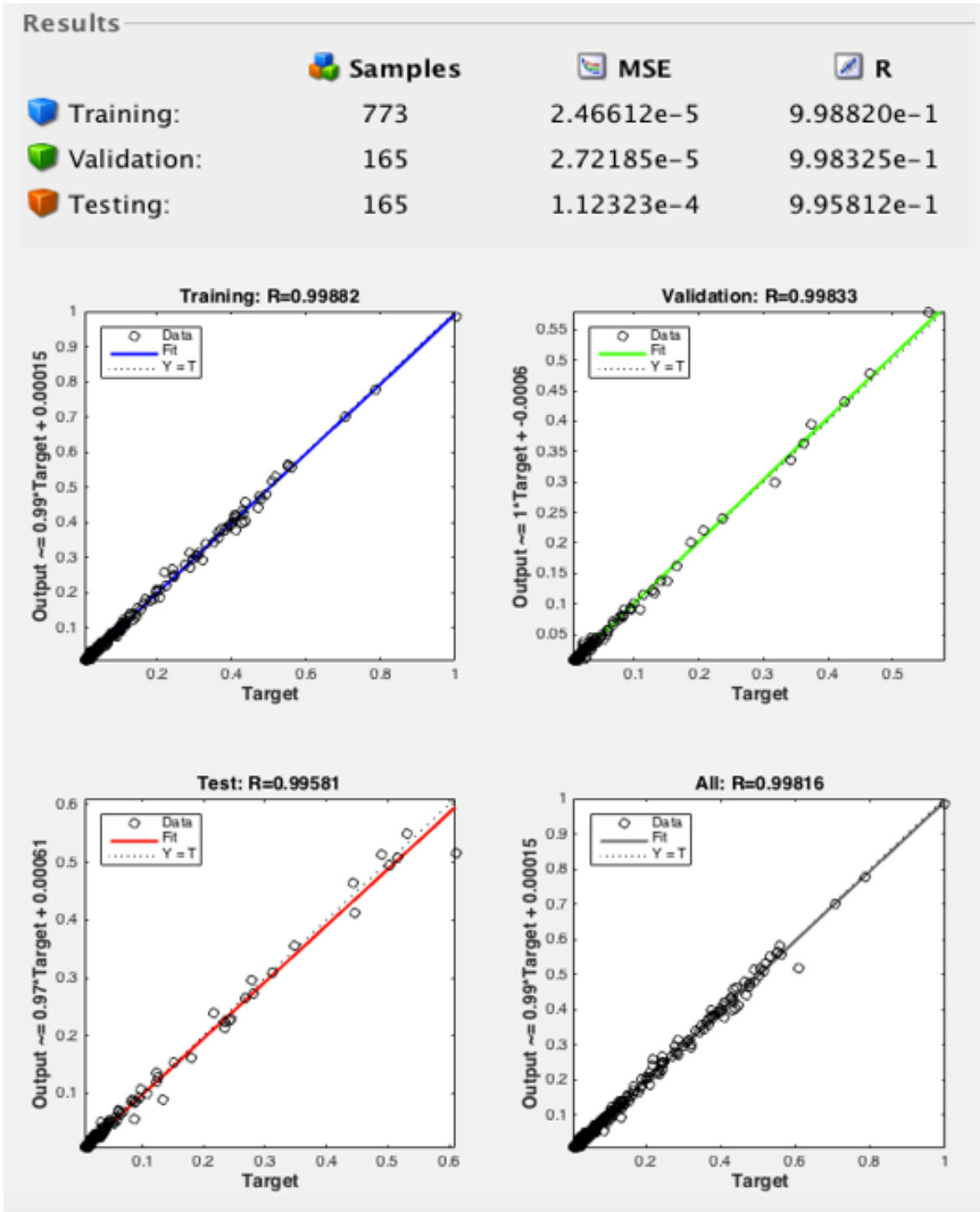
D) Comprising only $h_c < 20$ W/m^2.K data

Figure 49. Neural network fit for friction coefficient with convection heat transfer coefficient lower than 20 W/m^2.K.